Universitat Autònoma de Barcelona

Reflectance properties and mineralogy of asteroids by using carbonaceous chondrites

Safoura Tanbakouei

UNIVERSITAT AUTÒNOMA DE BARCELONA

DOCTORAL THESIS

Reflectance properties and mineralogy of asteroids by using carbonaceous chondrites

Author: Safoura Tanbakouei
Supervisor: Dr. Josep Maria Trigo-Rodríguez

Institute of Space Sciences
August 2, 2020

"This most beautiful system of the sun, planets and comets, could only proceed from the counsel and dominion of an intelligent and powerful Being."

Isaac Newton

Abstract

To understand the solar system and its current form, the evolution, and the formation process of the planets, small bodies are playing a key role. The surface composition of small bodies provide us the signs from the birth date of solar system and planets. These small bodies are the first solid materials of the Solar System had formed from aggregation and melting of dust and presolar grains with interplanetary particles and then larger bodies such as *asteroids*, *planetesimals* and planets formed. Some bodies have experienced chemical changes due to differentiation and some were small enough for not melting but conserve some of the very primordial materials of the Solar System. These preserved materials are hosted by undifferentiated *meteorites*. The *meteorites* coming from these objects, known as *chondrites* are samples of materials formed in the *protoplanetary disk* around the Sun about 4,600 million years ago. *Carbonaceous chondrite meteorites* are so far the only available samples representing carbon rich *asteroids* which are important to understand their physical properties and for future comparison with samples returned by missions such as Hayabusa 2 and OSIRIS-Rex.

This thesis focuses on the compositions, physical and mechanical properties and mineralogy of Solar system small bodies through laboratory measurements of their *meteorites*. These techniques allow the study of several physico-chemical properties of *chondrites*, and therefore provide clues about the complex accretionary histories of their parent bodies. The specific mineralogy related to *thermal metamorphism*, aqueous alteration, and the effects of shock in *chondrites* are described here in the context of their possible parent *asteroids*. Besides, spectroscopic techniques are applied as suitable method to link the *meteorite* samples to specific *asteroids*, although an exact association will require to complete future sample return missions.

In the first part of the work, the reflectance spectra of two chemically-related *carbonaceous chondrites* groups, precisely the *CVs* and *CKs* are measured and compared. The available sample suite includes multiple grain sizes and samples with *petrologic types* varying from 3 (very low degree of *thermal metamorphism*) to 5 (high degree of *thermal metamorphism*). The reflective properties of these two *chondrite* groups and the comparison with the Cg *asteroid* reflectance class suggests in a plausible formation scenario. In our opinion, the similarities point toward a common chondritic reservoir from which the *CV-CK asteroids* collisionally evolved. In that scenario the *CV* and *CK chondrites* could be originated from 221 Eos *asteroid* family, but because of its collisional disruption, both *chondrite* groups evolved separately, experiencing different stages of *thermal metamorphism*, annealing and *space weathering*.

Asteroids have been exposed to impacts since their formation, and as a consequence their surfaces are covered by small particles, pebbles, and boulders. The Japanese JAXA/ISAS Hayabusa mission collected micron-sized particles from the regolith of *asteroid* 25143 Itokawa. The study in terrestrial laboratories of these particles provides a scientific opportunity as their physical properties can be compared with those characteristic of chondritic *meteorites* that are often considered proxies of the building materials of *potentially hazardous asteroids (PHAs)*. In the second part of the thesis, I present the results from a study of the mechanical properties of three

of these particles using a precise technique called nanoindentation. The reduced *Young's modulus* values obtained for the Itokawa samples are higher than those measured for the Chelyabinsk *chondrite*, so these specific particles of *asteroid* regolith are more compacted than the minerals forming the particular *LL chondrite* associated with *PHAs*. This might be a natural consequence of particles surviving long exposure times on the surface of a *NEA* (Near-Earth Asteroid). These results are relevant to increase the efficiency of impact deflection in *asteroids*, as the future Double Asteroid Redirection Test (DART) mission plans to excavate a *crater* in the surface of the (65803) Didymos satellite of the (65803) Didymos binary asteroid.

I also studied the properties of dark bodies, associated with evolved short-period comets. In that sense,*Comet* 2P/Encke is one of the largest object of the so-called *Taurid complex*. It has been proposed that its spectral behaviour makes it similar to pristine carbonaceous *asteroids*, but little is known about its real nature. During the last decades other *NEOs (Near-Earth Objects)* have been discovered with orbits that can be linked to 2P/Encke and to the *Taurid complex*. Thirdly, I compared the spectral behaviour of 2P/Encke with laboratory spectra of *carbonaceous chondrites*. Different specimens of the common *carbonaceous chondrite* groups do not match the overall features and slope of *comet* 2P/Encke. Trying ungrouped *carbonaceous chondrites*, I found two *meteorites*, Meteorite Hills 01017 and Grosvenor Mountains 95551, which could be good proxies for the dark materials forming this short-period *comet*. These two *meteorites* could be rare surviving samples, either from the *Taurid complex* or another compositionally similar bodies. Finally, I think that identifying good proxies of 2P/Encke-forming materials might have interesting implications for future sample-return missions to evolved, potentially dormant or extinct, *comets*. To understand the compositional nature of evolved *comets* is particularly relevant in the context of the future mitigation of impact hazard from these dark and dangerous projectiles.

Acknowledgements

Firstly, I would like to express my sincere gratitude to my advisor Dr. Josep M. Trigo Rodríguez for the continuous support of my Ph.D study and related research, for his patience, motivation, and immense knowledge. His guidance helped me in all the time of research and writing of this thesis. Also, he provided me several great opportunities to travel, participate in conferences and work with different teams.

I also want to thank the coauthors and collaborators of the papers published and researched done during the process of this thesis. I would like to thank Prof. Jordi Sort to give me the oppurtunity to take advantage of UMIS Equipment from Fischer-Cripps Laboratorie and Prof. Jordi Llorca to provide us the oppurtunity to use A Shimadzu UV 3600 UV–Vis–NIR spectrometer.

A special mention to Prof. Andrew Rivkin, Prof. Iwan P. Williams, Prof. Tomoki Nakamura and Prof. Jurgen Blum, whose provided generous advise contributing to the publication of our papers. We also thank the Hayabusa team for providing the Itokawa particles and NASA Meteorite Antarctic Collection for providing the samples of Antarctic meteorites.

I would like to thank the jury committee: Dr. Adriano Campo Bagatin, Dr. Eva Pellicer, Dr. Maria Gritsevich, Dr. Julia de Leóna nd Dr. Elisabetta Dotto for evaluating my work, and for their constructive and helpful suggestions.

Last but not the least, I would like to thank my husband for his love and support over the past four years, my parents and my sister for supporting me financially and spiritually throughout the years of my PhD and writing this thesis to accomplish my goals. I am grateful for their support and encouragement.

Contents

List of Figures

List of Tables

Chapter 1

Introduction

This PhD thesis is addressed to increase our understanding about the physical and reflective properties of the smallest Solar System objects: *asteroids*, *comets* and meteoroids. The relevance of these bodies to get additional insight on the formation of the Sun and the planets is enormous as *asteroids* and *comets* represent the last surviving pieces of the Solar System evolutionary puzzle. Not only that, as the study of sample-returned materials and *meteorites* reveals that undifferentiated *asteroids* and *comets* have kept rock-forming minerals in their interiors that condensed and aggregated about 4.565 million years (Myrs) ago.

1.1 Minor bodies as remnants of solar system evolution and formation

Undifferentiated bodies in our planetary system provide valuable clues on the conditions of the solar system during its formation as well as planets and minor bodies formation and evolution. One of the favoured *accretion* models is the so-called hierarchical dust *accretion* hypothesis that describes how the *protoplanetary disk* aggregates grow into sub-millimeter, porous clusters (Rietmeijer, 2002). These primordial clusters were probably compacted into cm- to meter-sized bodies that were the origin of *planetesimals*. These Solar System building blocks accreted into km-sized bodies that never experienced chemical *differentiation* like much later happened in the largest (thousand of km in diameter) planetary bodies. These undifferentiated bodies are formed by a type of primordial accretionary solid blocks accreted around the Sun that is known as *chondrites*. This name comes from the fact that they are accretionary rocks containing igneous spherules basically made by silicates, sulphides and metal, generically known as *chondrules*.

The isotopic study of undifferentiated *meteorites* has revealed that the Solar System formed around 4.6 Gyr ago (Bouvier and Wadhwa, 2010). Blum et al. (2006) simulated the formation conditions of large bodies in the solar system and demonstrated the *accretion* of primordial materials in short timescales. The planetary formation process of minor bodies occurred over an extremely short period of less than 10 millions years (Yin et al., 2002). After this period, strong solar winds cleared the gas and fine dust from the Solar System, and the leftovers were the so-called *planetesimals*. Depending of the materials available on the *protoplanetary disk* (Fig. 1.1) that surrounded the Sun, rocky *planetesimals* formed close to the Sun, while weakly bounded aggregates formed by ices, organics, and tiny mineral grains accreted in the outer disk (Armitage, 2011). Collision velocities and energies increased while growing in size (to several cm at 1 AU and $\sim$ 1 mm at 30 AU) and mass, so the process ended in the formation of fragile dust aggregates, that also suffered fragmentation processes (Blum and Wurm, 2000; Blum, 2004).

The Ca and Al-rich Inclusions (*CAIs*) are *refractory* inclusions contained in the undifferentiated *meteorites* known as *chondrites*. The *CAIs* formed part of the first materials that survived the extreme environment of the young Sun. The original minerals condensed from a cooling gas of solar composition, but under such extreme heating conditions some of their components evaporated to become *refractory* oxides (Jones et al., 2000). In few million of years after their formation, chondritic aggregates started to survive as igneous *chondrules*. Then grew enough to become porous bodies in the km scale and attract each other through their mutual gravity which called *planetesimals* (Weidenschilling and Cuzzi, 1993). In the whole lifetime of the Solar System, *planetesimals* experienced big quantities of collisions by different-sized impactors at different velocities. These processes made them to compact but the largest impacts produce catasrophic disruption and reaccretion (Michel et al., 2001). Over the eons their surfaces became processed by collisional *gardening* (Beitz et al., 2016). The rest of planets and moons, remained as *comets* in the outer regions of the solar System, and a large fraction formed as minor bodies and *asteroids* in the Main Asteroid Belt between Mars and Jupiter (Beitz et al., 2016).

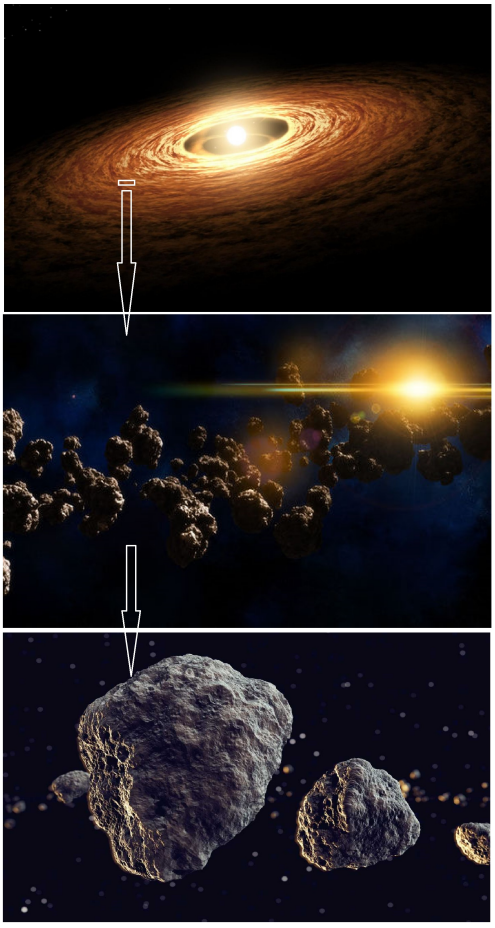

FIGURE 1.1: A protoplanetary disk sketch to exemplify hierarchical accretion, and the steps in accretion: from dust aggregates up to the final consolidation of planetesimals

1.1.1 Asteroids, NEOs and comets

There are millions of small bodies in the Solar System, including *asteroids* and *comets*. *Asteroids* are rocky bodies orbiting the Sun at different heliocentric distances. These minor bodies are the remnants of the *planetesimal* original population, being rocky or metal in the regions close to the Sun or ice-rich bodies in the farthest regions in the Solar System (Brearley and Jones, 1998; Trigo-Rodríguez, 2015).

Most current *asteroids* of the solar system are formed by re-aggregation of large rock fragments from the huge and continuous impacts of previous *asteroids* and variable size objects (Michel et al., 2001; Holsapple, 2001; Beitz et al., 2016). These collisions produce huge amounts of impact ejects. Continuously, the larger *asteroids* (sizes above few km) collided, merged and retook more than half of these ejected material to grew as planetary sizes and form a regolith layer on their surface (O'Keefe and Ahrens, 1985; DeMeo, 2010a).

At this early stage, a strong temperature gradient across the disk, made different components to condense separately. The inner disk was too hot for the condensation of volatiles, so it was dominated by rocky material, while the outer disk had a mixture of fine mineral grains, organics and ices as revealed Stardust (NASA) mission from the sample return of materials from *comet* 81p/Wild 2 (Brownlee et al., 2006). Within the disk, micron-size dust grains formed bodies up to a kilometer in size. Many of these large bodies collided and merged other bodies and eventually grew to planetary sizes (DeMeo, 2010a).

Near-Earth Objects (NEOs) include *asteroids* and *comets*. They have orbits lying within the Earth's orbit or well crossing the near-Earth space. According to the Center for Near Earth Object Studies (CNEOS) at the Jet Propulsion Laboratory there are 22,189 *NEOs* up to Feb. 2, 2020 (Barbee, 2020) which around 8% of them have orbits, *albedos* and spectra similar to a cometary origin with the dynamical and physical criteria (DeMeo et al., 2009). Some of the *NEOs* are ideal target mission for National Aeronautics and Space Administration (NASA), European Space Agency (ESA) and Japan Aerospace Exploration Agency (JAXA) that they dedicate space missions to explore these objects.

Among the *NEOs* there is a subgroup known as *Near Earth Asteroids (NEAs)*. These rocky or rocky-metal bodies approaching to Earth have orbits with perihelion distance q < 1.3 astronomical units (AU) and aphelion distance Q > 0.983 AU (see the different recognized groups in Tab. 1.1). *Asteroids* are dominant in the near-Earth region because represent a population of thousands of bodies compared with about one hundred dark objects that share dynamic and physical properties of being dormant or extinct *comets* (Jenniskens, 1998; Jenniskens, 2006).

On the other hand, the most distant *comets* are weakly-bounded aggregates that contain ices, organics and micron-sized rocky minerals as revealed Stardust mission (Brownlee et al., 2006). When they approach to the Sun the ices are sublimated, forming a halo of gas and dust surrounding the *comet* nucleus. In addition, the release of the *comet* components in form of gas and dust produces two tails: a dust tail drawing along the opposite trajectory to the *comet* and an ion tail in the anti-Sun direction, which are mostly developed during the close approach of the *comet* to the Sun. Our discovery of a cometary fragment in the interior of a *chondrite* make suspect that *comets* have very significant compositional differences (Nittler et al., 2019a).

As *comet* nuclei contain ice species more volatile than water ice, a coma and tail may be formed even at large heliocentric distances. Sublimation of water typically begins at a distance of 3 AU, but other species appear to sublimate far away from the Sun, creating a coma even at 6 AU (Brandt and Chapman, 2004). When a new

TABLE 1.1: Orbital definitions of the Near Earth Object groups and their respective acronyms (Adapted from NEO JPL).

Groups	Description	Orbital Definition
NECs	Near-Earth Comets	q < 1.3 AU, P< 200 yrs
NEAs	Near-Earth Asteroids	q < 1.3 AU
Atiras	NEAs named after asteroid 163693 Atira	Orbits are contained entirely with the orbit of the Earth a < 1.0 AU, Q < 0.983 AU
Atens	NEAs named after asteroid 2062 Aten.	Earth-crossing NEAs with semi-major axes smaller than Earth's a < 1.0 AU, Q > 0.983 AU
Apollos	NEAs named after asteroid 1862 Apollo	Earth-crossing NEAs with semi-major axes larger than Earth's a >1.0 AU, q < 1.017 AU
Amors	NEAs named after asteroid 1221 Amor	Earth-approaching NEAs with orbits exterior to Earth's but interior to Mars' accomplishing: a >1.0 AU, 1.017 < q < 1.3 AU
PHAs	Potentially Hazardous Asteroids: NEAs whose Minimum Orbit Intersection Distance (MOID) with the Earth is 0.05 AU or less and whose absolute magnitude (H) is 22.0 or brighter.	MOID <= 0.05 AU, H <= 22.0

Solar System body is detected exhibiting a blurry appearance, just a distinguishable presentation of a coma surrounding a false nucleus, is named and catalogued as a *comet*. *Comets* are classified into long period *comets* with periods greater than 200 years and highly eccentric orbits or short period comets with periods less than 200 years. Among them are Halley Family Comets (P > 20 years) like 1P/Halley, or Jupiter Family Comets (P < 20 years) (Hsieh and Jewitt, 2006). Other so-called evolved comets have periods smaller than 20 years, like e.g. 2P/Encke that probably appeared from the disruption of a larger *comet*. In addition, a new type of comet has been defined and catalogued as interstellar, like e.g. 2I/ Borisov. It is not surprising as we expect that *asteroids* and *comets* are scattered by planetary perturbations during the first stages in the formation of planetary systems.

1.2 Undifferentiated meteorites: chondrites

Chondrites are agglomerate rocks mostly composed by silicate, sulfide and usually, metal that have quasi, solar bulk compositions (Brearley and Jones, 1998). Within this definition, *chondrites* show systematic variations of major non-*volatile elements* such as Si, Mg, Al, Ca and Fe that allow us to assign them to three classes: carbonaceous, ordinary and *enstatite* (see e.g. Hutchison (2006)). Chondrites are very diverse compositionally, and are classified in groups according to the affinities in bulk composition (Wasson, 1985). *Chondrite* properties are also diverse and representative of the different formation environments and evolutionary histories suffered by their respective chondritic parent bodies (Alexander, McKeegan, and Altwegg, 2018). Among the physical processes experienced by chondritic parent bodies, primordial radiogenic heating and impacts, promoted different degrees of *metamorphism* as a function of the *parent body* diameter, and the collisional history, respectively. As an outcome of these processes (Fig. 1.1): ice ratios, aqueous alteration, gravitational sintering, and shock-induced *metamorphism* or annealing depending of the energy of collisions with other bodies during *parent body* processing (Ormel, 2008; Hutchison, 2006) may happen.

Meteorites are then fragments of the bodies formed in our Solar System. These rocks are characterized as *falls* if they are recovered soon after their delivery to Earth's surface, while we call them *finds* if they have expended a long time since

its unknown arrival to our planet. We are going to concentrate in the study of *chondrites* as they are able to provide unique information about the early evolution of solid bodies in our planetary system. Obviously, they are not only chondritic in nature as the largest bodies product of the *accretion* of embryos experienced *differentiation* and developed a metallic core, a silicate mantle and a crust. Most of the first planetary embryos were either impacting to form planets or disrupted by gigantic catastrophic collisions (Petit and Morbidelli, 2005). As consequence of these evolutionary processes today we have samples of bodies that experienced igneous processes, recrystallizing their forming minerals and modifying their bulk compositions. The *meteorites* arrived from these differentiated bodies are known as *achondrites*.

Compositionally, *meteorites* are divided into three main classes: stones, stony-irons, and irons. Large majority of *meteorites* are stony, but it is important to remark that they include ordinary and *carbonaceous chondrites*, plus *achondrites*. The name *achondrite* makes reference to the absence of *chondrules*, given that these are recrystallized *meteorites* formed by igneous processes at work in large *asteroids* and planetary bodies.

In general, more than 67.5% of all of the *meteorites* known are undifferentiated and classified as *chondrites* (Grady, Hutchison, and Graham, 2000). Many finds are still not characterized or difficult to characterize due to having experienced significant terrestrial weathering, so about a 26% of the stony *meteorites* are *ungrouped*. Finally, a 3.8% of *meteorites* are *stony-irons* or *irons*, and a 2.7% are *achondrites* (Grady, Hutchison, and Graham, 2000). We are going to concentrate in the study of *chondrites*, so the next sections are devoted to study them and infer some of the processes experienced by their parent bodies.

1.2.1 Petrologic types

Larger bodies retained most of the radiation in their interiors, so the temperature increased. The high pressure due to the self-gravity and high temperature due to the radioactive decay which happen in the interior of *planetesimals*, cause a compaction process known as sintering which becomes active at temperatures $\sim 700K$ (Henke et al., 2012). The process of sintering ended in considerable compaction for silicates and metals in *asteroids*, but it also produces the crystallization of amorphous ice and phase transition of volatiles in highly porous icy bodies (Gail et al., 2013). Through this heating, the iron melt and sink to the core of the body, while the silicate melts and go up towards the surface due to its lower density (Yomogida and Matsui, 1984). The extent of melting and *differentiation* of a body depends on its composition, size and *accretion* time which determines the amount of short-lived radionuclides in a body before they decay. This compaction increases thermal conductivity and transport more heat from the core to the outer layers of the body (Krause et al., 2011). Thermal and structural evolution of chondritic *asteroids* is also affected significantly by water (Alexander, McKeegan, and Altwegg, 2018). Water ice absorb big amount of heat while melting and the warm water moves within the porous material and spread the heat through the body (Grimm and McSween, 1989).

Given the different "cooking" experienced by the chondritic *asteroids* is particularly important to define the concept of *petrologic type*. Depending on the degree of heat imposed to undifferentiated *asteroids*, the rocky components experienced different degrees of sintering. Following the method originated by Van Schmus and Wood (1967), *meteorites* from undifferentiated bodies are divided in a 1 to 6 scale of *petrologic type* (see Fig. 1.2). Types 1 and 2 describe the degree of aqueous alteration,

and types 3 to 6 describe the degree of *thermal metamorphism* (Weisberg, McCoy, and Krot, 2006).

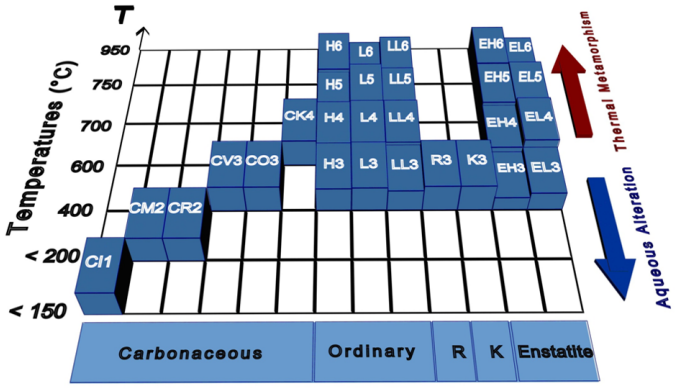

FIGURE 1.2: A schematic figure of the petrologic types in chondrites that are representative of the thermal metamorphism and aqueous alteration experienced by their parent asteroids.

In general, a *petrologic type* 3 is recognized as primordial, almost unaltered material. *Chondrites* of this specific petrologic type are considered representative of the accretionary materials that accreted 4.565 Myrs ago. Type 3 includes the so-called unequilibrated *meteorites*, because their minerals show compositions that were not homogeneized by heat, and reflect those that the mineral components had in the solar nebula (Jones, 1967). This type, heated between 600 and 900 K and has been divided in subtypes 3.0 to 3.9, with increasing *thermal metamorphism* releasing their elements of different composition, from the *matrix* to the *chondrules* (Huss, Rubin, and Grossman, 2006).

Increasing such *petrologic type* like e.g. types 4 to 6 we find rocks that have experienced increasing changes in mineralogy and texture due to the different degrees of *thermal metamorphism* experienced, while in general most of them have little evidence of aqueous alteration (Brearley and Jones, 1998; Huss, Rubin, and Grossman, 2006). It has been invoked that such relative absence of water is consequence of the initial *porosity* of *asteroids*, so most of the water was significantly released to space before sintering was efficient (Alexander, McKeegan, and Altwegg, 2018; Trigo-Rodríguez et al., 2019). It is accepted that the *chondrites* of *petrologic types* 3 to 6 were produced at different levels of sintering in their parent bodies. In other words, the rocks forming chondritic bodies, given the different temperature and pressures achieved in their interiors ended with a distinctive *petrologic type* (Göpel, Manhes, and Allegre, 1994). Types 4 to 6 include equilibrated *meteorites* with homogeneous minerals that were heated to between ∼900 and 1200 K and resulted in *matrix* re-crystallization and grain size increase (Van Schmus and Wood, 1967; Huss, Rubin, and Grossman, 2006). Above 1200 K, the parent bodies of these *meteorites* started melting and differentiating (Henke et al., 2012; Neumann, Breuer, and Spohn, 2012). Increasing degree of *thermal metamorphism* make type 5 *meteorites* more indistinct and make the *matrix* indistinguishable. In type 6, *chondrules* integrate with the *matrix* and *feldspar* form (Van Schmus and Wood, 1967; Huss, Rubin, and Grossman, 2006).

There are *chondrites* that have experienced different degrees of aqueous alteration, but relatively small effects of *thermal metamorphism*. These groups of *chondrites* belong to the carbonaceous class, and are represented by *petrologic types* below 3. In fact, *petrologic type* 1 refers to extremely altered *chondrites* up to the point that the *chondrules* were transformed into hydrated phases (phyllosilicates) by the

extensive aqueous alteration of the primordial *olivine* and *pyroxene*. Most of these *meteorites* experienced extensive aqueous alteration in their parent bodies at temperatures between ∼320 and 420 K (Van Schmus and Wood, 1967; Brearley and Jones, 1998; Weisberg, McCoy, and Krot, 2006). More moderate action of water is described for *petrologic type* 2 that probably experienced aqueous alteration during a more limited time, but at higher temperatures, between ∼470 and 600 K (Brearley and Jones, 1998). Probably due to the low initial ice ratios of their carbonaceous *asteroids*, at such temperature *thermal metamorphism* did not happen, so silicate *chondrules* survived (Trigo-Rodríguez et al., 2019). According to the different degrees of aqueous alteration experienced by hydrated *carbonaceous chondrites*, type 2 was divided in subtypes between 2.0 and 2.6 (Rubin et al., 2007).

1.2.2 Chondrite types

The noticeable differences in bulk elemental composition of the *chondrites*, also including oxygen isotopic compositions, concentration of *refractory* lithophile elements, and abundance of Fe in metallic or oxidized form, are used to classify the *chondrites* (Wasson, 1985). Other differences between *chondrite* groups come from the different formation regions in the Solar System and distances to the sun, so they ended in particular composition and level of oxidation (Weisberg, McCoy, and Krot, 2006; Alexander et al., 2007; Alexander, McKeegan, and Altwegg, 2018; Rubin, 2011).

Chondrites contain small grains- called *chondrules*- that accumulated during formation of the *asteroid* and have not changed over time. *Ordinary chondrites* (OCs) according to their iron content, classified into H (high iron content), L (low iron content), and LL (very low iron content). *Carbonaceous chondrites* (CCs) with significant amounts of carbon and water, depending on their composition, amount of aqueous and thermal alteration, are divided among classes *CI, CM, CV, CR, CO, CK,* CH and CB. *Enstatite chondrites* (ECs) are the most reduced class of *chondrites*.

Ordinary chondrites are the most common class of stony *meteorites*, representing more than 85% of all witnessed *chondrite falls* (Grady, Hutchison, and Graham, 2000). As genuine pieces of primordial matter, *ordinary chondrites* are everything else but ordinary since they are much rare than gold or diamonds and older than any rock known on Earth. More importantly, *ordinary chondrites* might not be that common at all when it comes to the actual distribution of chondritic matter in our solar system. In fact, the majority of *NEAs* exhibit *ordinary chondrite* composition, as also reflects the higher percentage of *ordinary chondrite falls* (Burbine et al., 2002). This is a natural consequence of a significant bias in the population of objects around the Earth. It is dominated by *ordinary chondrites* as these rocks have experienced higher degrees of *metamorphism*, are the common outcome of collisions in the Main Asteroid Belt, and are rocks with a higher strength, so they survive longer in interplanetary space (Trigo-Rodriguez and Blum, 2009; Trigo-Rodríguez, 2015).

In terms of mineralogy, *ordinary chondrites* are primarily composed of *olivine, pyroxene*, and a certain percentage of more or less oxidized nickel-iron. Based on the differing content of metal and differing mineralogical compositions, the OCs have been subdivided into three distinct groups that are designated as *H, L, and LL chondrites* (Brearley and Jones, 1998; Hutchison, 2006).

Carbonaceous chondrites represent about the 4% of the all *chondrites* known (Grady, Hutchison, and Graham, 2000), and their bulk chemical compositions match the chemistry of the Sun more closely than any other class of *chondrites* (Lodders and Fegley, 2015). *Carbonaceous chondrites* are primitive and undifferentiated *meteorites* that formed in oxygen-rich regions of the early solar system so that most of the metal is

not found in its free form but found as silicates, oxides, or sulfides. Most of them contain water or minerals that have been altered in the presence of water, and some of them contain large amounts of carbon as well as organic compounds or in inorganic form (*graphite*). Some *carbonaceous chondrites* have been relatively unaltered by heating during their history. The most primitive *carbonaceous chondrites* have never been heated above 50° C (Wasson, 1985). However, there are different clans and groups of *carbonaceous chondrites* that formed on different parent bodies presumably in different regions of the early solar nebula. The most important groups are designated as *CI, CM, CV, CO, CR, CK* and *CH chondrites* (Hutchison, 2006).

Enstatite chondrites (ECs) characterized by silicate *enstatite* in their *chondrules* and Mg-rich *pyroxene*. ECs cover less than 600 of recovered samples and show a range of *petrologic types* between 3 and 6. They show unique mineralogical features that have formed under highly reducing nebular conditions as Fe-poor silicates, Si and Sulphides (Keil, 1968). They show a lower abundance of *matrix* (between 0.1 and 10% in volume) and a higher abundance of metal clasts (between 8 and 15% in volume), very low volume of *CAIs* and other *refractory* inclusions below the 0.1%, a 60-80% volume of *chondrules* (Keil, 1968). ECs are divided in two different groups: EH (high-iron) with an average *chondrule* size $\sim$0.2 mm, up to 3% abundance of Si and $\sim$8% volume metal content, EL (low-iron) with $\sim$0.6 mm *chondrule* size, below 1% abundance of Si and $\sim$15% volume metal contents (Moyano Cambero, 2017). EHs also characterized by lower abundance of Ni in the NiFe metal grains, higher variation in the abundance of sulphides, and lower abundance of *enstatite* (Keil, 1968).

1.3 Rock forming materials in chondrites

The term *chondrule* is restricted to near-spherical, mm-sized igneous silicate objects, or fragment thereof, composed of the ferromagnesian minerals *olivine* and *pyroxene* $\pm$ feldspathic mesotasis. Before they became part of their parent bodies *chondrules* were thermally processed while they were floating in the *protoplanetary disk*, the effects of which ranged from total or partial melting to the sintering of precursor mineral grains (Hutchison, 2006). In other words, *chondrules* were produced from the thermal processing micron-sized clusters of particles that were thermally processed during the first stages of the *protoplanetary disk* evolution (Brearley and Jones, 1998; Trigo-Rodríguez, 2015). Calcium aluminium inclusions (*CAIs*) are another conspicuous components of *chondrites* that formed even earlier. Although much rarer, they are typically a factor of 10 larger than *chondrules*. As *chondrites* formed out of these *chondrules* and *CAIs*, this would also indicate that *planetesimal* formation was a relatively prolonged process, i.e., happening over much of the life-span of the solar nebula (Ormel, 2008; Hutchison, 2006). *CAIs* were overheated to the point that moderately *volatile elements* were depleted and only *refractory* oxides were preserved. Although the precise interpretation is disputed (Metzler, 2004; Trigo-Rodriguez, Rubin, and Wasson, 2006), *chondrites* consists of another component in the form of micron size dust particles of different compositions: silicates, sulfides, carbonates, organics, *graphite*, etc. These are present throughout the *chondrite* in a *matrix* component that is cementing the *meteorite*. This configuration suggests that *chondrules* and dust accreted together into the *chondrites* which implies that the *matrix* and rim material mimics the environmental conditions existing during the *protoplanetary disk* phase, i.e., when *chondrules* were still freely floating objects, although the precise interpretation is disputed (Ormel, 2008).

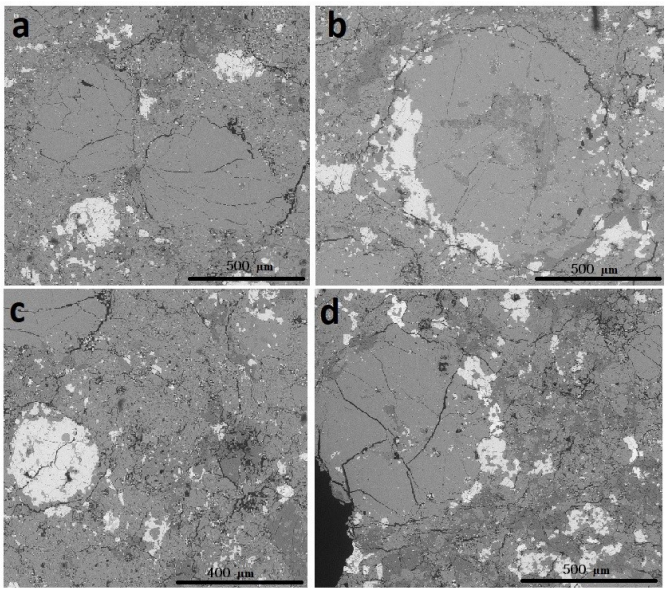

FIGURE 1.3: Back- scattered electron (BSE) image of regions of CK4 chondrite ALH 85002, consists mainly of well compacted silicate-rich chondrules, sulfides and accessory minerals. The matrix is formed by comminuted chondrule fragments that have experienced significant crushing, presumably due to impact processes. Olivine – light gray; orthopyroxene – medium gray; plagioclase – dark gray; sulfide and magnetite – white; fractures and pores being black. The black scale bars are 500, 500, 400 and 500 μm, respectively.

1.3.1 The surfaces, structures and composition of small bodies

Solar system bodies contain different composition according to their temperature they have based on their distance from the sun. As explained further in `chapter 3`, the composition of *asteroids* is primarily determined through spectroscopic observation and analyzing their reflectance properties. Different taxonomic categories of *asteroids* correlate with surface composition of these bodies. Silicate rich *asteroids* primarily located in the inner Solar System, contain the SiO_4. There are three major categories that describe *asteroids*: primitive, partially melted, and differentiated. Primitive material includes C, X, T and D types and are mainly made of silicates, carbon, and organics and are nearly similar to *CI* and C *meteorites*. Partially melted (thermally altered) include the S-complex *asteroids* and primarily contain *olivine, pyroxene* and metal. Their *meteorite* analogs are OCs and other *chondrites*. Differentiated bodies include basaltic V-types, nearly-pure *olivine*, A-types and metallic bodies, that represent pieces of the crust, mantle, and core.

Other processes which cause physical and chemical changes on the surfaces of small bodies include collisions, aqueous alteration and thermal alteration. Low *albedo asteroids* with a weak feature at 700 nm would be the evidence of aqueous alteration, caused by water interacting with anhydrous rock (Vilas and Gaffey, 1989). Bodies located in the inner solar system or with elliptic orbits have higher temperatures and therefore experience thermal effects. About 80% of all *meteorite falls* are *ordinary chondrites* although Q-type *asteroids*, which is spectrally most similar to *ordinary chondrites*, are minority among *NEAs*.

Space weathering is a process which changes the spectrum of bodies with no atmosphere, since there is no protection of the surface. Effects like bombardment by micrometeorites, solar wind ions, and cosmic ions would cause *space weathering*, with different strengths according to the *porosity*, grain size, composition, and the amount of time a surface has been exposed to space. Decreasing the size of S-type *NEOs* from 5 to 0.1 km resulted in decreasing the average spectral slope of the objects (Binzel et al., 2004), since smaller *asteroids* have shorter collisional lifetimes. Evidence for *space weathering* has been seen by in situ observations of *near-Earth asteroids* (Binzel et al., 2004). On *asteroid* 25143 Itokawa, visited by the Hayabusa spacecraft, the brighter fresher regions are also seen at inclined areas of the Little Woomera region (Saito et al., 2006).

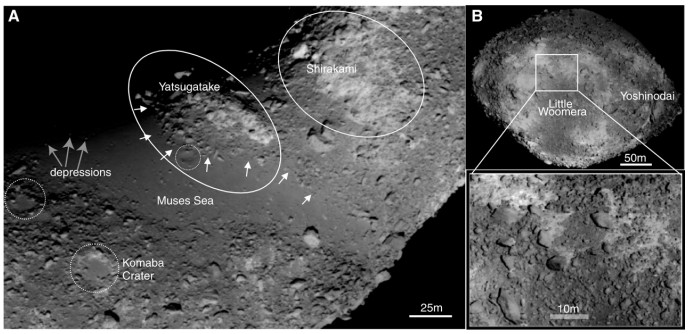

FIGURE 1.4: (A) Muses Sea, with the Shirakami area composing the southern part of the "neck" region (ST2474731509). Small white arrows near Yatsugatake indicate the thin, boulder-rich layer similar to landslide deposits. Depressions in Muses Sea are marked by long gray arrows. The Komaba crater and some crater candidates are also indicated. (B) The darker depressed region in Little Woomera, which is one of the largest facets, is surrounded by a brighter rim (Saito et al., 2006).

1.4 Chondritic meteorites and asteroid classes

UV to NIR spectroscopy provides clues on the mineralogy of *asteroids* (Gaffey and McCord, 1978; Gaffey, Bell, and Cruikshank, 1989; Bottke, 2002; DeMeo et al., 2009; Trigo-Rodriguez et al., 2014; Moyano-Cambero et al., 2017a). It is essential to take into account that spectral information of *asteroids* represent only their surface which covered by regolith, while *meteorites* might be separated from deeper layers of the *asteroid* by strong collisions, and therefore affected by processes such as impact processing, aqueous alteration or *thermal metamorphism*, which can alter their spectra (Keil, Bell, and Britt, 1992; Vernazza et al., 2008; Gaffey, 2010). Also, the separated fragments would have been taken apart from their parent *asteroid* for Myr, according to their CREAs (Llorca et al., 2005) which leads to different impact processing, *space weathering* alteration for the parent *asteroid* and the *meteorite* (Chapman, 2004).

In this thesis we will use spectroscopy to establish connections between *CV-CK chondrites* and C-type *asteroids*, which show similar *albedos*, flat reflectance type spectra, and common absorption features. *LL chondrites*, the least common OCs are representative of over 70% of the population of S and Q-type *NEAs*, according to their spectral features and mineralogy (Vernazza et al., 2008). Samples recovered from both the *asteroid* Itokawa and the Chelyabinsk *fall* are also *LL chondrites* (Nakamura et al., 2011; Galimov, 2013; Tanbakouei et al., 2019b). OCs are correlated with S and

Q-type *asteroids*, CCs are related to C-type *asteroids* (although K and X-type *asteroids* also could be associated to some CC groups), and ECs are correlated with X-type *asteroids* (Burbine et al., 2002; DeMeo et al., 2009).

C-type *asteroids* are more abundant than S or Q-type *asteroids* in the main asteroid belt (Zellner, 1979). C-type are mostly located in the outer regions of the MB, while S-type are in the inner MB (Dunn et al., 2013). As *asteroids* of CC composition are more fragile than those similar to OCs (Trigo-Rodriguez and Blum, 2009; Popova et al., 2011), they have less opportunity to survive impacts during their travel in space and the entrance through Earth's atmosphere.

S-type *asteroids* like Itokawa, is one of the most common spectral types among Main Belt Asteroids and *NEOs*. The spectrum is similar to the ordinary *chondrite* spectrum but significantly redder with weaker bands. Spectral differences between some of the *ordinary chondrites*, and S-type, reveals that *space weathering*, had happened and affected the surfaces of *asteroids* and altered their spectra (Thomas and Binzel, 2010).

To obtain a more precise knowledge on the surface mineralogy and composition of these minor bodies, two successful sample return missions to *asteroids* or *comets* have been achieved: the Stardust mission, brought to Earth dust from the tail of the comet 81P/Wild 2 in 2006 (Brownlee et al., 2006), and the Hayabusa mission, brought back samples from the *asteroid* 25143 Itokawa (Nakamura et al., 2011) in 2010. Other ongoing missions are NASA OSIRIS-REx and Hayabusa 2 missions. The thesis is focused in comparing *asteroid* spectra with chondritic *meteorites*. Comparing is not easy because the secondary processes occurring in space, like e.g. Impact collisions that modify the spectral reflectance of materials (Chapman and Salisbury, 1973).

1.5 Outline of the thesis

In this thesis we emphasize the relevance of studying the physico-chemical properties of chondrites as the building blocks of *asteroids* and rocky planets. We deal with the mechanical and reflective properties of chondritic *meteorites*, and returned samples. Different samples have been analyzed and studied to better understand the processes that took place in their parent *asteroids*.

To gain insight in the study of chondritic *meteorites* different instruments and techniques were used. Experimental techniques and specific instruments used in this thesis are explained in `chapter 2`.

In `chapter 3`, *CK* and *CV chondrites* are compared with the reflectance spectra of C-type *asteroids* from the ultraviolet to near-infrared range. It provides a possible connection between *chondrite* groups and this type of *asteroids*.

In `chapter 3` section 2, nanoindentation technique is described, which provide insight in the mechanical properties of regolith grains of Itokawa *asteroid* brought to earth by Hayabusa sample-return mission. This technique allows to infer the mechanical and physical properties of the samples in a non-destructive way, allowing the study of fragile samples without damaging them (Moyano-Cambero et al., 2017a; Tanbakouei et al., 2019b). This study provides a method for accurate measurement of the mechanical response of regolith grains on the surface of chondritic *asteroids*.

In the third section of this chapter, the spectral behavior of 2P/Encke are compared with laboratory spectra of *carbonaceous chondrites*. Two anomalous *carbonaceous chondrites*, the Meteorite Hills 01017 and Grosvenor Mountains 95551 could be good proxies for the dark materials forming this short-period *comet*. These two

meteorites could be rare surviving samples, either from the *Taurid complex* or other compositionally similar body.

The last section of `chapter 3` addresses the astrometry and photometric measurement of *comet* 2I/Borisov. Joan Oró robotic telescope and two small-size instruments have been used. This faint *comet* exhibits very uniform behavior in its magnitude changes over several nights.

Finally `chapter 4` discusses the results and emphasize the main conclusions obtained in this PhD work. Considering the asteroid-meteorite connection described in `chapter 3`, a general overview has obtained on how space collisions, *thermal metamorphism*, and *space weathering* affect *meteorite samples*, and how we should consider them to study the the compositional properties of *asteroids* and *comets*.

Chapter 2

Analytical instrumentation, and observational methods

This thesis focuses in the study of *asteroids* and *comets* using two approaches: laboratory studies, and remote telescopic observations. To perform the study of the materials forming these undifferentiated bodies we will perform laboratory studies of *meteorites* and returned samples, by space missions (Tanbakouei et al., 2019b). In addition, we have followed *asteroids* and *comets* using a medium-size telescope to exemplify the main techniques in which we can follow and track these objects. In section 2.1 the laboratory study of *meteorites* is described. These free-delivered rocks can be considered a good proxy of the rocky materials forming *asteroids* and *comets* (McSween and McSween, 1999; Trigo-Rodríguez, 2015; Tanbakouei et al., 2019b). In our studies of *meteorites*, we usually focus on the particular physical and mineralogical properties of the samples and the effect that some physical processes make on them. To quantify these effects (see e.g. Trigo-Rodríguez et al. (2017)), we use different analytical techniques. Thanks to the analytical results on the physico-chemical properties of *meteorites* we can get answers to a wide range of questions about the origin and evolution of their parent *asteroids* and *comets*. Then, to achieve the goals of this thesis, we have used diverse instrumental techniques described in this chapter.

In section 2.2 a follow-up of *comet* 2I/Borisov was programmed to exemplify the photometric technique using the 0.8 m in diameter Joan Oró Telescope was performed (see e.g. Trigo-Rodríguez et al. (2017)). This section describes the instrumentation and techniques used to pursue that monitoring. Then a brief summary of astrometric description and observational techniques are presented. Consequently, a brief summary of astrometric and photometric observational techniques is presented.

2.1 Laboratory work on meteorites

In order to get the proper characterization of the *meteorites* from different points of view - mechanical properties, mineralogy, spectral features- and to make a first connection between *meteorites* and their possible parent bodies, several techniques were combined. In this part I mostly focused on the techniques used to study the spectroscopic characteristics of the *find/fall meteorite* and returned samples (Tab. 2.1).

2.1.1 Scanning electron microscopy (SEM/EDX)

To study the mineralogical composition and the structure of samples, two Scanning Electron Microscopes (SEMs) were used: a FEI Quanta 650 FEG with a Back Scattered Electron Detector (BSED), at the Catalan Institute of Nanoscience and Nanotechnology (ICN2) and a Zeiss Merlin field emission (FE) SEM at the Autonomous

TABLE 2.1: All chondrites studied in the thesis

Meteorite	Group	Weight (g)
MET 01017	CV3-an	238.00
GRO 9551	C-ung	213.389
PCA 82500	CK3	O90.9
LAR 04318	CK4	53.5
ALH 85002	CK4	438
LAR 12265	CK5	14.3
MET 00430	CV3	151.7
MET 01074	CV3	46.2
Allende	CV3	20000
MIL 07002	CV3	758
ALH 84028	CV3	736
NWA 6013	Diogenite- olivine	357

University of Barcelona (UAB). In this type of microscopes, the electron beam passes across a sample's surface and some images are produced by scanning the surface of the sample. When the electrons strike the sample, a variety of signals are generated, and it is the detection of specific signals which produces an image or a sample's elemental composition. The three signals which provide the greatest amount of information in SEM are the secondary electrons (SE), back scattered electrons (BSE), and X-rays.

Secondary electrons are emitted from the atoms occupying the top surface and produce a readily interpretable image of the surface. The contrast in the image is determined by the sample morphology. A high resolution image can be obtained because of the small diameter of the primary electron beam. Back scattered electrons (BSE) are primary beam electrons which are reflected from atoms in the solid. The contrast in the image produced is determined by the atomic number of the elements in the sample. The image will therefore reflect the distribution of different chemical phases in the sample. Because these electrons are emitted from depth in the sample, the resolution in the image is not as good as for secondary electrons.

Interaction of the primary beam with atoms in the sample causes shell transitions which result in the emission of an X-ray. The emitted X-ray has an energy characteristic of the parent element. Detection and measurement of the energy permits elemental analysis (Energy Dispersive X-ray Spectroscopy or EDS). The EDS techniques can provide rapid qualitative, or with adequate standards, semi-quantitative analysis of elemental composition with a sampling depth of 1-2 microns. X-rays may also be used to form maps or line profiles, showing the elemental distribution in a sample surface.

SEM/EDS allows identification and characterization of mineral phases in chondrules and in *matrix*. It also enables determination of micro structures in chondrules and chemical composition of micro fracture-fill components. SEM/EDS is frequently a method of choice in *meteorite* studies worldwide. Using SEM/EDS, chemical compositions of *olivine, pyroxene, plagioclase* and metal phases were determined, which were consistent with the L-group, equilibrated ordinary *chondrite*. The IEEC-CSIC group often uses SEM+EDX techniques plus microprobe analysis for accurate quantitative analysis of the bulk mineral composition in order to characterize new *meteorites* (see e.g. Trigo-Rodriguez et al. (2014). By using the EDS technique, a big diversity in chemical and mineralogical compositions at micrometer scale is noticeable. The SEM investigations showed great variations in the chemical composition of the *meteorite* at small distances from grain to grain.

2.1.2 Raman spectroscopy

Generally, spectroscopy is measuring the reflectance of the incoming light from a source when the light is dispersed according to its wavelength. Specific inclines and slopes in the spectrum infer to absorbing light at that wavelength due to a particular material. Analyzing these absorption features provide essential information about the composition on the surfaces of these bodies (DeMeo, 2010a).

Micro-Raman spectra with a spot size of approximately 1 μm and laser power below 0.6 mW cm^{-2} were obtained by a Jobin-Yvon T-64000 Raman spectrometer at the Institute of Material Sciences of Barcelona (ICMAB-CSIC) in order to identify mineral phases. The crystalline structure of the minerals is often affected by the collisional history of each sample, so this Raman technique allow us to infer the degree of shock experienced by the rock-forming minerals and the structural information of different phases. The latter is because the Raman spectra is characteristic of the crystalline structure of each mineral.

In general, backscatter measurements were carried out at room temperature using the 5145 Åline of an Argon-ion laser with a Jobin-Yvon T-64000 Raman spectrometer attached to an Olympus microscope (Fig. 2.1), which is equipped with a liquid nitrogen–cooled CCD detector. The Raman spectrometer operated between 100 and 1400 cm^{-1} allow us to acquire high-resolution spectra, with a step of about 1 cm^{-1}. To calibrate our Raman spectrometer, we used the sharp peak of stress-free Si that is measured at 520.3 cm^{-1} (Kim et al., 2014). The instrument was used to better characterize mineralogy, composition and possibly also to detect shock features (Moyano-Cambero et al., 2017a). The software Crystal Sleuth was used to infer the exact location of the peak associated with each mineral. The Origin software also have been used to remove the base slope of Raman spectra and substrate the baseline of the spectra of three Itokawa samples and NWA 6013 achondrite.

FIGURE 2.1: Jobin-Yvon T-64000 Raman spectrometer at ICMAB-CSIC.

2.1.3 UV-VIS-NIR spectroscopy

Another key part of the research consisted in obtaining reflectance spectra of *meteorites*. To do so a Shimadzu UV3600 ultraviolet-visible-near infrared (UV-Vis-NIR) spectrometer was used. We obtained the reflectance spectra of thick and thin *meteorite* sections in the 300 to 1800 nm range following previous work of the team (Moyano-Cambero, Trigo-Rodríguez, and Llorca, 2013; Trigo-Rodriguez et al., 2014)

at the Polytechnic University of Catalonia (UPC). The standard setting for the spectrometer is an integrating sphere (ISR) with a working range of 180-2600 nm, although the signal becomes noisy beyond about 2000 nm.

In order to cover a wide range of wavelengths, the spectrometer uses multiple lamps, detectors and diffraction gratings that produce some artefacts that are avoided in the spectra presented here. We used thin ($\sim$30 μm) and thick ($\sim$1 mm) *meteorite* sections to obtain the reflectance spectra. All our samples had a larger area than the spectrometer beam to avoid signal reflections by other materials, following Trigo-Rodríguez (2015) procedure. Moyano-Cambero et al. (2016) explained that the incident light is not transmitted through the section. There are also several peaks of instrumental origin around 1450 nm and 2000 nm approximately. We applied some corrections to avoid the unreliable data. The spectra presented in this thesis covers the 400 to 1800 nm spectral range and allows comparison with asteroidal spectra taken from ground or space-based telescopes.

The spectrometer diffraction illumination originates from one of two lamps and passes through a variable slit, then is filtered with a grating to select the desired wavelength and afterwards is split into two alternating but identical beams with a chopper. Next the beam interacts with the sample and is routed to the detector. The reference beam interacts with the material and then goes to the same detector. The interior of the ISR is coated with a duraflect reflecting polymer. The spectra obtained via this specific spectrometer, always shows noise between 800 and 900 nm plus two instrumental peaks (one from 1400 to 1600 nm and the other from 1900 to 2200 nm) (Moyano-Cambero et al., 2016). Above 2000 nm, the spectra become noisy and loses uniformity, due to being obtained under laboratory conditions, so the signal is affected by atmospheric components.

To avoid displaying unreliable data, we cut the spectra above the 1800 nm. The peaks at 1400-1600 nm and at 1900-2200 nm are attributed to an unsuccessful instrumental correction applied by the software to remove the presence of the $BaSO_4$ substrate of the final spectra. A new correction had been applied to the spectra to remove those peaks, but the final result in those regions became a bit noisier than desired. The region between 800 and 900 nm was deleted, as it does not include usable data and was too noisy to be reliable (Fig. 2.2).

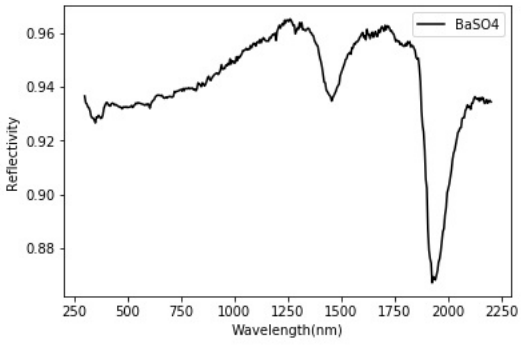

FIGURE 2.2: Barium sulphate ($BaSO_4$) standard baseline, used in the correction applied to calibrate the detector (Moyano-Cambero et al., 2016)

2.1.4 Nanoindentation

We applied nanoindentation to *asteroid* 25143 Itokawa regolith particles collected by Hayabusa mission of the Japanese Space Agency (JAXA). The mechanical properties of those samples, which were prepared by JAXA embedded in resin and polished using diamond paste, were evaluated by nanoindentation. It has been the first time that this technique was used to infer the mechanical properties of materials brought to Earth from a sample-return space mission (Fig. 2.3) (Tanbakouei et al., 2019b).

In this technique, an Ultra Micro Indentation System (UMIS) from Fischer-Cripps Laboratories was used at Autonomous University of Barcelona (UAB). The team used the same instrument to perform the first known study of the mechanical properties of a *meteorite*, precisely of Chelyabinsk ordinary *chondrite* (see e.g. Moyano-Cambero et al. (2017a)). During nanoindentation a controlled load is applied to some parts of a sample through the use of a diamond indenter. The indenter pushes the surface while the load increases to a specified maximum. After loading, the force is progressively brought back to zero and the sample surface retracts because of elasticity. The penetration depth is acquired during the whole load-unload cycle. Final data reduction depends on the interpretation of the extracted load-depth curves. These graphs provide information concerning the deformation mechanisms (elastic and plastic) and about the *elastic recovery* (Tanbakouei et al., 2019b). The mechanical properties such as hardness and the reduced *Young's modulus*, were evaluated by the method developed by Oliver and Pharr (1992) for general solid materials. Some proper corrections such as initial penetration depth and instrument compliance are applied to the contact area (Fischer-Cripps, 2004).

The two mechanical properties measured by using load and depth indentation techniques are the elastic modulus, E and the hardness, H. In a commonly used method, data are obtained from one complete cycle of loading and unloading. Methods for independently estimating the contact area from the indenter shape function are then used to provide separate measurements of E and H (Oliver and Pharr, 1992).

According to Fischer-Cripps (2004), the validity of the results for hardness and modulus depends largely upon the analysis procedure used to process the raw data which are concerned with the extraction of modulus and hardness, also with correcting the raw data for various systematic errors that have been identified for this type of testing. The forces involved are usually in the millinewton (10^{-3} N) range and are measured with a resolution of a few nanonewtons (10^{-9} N). The depths of penetration are on the order of microns with a resolution of less than a nanometre (10^{-9} m) (Fischer-Cripps, 2004).

2.2 Observational follow-up of minor bodies

To get valuable and important information about the remote behavior of small bodies, we have scheduled observations using our TJO telescope at Montsec Astronomical Observatory (OAdM:). In this chapter I mention a summary about the techniques used, particularly photometry, describe the telescope used to get data of the 2I/Borisov comet, and explain the data reduction processes (DeMeo, 2010a).

2.2.1 Photometry/Astrometry of asteroid and comets

Photometry is an observational technique that measures the flux of incoming light from an object, here the small bodies of the solar system and comets. The total flux of light is measured in a specific band-filter and converted into a magnitude. The

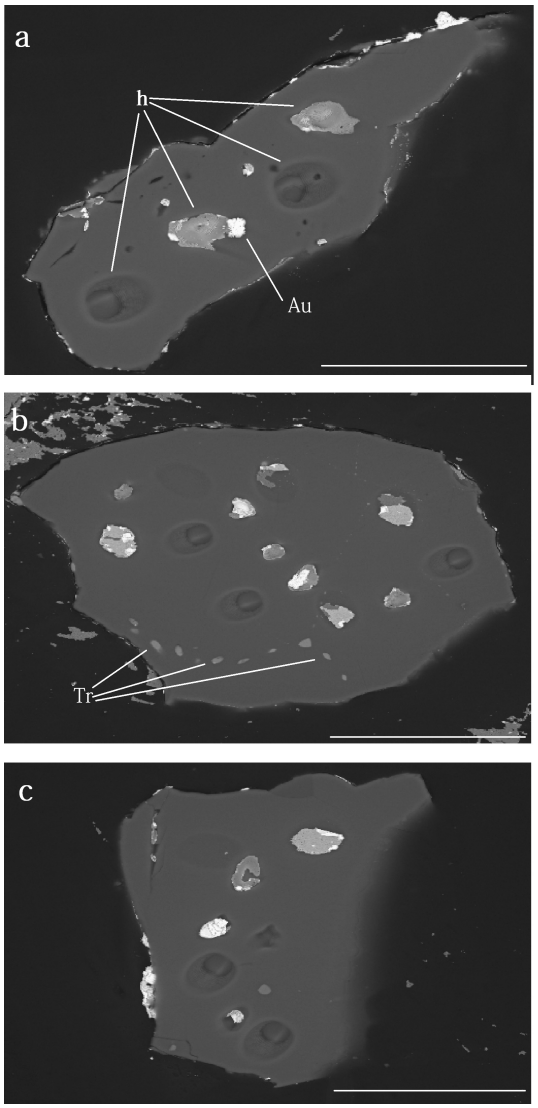

FIGURE 2.3: BSE images of the three Itokawa grains. (a) RA-QD02-0014, (b) RA-QD02-0023, and (c) RA-QD02-0047. The white scale bars are 50, 70, and 60 μm respectively. Labeled in panel an are several holes (h) and Au patches from previous analyses. A chain of troilite (tr) grains is also labeled in panel b.

frequency of the magnitude with time – which is due to the unshaped physical status of an object or heterogeneity on the surface - is calculated to define the rotation rate of a comet (DeMeo, 2010a).

2.2.2 Telescopes and Instruments

The Joan Oró telescope (TJO) is a Ritchey-Chrètien telescope with a 0.8 m primary mirror and an effective focal ratio of f/9.6, with open fork equatorial mount. The automatic station of the Meteorological Service of Catalonia (SMC) and the environmental quality measurement station of the XVPCA network (IDAEA), and several antennas for low orbit satellites' communications installed and managed by the Universitat Politècnica de Catalunya and IEEC. TJO is at the Montsec Astronomical Observatory (OAdM), at a height over the sea level of 1.570 meters, and located in

one of the most suitable areas on the European continent for astronomical observation, due to the combination of weather conditions and low level of light pollution. The pointing precision of TJO is of 20″ and, even though it has not an auto guiding system, a pointing mesh allows making exposure times between 300 and 600 s with good tracking precision. The polished quality of the primary mirror is better than lambda/16 in 633 nm. The instrumentation is installed in the Cassegrain focus. The telescope control system is based on a suite of applications and subsystems that guarantees the reliability and robustness of the operation, while optimizing the scientific return of this facility.

2.2.3 Basic Photometry Reduction

The magnitude of the observed object is obtained by direct comparison with the flux of standard stars that are in the observed stellar fields. This is possible because the CCD sensor collects the focused telescope image in pixels, so the electronic image is proportional to the photons arrived to the device. This is clearly emphasizing that semiprofessional observatories have something to say in front of the more systematic searchers made nowadays by professional automatic surveys. Then, this triumph of small-telescope astronomy in the field of solar system minor bodies suggest that there is room for amateur research, not only in the systematic follow-up of interesting objects that experience unexpected photometric changes (Trigo-Rodríguez et al., 2008; Trigo-Rodríguez et al., 2010).

From Catalonia we observed comet 2I/Borisov using Telescopi Joan Oró (TJO), a 1 m-class telescope working in a completely unattended manner. It operates in the Observatori Astronòmic del Montsec (OAdM: www.oadm.cat), a site devoted to host astronomical research facilities under dark skies. In fact, the TJO is the largest telescope in Catalonia and named after the famous Catalan biochemist and pioneer of astrobiology who promoted the construction of this facility. There is an obvious interest in increasing our understanding of the real nature of interstellar *comets* (Trigo-Rodríguez et al., 2010). In this study we compile the photometric measurements made from Catalonia and Crimea in order to exemplify the relevance of a systematic photometric study of interstellar visitors using meter-class instruments. To study the photometric behavior of 2I/Borisov we have used the 0.8 m in diameter Joan Oró robotic telescope, and other small-size instruments compiled in Table 2.2. TJO CCD detector is an iKon XL camera, with a back-illuminated 4k $\times$ 4k chip manufactured by Andor. This CCD camera provides a FoV of about 27.5 $\times$ 27.5 arcmin, with a resolution of 0.4 arcsec given the pixel size of 15 μm. The 0.65 m telescope used a FLI ML16803 camera in the Johnson V, R and I filters.

Given the faintness of this *comet*, we decided to made unfiltered CCD imaging, and the photometry was made using LAIA (Laboratory for Astronomical Image Analysis) and Astrometrica software successfully tested for obtaining high-precision stellar photometry (Juan-Samsó et al., 2005). The data reduction process basically consists of bias subtraction, flat-field correction and flux calibration. We have used similar reduction procedures than in the previous papers (Trigo-Rodríguez et al., 2010), but this time the photometry was measured for a circular aperture of about 20 arcmin centered in the comet false nucleus (Stetson, 2000). Using these standards, we were able to quantify the typical data accuracy to be better than 0.1 mag (for further details see Trigo-Rodríguez et al. (2010)).

The reduction process of the observational data consists in receiving the flux as a function of wavelength from the CCD images, and the basic process for photometry (Howell, 2006) are introduced here (McLean, 2008; Popescu, 2012).

TABLE 2.2: Observatories and instruments used in this study.

Observatory	MPC code	Telescope
MARGO Astron. Obs., Ukr.	051	SC 65 f/10
TJO, Montsec (OAdM), Cat	C65	RC 80 f/9.6
Montseny, Cat	B06	SC 25 f/10

Optical photometry in the Johnson V, R and I filters was obtained with the Joan Oró telescope (TJO) equipped with the Andor CCD camera (see, for example, [1] for more details). The Johnson VRI magnitudes were derived using standard aperture photometry tasks in Astrometrica and an additional software called LAIA (Laboratory for Astronomical Image Analysis), successfully tested for obtaining high-precision stellar photometry (Garcia-Melendo and Clement, 1997). The data reduction process basically consists of bias subtraction, flat-field correction and flux calibration. The photometric accuracy given for a standard aperture of 10 arcsec was sometimes improved using Landolt and Stetson calibration fields (Landolt, 1992; Stetson, 2000). Using these standards, we were able to quantify the typical data accuracy to be better than 0.05 mag in the different VRI bands (for further details see Trigo-Rodríguez et al. (2010)).

[1] http://www.ieec.cat/en/content/227/laia

Chapter 3

Results and discussion

3.1 Characterization of asteroids using reflectance spectroscopy

The light reflected from an *asteroid* depends on the rock-forming minerals of the body, but also of the size and roughness of the regolith that often covers their surfaces. Each specific mineral exhibits a characteristic reflectance spectrum with distinctive spectral features (Gaffey and McCord, 1978). Reflectance spectroscopy is a technique that can provide insight about the mineralogy of *asteroids* with the added value to be used remotely.

The materials forming an *asteroid* surface, contain minerals with their own reflectance response to solar light. The spectral parameters such as band positions and peaks are characteristic of the specific composition of the exclusive mineral forming the body. Remote spectroscopy provides a blended spectrum with features characteristic of the mineralogy of the entire body. Despite the different scale, the mineral spectra of *meteorites* have distinctive features in the UV-NIR range that can be compared with those found in *asteroid* spectra.

Generally, the most common UV to Near-Infrared range involves a spectral interval from about 400 to 2500 nm. The study of the features in such interval allows to characterize the minerals forming an asteroidal, or planetary surface. Chondritic *asteroids* are dominated by silicates, so several absorption bands located between 1000 and 2000 nm are associated with *olivine* and *pyroxene* forming their surfaces.

TABLE 3.1: Main minerals found in chondrites

Mineral name	Mineral composition	Possible Occurrence
kamacite	α-(Fe,Ni); $Fe^{0+}_{0.9}Ni_{0.1}$	In iron, stony-iron and most chondrites
Taenite	γ-(Ni,Fe)	In iron, stony-iron and most chondrites
Troilite	FeS	Present in most meteorites
Chromite	$FeCrO_4$	In most meteorites
Magnetite	Fe_3O_4	In most CCs
Graphite	C	Common is irons and some stones
Orthopyroxene	$(Mg,Fe)SiO_3$	Common in stones and stony-irons
Clinopyroxene	$(Ca,Mg,Fe)SiO_3$	Common in stones and stony-irons
Enstatite	$Mg_2Si_2O_6$	Mostly in E-chondrites
Olivine	$(Mg,Fe)_2SiO_4$	Common in stones and stony-irons
Plagioclase	$(Na,Ca)(Si,Al)_4O_8$	Common in stones and stony-irons
Phylosilicate	$(Na,Ca)(Al,Mg_6(Si_4O_{10})_3OH_6\text{-}nH_2O)$	Common in most CCs

In general terms, the wavelengths at which the features are located in the spectrum depends on the mineral structure and ionic (Fe^{2+}, Fe^{3+}, etc.) or molecular (H_2O, OH, CO_3) species involved (Gaffey, Burbine, and Binzel, 1993; Popescu, 2012). Most *asteroids* are composed by a mixture of the abundant mineral composing the *meteorites: olivine, pyroxene*, Iron-Nickel alloy, spinel and *feldspar*. The abundance of

one particular species establish the presence of the feature, so the high quality spectra of simple mineral mixtures, the average composition and relative abundances can be also determined. The relative abundances of *olivine-orthopyroxene* mixtures are determined by a method which had developed by Cloutis et al. (1986) (Popescu, 2012).

3.1.1 Distinctive asteroid classes from the Bus-DeMeo Taxonomy

Significant progress in the characterization of *asteroids* was achieved when reflectance spectra indicated that they exhibit different compositions and the diverse rock-forming mineralogy is produced (Gaffey, Burbine, and Binzel, 1993). The first taxonomy classification system was based on *asteroid* broad band filter colors; two separate types of objects denoted as S and C (Wood and Kuiper, 1963; Chapman, Johnson, and McCord, 1971). With time the number of *asteroids* with reflectance spectra increased, and so did the number of asteroidal classes, distinguishable by specific features representing the surface composition, age and alteration based on much higher resolution spectra obtained by more modern digital spectrographs. That progress allowed the new system developed a new taxonomic system (DeMeo, 2010b). Other specific taxonomic systems are used to specify mineralogy for each of the defined classes (see e.g. Popescu (2012)).

In fact, the evolution of *asteroid* taxonomies has grown in parallel with *asteroid* discoveries. First, Gaffey, Burbine, and Binzel (1993) created a S-complex taxonomy of *olivine* and pyroxene-rich *asteroids* based on near infrared data. This taxonomy was followed by the Tholen (1984) based on the Eight-Color Asteroid Survey data (ECAS, Zellner, Tholen, and Tedesco (1985)), the SMASSII spectral survey taxonomy (Bus, 1999; Bus and Binzel, 2002) and the Bus-DeMeo taxonomy (DeMeo et al., 2009).

The Bus-Demeo taxonomy is an extension of a previous taxonomy scheme into the near-infrared and was created using Principal Component Analysis which contain 24 classes compared to 26 in the Bus system, three Bus classes eliminated (Sl, Sk, Ld) and one (Sv) created (see Fig. 3.1). The objects in the S-complex had widely varying spectral slopes. To distinct the objects with higher slope, W notation is added which means that the objects has similar spectral features but higher spectral slope. To relabel these objects, instead the S, Sq, Sr, and Sv, they receive a notation of w added to their name which is commonly represents an increase in slope arising from *space weathering* (Clark et al., 2002). The taxonomy classes are defined by covering the data in the wavelength range 450 to 2045 nm as compared with 340 to 1040 nm for Tholen (1984) and 435 to 925 nm for Bus (1999) (Burbine and Binzel, 2002; DeMeo et al., 2009).

3.1.2 Connection of carbonaceous chondrites with a C class asteroid

One primary goal of this PhD has been to identify *carbonaceous chondrite* groups with specific *asteroid* classes. *Space weathering* processes change the reflectance properties of *asteroid* surfaces, so establish a clear link between dark asteroids and the CCs arrived to our *meteorite* collections is a big challenge. So far most *chondrite* groups are not clearly associated, and currently ongoing sample-return missions try to establish candidates (Trigo-Rodriguez et al., 2014; Watanabe et al., 2019).

An example of *carbonaceous chondrite* clan is the affinitude found between the CV and CK groups (see section 3.1.4), probably associated to each other. In order to gain insight on this we have compared our mean reflectance spectra with the Cg asteroidal reflectance class of the Bus-DeMeo Taxonomy Classification (DeMeo et al.,

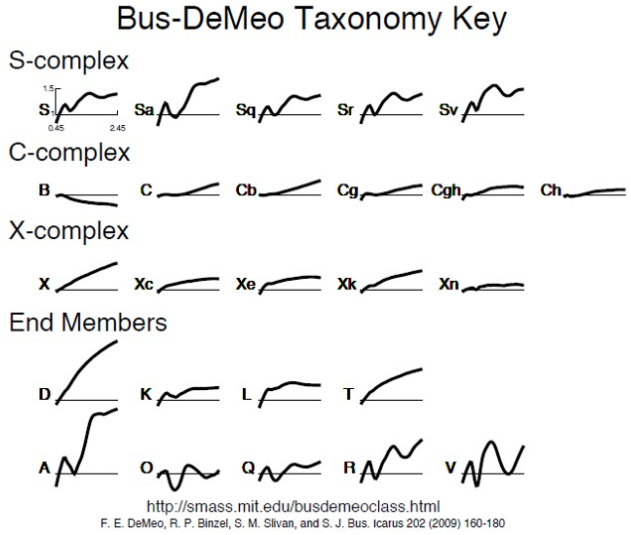

FIGURE 3.1: Asteroids Taxonomy (DeMeo et al., 2009). The characteristic spectral shapes go from X to Y nm.

2009). We have used a Cg class averaged spectrum for comparison with the spectra of *CK chondrites* in the range of 400-1800 nm (Fig. 3.2).

The progressive collisional sequence of *CV-CKs* produces shock darkening similar to what was found in Chelyabinsk (Moyano-Cambero et al., 2017b). One of the main interests of the Hayabusa 2 mission, which will return samples from the rare Cg-type *asteroid* 162173 Ryugu, is the effect of secondary minerals on impact darkening in *carbonaceous chondrites*. Some of these secondary minor minerals were probably formed due to impact-induced *metamorphism* plus aqueous alteration. The smoothed spectrum of Ryugu suggests two broad absorption bands near 1000 and 2200 nm, which are consistent with *CV chondrites* (Cloutis et al., 2012; Trigo-Rodriguez et al., 2014). *CV chondrites* have reflectance from 50 to 180 at 560 nm, while Ryugu has a value of 48 at the corresponding point (Trigo-Rodriguez et al., 2014). As Loeffler, Dukes, and Baragiola (2009) suggested, darkening and reddening of CCs and their associated *mafic* silicates are possibly due to *space weathering* (Gillis-Davis et al., 2017).

Moreover, the recent simulated *space weathering* experiments on CV3 *meteorite* Allende by Gillis-Davis et al. (2017) showed that the weathered *meteorite* shows a different weathering trend for the continuum slope between 450-550 nm. Although the absorption bands in the 900-1400 nm region spectrum of Ryugu are not well-defined, this implies some constraints on possible *meteorite* analogues. The absorption bands in the range of 1050 to 1250 nm in ureilites corresponds to *olivine*, so we infer that the same bands in *CVs* and *CKs* are also associated with *olivine* (Cloutis et al., 2010; Cloutis et al., 2012; Trigo-Rodriguez et al., 2014). Our results show that Cg spectral type *asteroids* could match the spectra of *CK chondrites* according to what was found between 500 and 800 nm (Fig. 3.2). In general, several specific features in an *asteroid* reflectance spectrum display the effect of aqueous alteration in the *asteroid* surface (Barucci et al., 2005). As we combined our spectra with the Bus-DeMeo Taxonomy Classification tool, it is realized that the overall shape of most *CK* spectra seems to be similar to Cg-type *asteroids* (DeMeo et al., 2009).

Previously to our results, Mothé-Diniz et al. (2008) compared the reflectance

spectra of 221 Eos family members with the spectra of different CC group specimens. They realized that many members of that *asteroid* family are consistent with CK3, CK4 and CK5 *chondrites* in the NIR region, but differ in the visible region (Salisbury, Hunt, and Lenhoff, 1975). In fact, *asteroid* 221 Eos and its family members are classified as K *asteroids* in the Bus-DeMeo taxonomy (DeMeo et al., 2009).

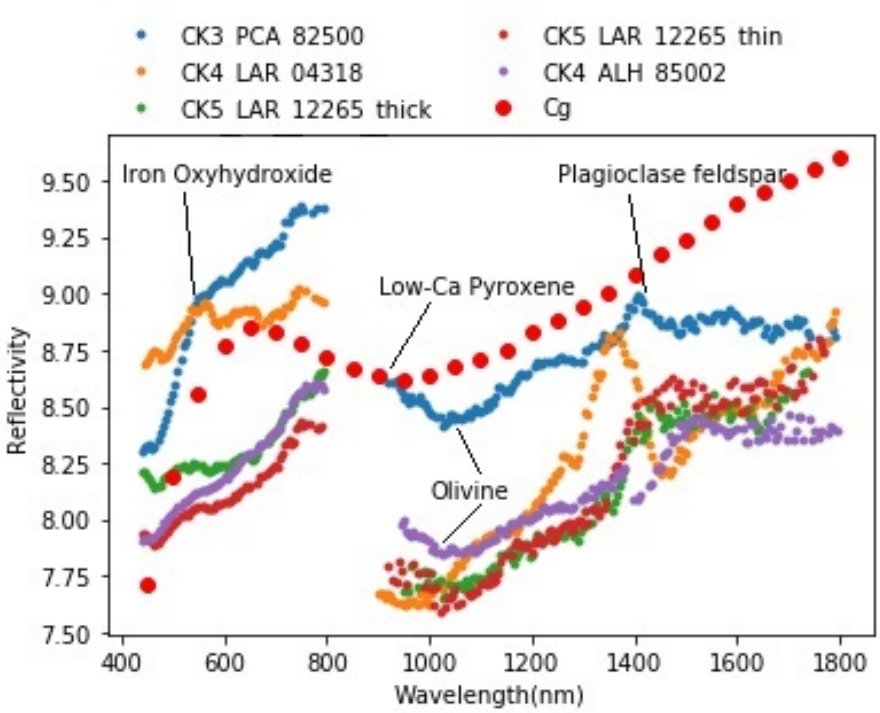

FIGURE 3.2: CK reflectance spectra compared with reflectivity of Cg-type asteroids in the UV-NIR range.

3.1.3 Reflectance spectra of CV-CK carbonaceous chondrites

The discovery of a significant number of new *CKs* in Antarctica has increased the availability of *CK chondrites*. Some of these new *CKs* exhibit low levels of terrestrial weathering, making them good candidates for spectroscopic comparison with other CCs and to some extent with *asteroids*. The reflectance spectra of five *CK chondrites* obtained in this work are shown in Figure 3.3. We used the average data among CK spectral reflectance and made the $BaSO_4$ correction above. Pecora Escarpment 82500 (PCA 82500) and Larkman Nunatak 04318 (LAR 04318) are corrected two times to reduce noises (Moyano-Cambero et al., 2016).

The newly-obtained reflectance spectra of *CK* sections included in this study are shown in Figure 3.5. They have slightly red to blue spectral slopes beyond 900 nm (mostly red in the 900 to 1800 nm region and a bit blue slopped, above 1500 nm), exhibiting an olivine-like absorption band in the 1000-1200 nm region (Fig. 3.3). We have noticed in the *CK* spectra that the centre of the absorption bands does not change its position with the metamorphic grades, but correlates with the *olivine* composition. The depth of the bands, however, increases with higher degrees of *thermal metamorphism*, with the deepest band depth being found in CK6 spectra, while CK3–5 petrographic grades display shallower band depths in Figure 3.4 and Figure 3.5.

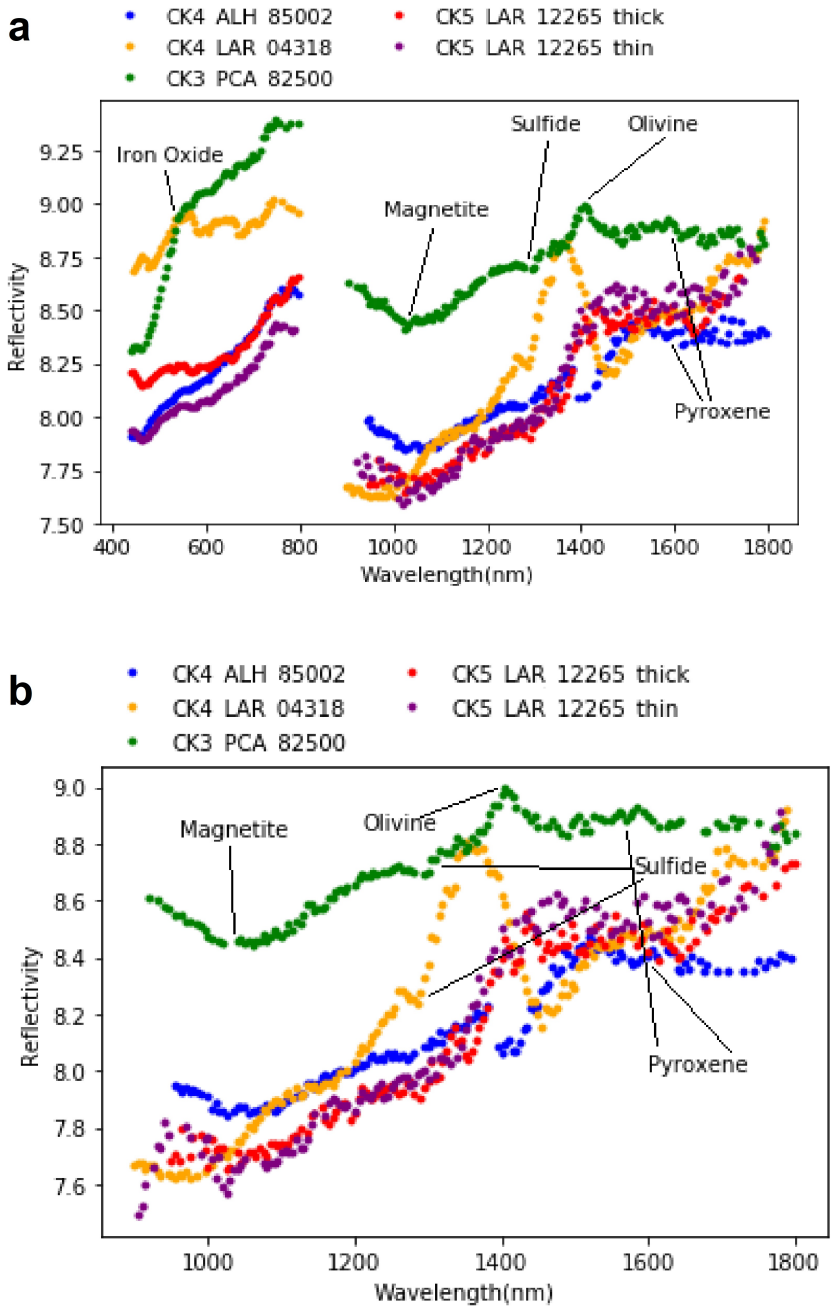

FIGURE 3.3: Reflectance spectra of CK chondrites. a) between 400 and 1800 nm, b) between 900 and 1800 nm. Features and absorption bands in b are easier to compare. Considering the $BaSO_4$ substrate spectrum, the peaks between 800 and 900 nm seem to be strongly related with it, so a correction applied to remove the substrate spectrum.

Several representative absorption bands are identified in *CK* and *CV* spectra. First, a narrow band at 600 nm, attributed to FeO and Fe_2O_3 contents (Hunt and Ashley, 1979) are described in several spectra (Lazzarin et al., 2004; Belskaya et al., 2010b). There is also a broader band around 650 nm, which is assigned to *plagioclase feldspar* (Geiger and Bischoff, 1995). Another commonly found band appears

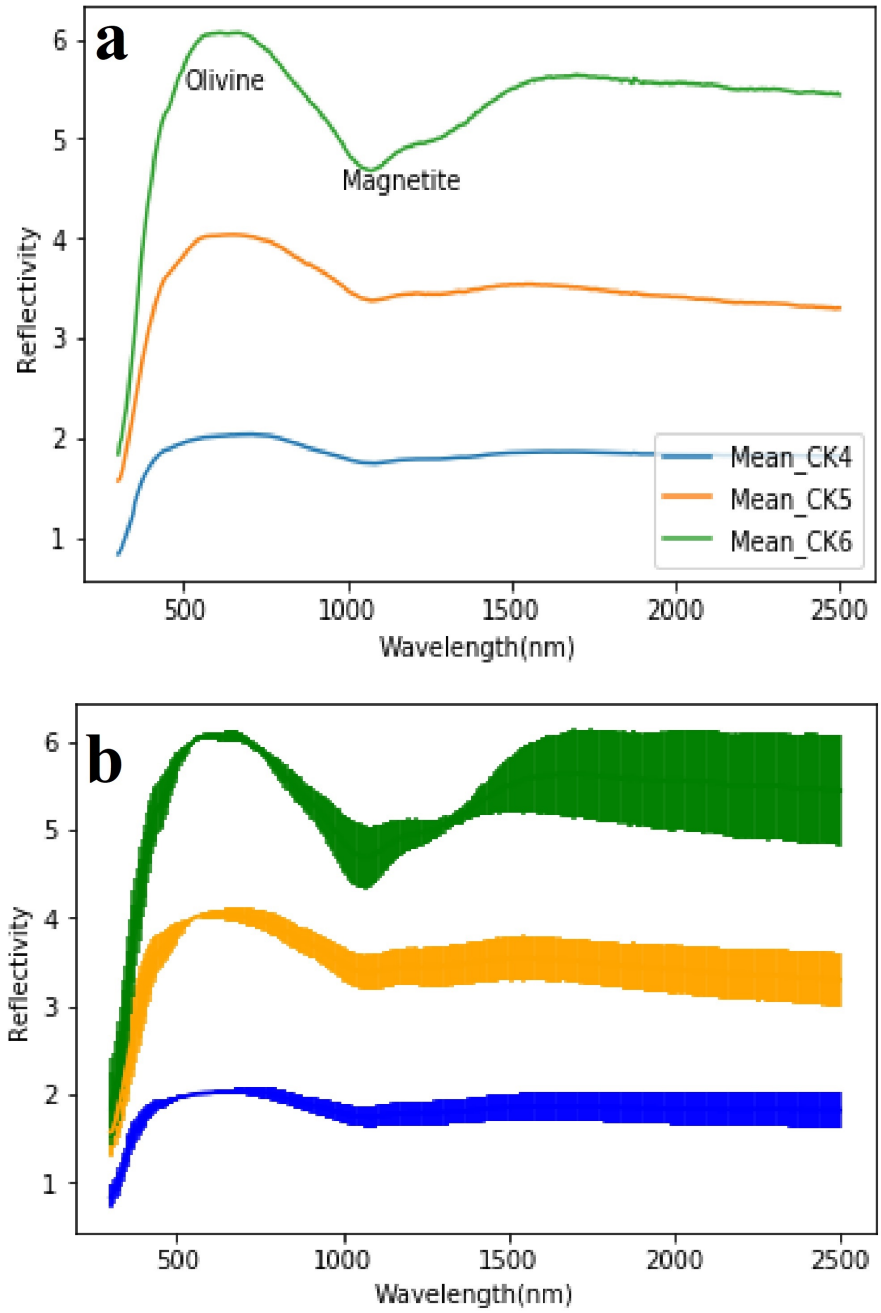

FIGURE 3.4: Comparison of CK reflectance spectra from meteorite powders studied in the RELAB spectral database in the range of 300 nm to 2500 nm range. a) Mean spectral reflectance of three different petrological types of CKs. b) Mean spectral reflectance of three different petrological type of CKs with error bars

between 900 to 1100 nm, being associated with *olivine* (Hunt and Ashley, 1979). The most common mineral in *CK chondrites* is indeed *olivine* (Cloutis et al., 2012). It exhibits an absorption feature centred near 1060 nm that can be seen in our spectra Figure 3.3. With increasing Fe^{2+} content, the centre of this absorption band moves to longer wavelengths, becomes deeper and darker by increasing the overall reflectance (see e.g. King and Ridley (1987)). In our data the olivine band extends between 950 and 1150 nm (see Fig. 3.3). *Plagioclase feldspar* is a minor silicate phase

in *CK chondrites* (<0.1 wt. %) that may exhibit a weak Fe absorption band near 1250 nm (Adams and Goullaud, 1978) which appears weakly represented in our spectra.

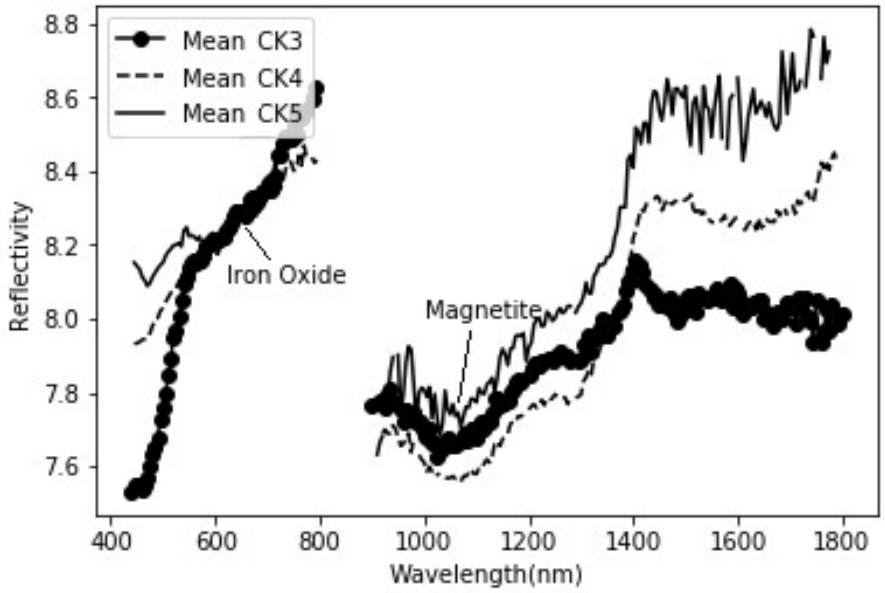

FIGURE 3.5: Comparison of reflectance spectra of two petrologic types of CK chondrites in our study (One CK3, two CK4 and two CK5 are mentioned in Table 3.3). $BaSO_4$ correction was applied to all.

The presence of *pyroxene* is noticeable as a 2000 nm absorption band in RELAB data, which varies from 1800 to 2080 nm when corresponding to low–Ca *pyroxenes*, to 1900-2380 nm for high–Ca *pyroxenes* (Cloutis et al., 2012). Due to the intrinsic noise introduced by using a spectrometer that is working in laboratory conditions, and not under vacuum. In consequence, we cannot properly characterize absorption bands like this of *pyroxene* at 2000 nm, but still the *CK* spectra shows a tail of this band near 1850 nm. The presence of *pyroxene* generally affects the *olivine* band positions, but this effect is less important in *CKs* than in other CCs (Cloutis et al., 1986). This is because *pyroxene* abundances in *CKs* are generally too low compared to *olivine* to appreciably affect *olivine* band positions (Cloutis et al., 2012).

Other relatively minor phases are also present in these spectra. Concerning the presence of *magnetite*, its spectral shape is known to be a function of grain size and location (Morris et al., 1985) but it commonly found as an absorption band near 1000 nm. In our *CK* spectra, the location of this absorption band varies from 980 to 1050 nm depending on the specimen analysed. We also noticed mineral oxides associated with *refractory* inclusions can be weakly featured as well, with fassaite, the most common mineral forming Ca- and Al- rich Inclusions (*CAIs*), being the best example at about 980 nm (Tab. 3.2).

3.1.4 CK and CV chondrites and the plausible connection between them

The *CK chondrite* group was defined by Kallemeyn, Rubin, and Wasson (1991) as having close compositional and textural relationship with the *CV chondrites*, but they are distinguishable from one another by their *refractory* lithophile abundances, *refractory* inclusions abundance, and the presence of igneous rims around *chondrules*, among other features. As previous author (Greenwood, Kearsley, and Franchi, 2003; Greenwood et al., 2004; Greenwood et al., 2010; Devouard et al., 2006) have suggested,

TABLE 3.2: Comparison between the main CK spectral bands in our UV-NIR spectra, Cloutis et al. (2012) and Brown University Keck/-NASA RELAB Spectrum PH-D2M-035/C1PH35 data.

Wavelengths (nm) (Ours)	Wavelengths (nm) (Cloutis et al., 2012)	Wavelengths (nm) (RELAB)	Minerals
600	650		Iron oxide (FeO)
900 - 1100	950	-	*Magnetite* (Fe_3O_4)
1950-2150	2000 – 2100		
600	600 - 700	700	*Olivine* ($(Mg,Fe)_2SiO_4$)
900 - 1100	1060	1050	
1270-1300	1250		
600 - 700	650	1350	*Plagioclase*
800 - 900	900		$((Na,Ca)(Si,Al)_4O_8)$
1250	1250		
980 - 1050	1100	1030	*Magnetite* (Fe_3O_4)
2050 - 2150	2100	-	Fassaite
			$(Ca,Na)(Mg,Fe,Al,Ti)(Si,Al)_2O_6$

there are some connections between *CV* and *CK chondrites*. *CKs* are also the most oxidized extraterrestrial rocks found so far, owing to their low abundance in Ni and Fe and their high content of *fayalite* and *magnetite* (Geiger and Bischoff, 1995). CV3-an Meteorite Hills 01017 (MET 01017) is possibly a reduced *chondrite* (Busemann, Alexander, and Nittler, 2007). CV3 MET 00430 and CV3 MET 01074 are highly oxidized Balilike type ($CV3_{OxB}$) (Brearley and Wagner, 2014; Jogo et al., 2018). CV3 Allende is an oxidized Allende-like type ($CV3_{OxA}$) (Bland et al., 2000). CV3 Miller Range 07002 (MIL 07002) is possibly oxidized and intermediate between CV_{OxA} and CV_{OxB} (Isa, Rubin, and Wasson, 2012). CV3 Allan Hills 84028 (ALH 84028) is also an oxidized Allende-like type (Bland et al., 2000) (Tab. 3.3).

TABLE 3.3: Petrologic types and meteorites from which reflectance spectra were obtained in this PhD section.

CK samples	**CV samples**
CK3 PCA 82500	CV3-an MET 01017
CK4 LAR 04318	CV3 MET 00430
CK4 ALH 85002	CV3 MET 01074
CK5 LAR 12265	CV3 Allende
	CV3 MIL 07002
	CV3 ALH 84028

The reflectance spectra of *CV chondrites*, with the exception of Allende, display a decreasing reflectance toward wavelengths short ward of 500 nm, which is the plausible result of the formation of iron *oxyhydroxides* due to terrestrial weathering. Significantly, the narrow absorption band in ALH 85002 and Allende, is due to its deep extinction below 400 nm and could be correlated with maghemite and *magnetite* (Tang et al., 2003). Figure 3.6 shows that fine-grained *CVs* have shallower *olivine* absorption bands. Particularly, the 1000 nm *olivine* absorption band is the main feature observed in *CK* and *CV* spectra, but it is deeper in *CKs* than in *CV chondrites*. In our reflectance spectra of *CK chondrites*, the *olivine* absorption feature at 1050 nm is dominant, indicating that it is a major rock-forming component. Another distinguishable bands are a low-Ca *pyroxene* band at 900 nm and a *plagioclase feldspar* band at 1250

nm. Although Cloutis et al. (2012) suggests that *CKs* do not have well-defined *olivine* absorption bands, due to not having experienced high enough temperatures to reduce the spectrum darkening effects of opaques or to recrystallize from preexisting *phyllosilicates*.

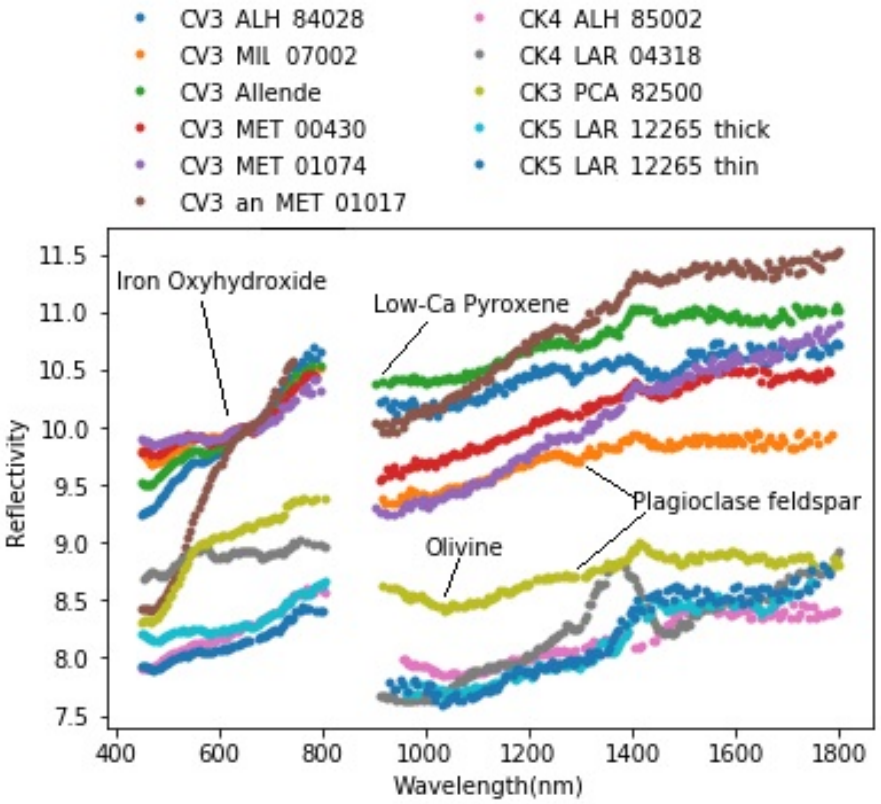

FIGURE 3.6: Reflectance spectra of CK and CV carbonaceous chondrites between 400 and 1900 nm. The differences between reflectivity of two groups are due to thermal metamorphism leading to a loss or aggregation of opaque phases. This would lead to an increase in reflectance of CVs. The spectra were normalized to 8 at 650 nm, and then the CV spectra were shifted to facilitate the comparison.

To explain these peculiar features and the diversity observed in between the different specimens is necessary to invoke some physical process. In fact, collisional *gardening* of the *CK* parent *asteroid* was proposed from the study of the minerals found in their matrices (Rubin and Ma, 2017). Matrix-rich regions in the *CK chondrites* formed by comminuted and ground materials, mostly micron-sized angular silicate grains that are pressed and crushed *chondrules*, demonstrate the degree of collisional processing in these samples (Rubin and Ma, 2017). Back-scattered electron (BSE) images of ALH 85002 exemplify the internal fractures usually contained in their rock-forming silicates and the subsequent comminution of the materials. As consequence of these processes secondary minerals were formed, acting as opaques that change the spectral reflectance behavior (Figure 3.7). On the other hand, the primary mineralogy of *CVs* seem to be better preserved than the *CKs*, so seems plausible that they suffered a minor extent of collisional processing. For example, in the *thin sections* of $CV3_{OxA}$ Allende, Norton (2002) reveal little evidence of crushing. Indeed, and although many reduced CV3 *chondrites* show impact signs (Scott, Keil, and Stöffler, 1992), they have not been extensively crushed (Kracher et al., 1985).

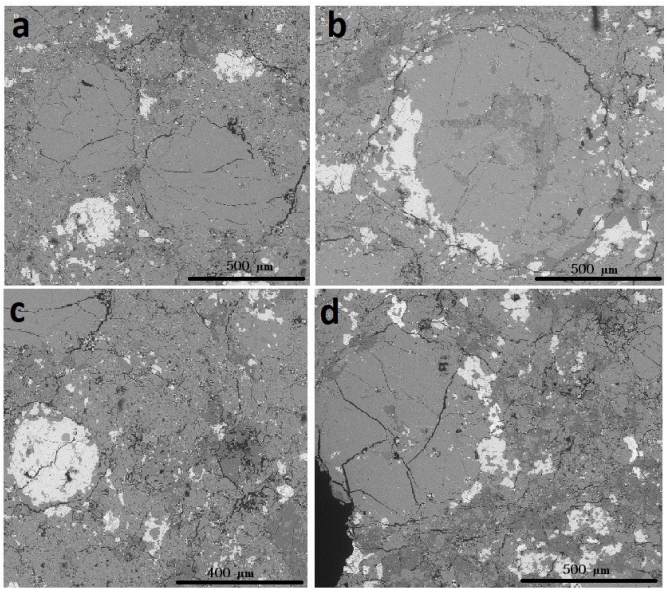

FIGURE 3.7: Back-scattered electron (BSE) image of regions of CK4 chondrite ALH 85002. It consists mainly of well compacted silicate-rich chondrules, sulfides and accessory minerals. Olivine – light gray; orthopyroxene – medium gray; plagioclase – dark gray; sulfide and magnetite – white; fractures and pores being black. The black scale bars are 500, 500, 400 and 500 $\sim$ μm, respectively.

As a result of the reflectance affinity and the chemical evidence found by (Wasson, Isa, and Rubin, 2013), it is plausible that *CV* and *CK chondrites* were associated with a common parent *asteroid* that experienced splitting and differentiated evolution by consequence of separated orbital evolution. Greenwood et al. (2010) and Cloutis et al. (2012) suggested that *CVs* and *CKs* may have a common *parent body*, Eos *asteroid* family should be its most likely source. It is also consistent with the suggestion that the 221 Eos *asteroid* collisional family proposed to be associated with *CV meteorites* (Greenwood et al., 2010), could be a possible source of *CK chondrites* since they share a blue-sloped feature in the NIR region (800-2500 nm) specially beyond $\sim$1500 nm (Cloutis et al., 2012). Then, collisionally processed fragments of 221 Eos family could be the source of CK4 and CK5 *chondrites*.

3.1.5 Comparison of the reflectance spectra of our samples with previous studies

In this section we compare the obtained reflectance spectra with previously published data. This is important, given that our procedure obtains the reflectance spectra using polished sections of the *meteorites*, while previous literature used powders from ground *meteorites*. Cloutis et al. (2012) identified compositions and spectral features in *CK chondrites* with small grain sizes (10-30 $\sim$ μm). The *CK chondrites* are highly oxidized with *petrologic types* from 3 to 6 with high abundance of the *fayalite* (Fe_2SiO_4) member of the *olivine* family (Geiger and Bischoff, 1995; Huber et al., 2006). The RELAB database at Brown University Keck/NASA also contains *CK chondrite* spectra covering a wavelength range from 400 to 1900 nm and measured on powders of various sizes (Cloutis et al., 2012). Our spectra show significant differences compared with RELAB data shown in Figure 3.8. The spectrum of ALH 85002 in RELAB has a lower reflectance than the spectrum obtained for this *meteorite* in

our studies. These differences may be due to measuring a polished *meteorite* surface instead of the fine-grained powders (<125 μm) which are used in RELAB. Moyano-Cambero et al. (2017b) also indicated that the behaviour of reflectance spectra in the UV region of the ground samples is remarkably different from our *meteorite* sections. In our data from ALH 85002 the steep slope found by RELAB below 600 nm does not exist. This is possibly produced by terrestrial weathering in the samples studied by RELAB (Moyano-Cambero et al., 2017b). Hendrix and Vilas (2006) also mentioned that flattening between 400 and 600 nm indicates high Fe content (Cloutis et al., 2010). As we work with polished samples, the metal grains contribute more to the spectrum than in the powder used in RELAB (Trigo-Rodriguez et al., 2014). As a result, the behaviour below 600 nm and other features in our spectra are very similar to changes in space-weathered *asteroids* (Hendrix and Vilas, 2006). It is notable that the narrow absorption band in ALH 85002 around 450 nm (Fig. 3.8) could be assigned to *magnetite*, due to its deep extinction below 400 nm (Tang et al., 2003).

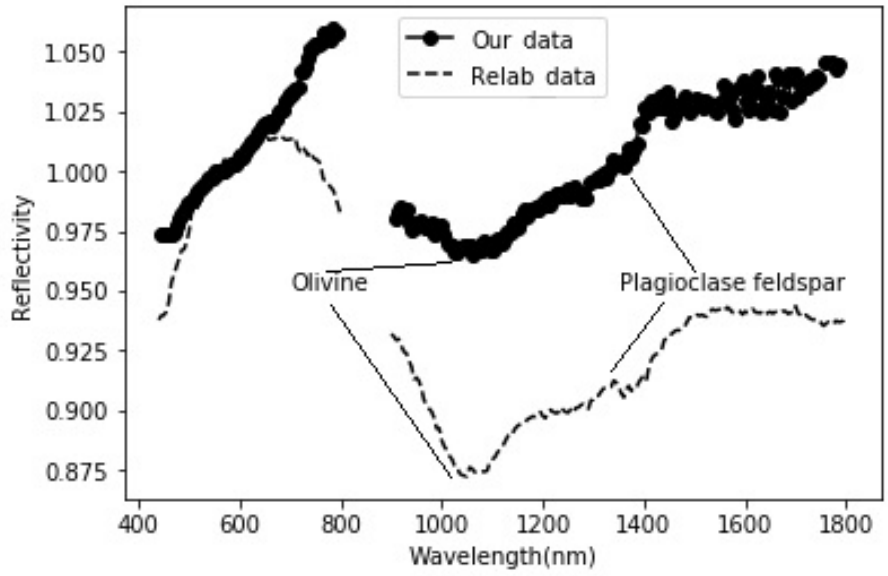

FIGURE 3.8: Comparison of the spectra of CK4 *chondrite* ALH 85002 obtained for this study, and another one from Brown University Keck-/NASA RELAB obtained from a powder of the same meteorite. They are normalized to 1 at 550 nm and $BaSO_4$ correction was applied to our spectra.

All *CK chondrites* contain some regions of shock-induced and darkened silicates that contain tiny (<0.3-10 μm) grains of *magnetite* and pentlandite throughout the interiors of many silicate grains (Brearley and Jones, 1998; Kallemeyn, Rubin, and Wasson, 1991). These opaque regions emerge because of progressive shock-darkening that creates vesicles and holes. The *olivine* in *CK chondrites* contains numerous spherical grains (0.1–5 μm) of *magnetite* and pentlandite, and other silicates. Noguchi (1993) and Geiger and Bischoff (1995) remarked that micron-sized *magnetite* grains act as opaque in the interior of silicates, thus contributing to shock darkening. The process of postshock annealing that follows shock compression of the samples as consequence of impact could led to minimize influence of shock in *olivine* (Rubin, 2012). Brearley (1991) also agrees that although silicate blackening could be due to shock, other processes like aqueous alteration could have been at work.

To compare with previous papers, Salisbury, Hunt, and Lenhoff (1975) found that

the spectrum of CK4 Karoonda, which is a well preserved *fall*, shows the shallowest absorption features in the 500-600 nm interval and a very weak *olivine* absorption band in 1000 nm region. Hiroi et al. (1993) also identified the blue-sloped reflectance spectra for <125 μm powders of CK4 ALH 85002 and CK4/5 Yamato 693 (Y 693) in the range of 500-2500 nm, and an olivine-like absorption band near 1050 nm.

Oxidation experienced by the possible presence of Fe^{3+} in low-calcium *pyroxenes*, and abundant Ni in *olivine*, are indicative of *metamorphism* occurred in most *CK* samples, since petrographic type 4 or higher types indicate *thermal metamorphism* (Noguchi, 1993). *Metamorphism* also leads to Fe enrichment in *CAIs* (Chaumard et al., 2014). The total carbon contents of *CKs* tend to decrease with increasing metamorphic grade (Jarosewich, 2006; Greenwood et al., 2010). In fact, Geiger and Bischoff (1995) suggested that *CK chondrites* formed by metamorphic heating of a *CV* like precursor under oxidizing conditions. Probably a part of the *metamorphism* experienced by these rocks was due to collisions, producing some rare secondary minerals identified in some of the our samples (Urzaiz, Trigo-Rodriguez, and Mestres, 2015). Huber et al. (2006) chose *CK* samples of un-weathered Antarctic *meteorites* to analyse the bulk elemental chemistry using INAA (Instrumental Neutron Activation Analysis) and petrographic techniques. These authors concluded that, as consequence of the aqueous alteration on the parent *asteroid*, *CK chondrites* became highly oxidized (Huber et al., 2006).

3.1.6 Conclusions

We have tested a working hypothesis for the formation of the parent bodies of *CV* and *CK* chondrites. The *CKs* could have formed from *CVs* after impacts and high temperatures, and these processes made them aqueously altered and annealed (Wasson, Isa, and Rubin, 2013). Such a working scenario implies an evolutionary processing of *CKs* from *CV* materials and suggests that *meteorite* collections should have specimens exhibiting gradational differences with significant consequences in their reflectance spectra. Such scenario is consistent with our current study of *CV* and *CK* reflectance spectra. From the study of these reflectance spectra we have reached the following conclusions:

1. We found a significant similitude between the reflectance spectra of *CV-CK chondrites* and *asteroids* belonging to the Cg spectral class. Specific diversity could be consequence of thermal heating due to collisional processing.

2. A common behavior for *CK chondrite* reflectance spectra is found. We realize that with increasing metamorphic grade, the reflectance decreases producing a deeper 1000 nm region absorption feature. But in general, higher petrographic degree is consistent with higher reflectivity, mainly in the visible region. The band depth of *olivine* in *CKs* increases while the *thermal metamorphism* increases: the CK3 petrographic grades of *meteorites* display shallower band depths, while the CK5 spectra exhibit the deepest band depths.

3. The correlation between *CV* and *CK* reflectance spectra, together with the chemical similitude claimed in previous studies, suggest that both groups could have originated from a common *parent body* that was broken apart a long time ago. In this evolutionary scenario, different *asteroid* fragments could have been dynamically separated by the action of non-gravitational forces. As a consequence of differentiated collisional evolution, each *asteroid* ended with different degrees of *space weathering*, aqueous alteration and *thermal metamorphism*.

4. If our evolutionary scenario is correct, secondary minerals formed as consequence of collisional processing and aqueous alteration in their parent *asteroids*, having direct influence on the progressive darkening found in the spectra of *CV-CK chondrites*.

3.2 Mechanical properties and shock metamorphism of Itokawa particles

The JAXA/ISAS Hayabusa spacecraft had a rendez-vous with *asteroid* 25143 Itokawa, and collected regolith samples from its surface after landing on the *asteroid* in November 2005. The collector sample-return capsule returned to Earth in June 2010 (Yano et al., 2006). The remote study of Itokawa reflectance properties revealed that the *asteroid* spectrum was consistent with that of an S-type *asteroid* and its bulk mineralogy characteristic of the LL group of *ordinary chondrites* (Abe et al., 2006). The surface of Itokawa consists of large stones and rocks, confirmed by the analysis of the return sample (Nakamura et al., 2011), which are not uniformly distributed, and a regolith essentially made of pounded stones and gravel-sized particles (Saito et al., 2006). A variety of boulders ranging from meters to hundreds of meters in diameter were also identified by the Hayabusa spacecraft (Saito et al., 2006). The re-arrangement of rocks and boulders on the surface of this rubble pile *asteroid* and the observed displacement of the regolith can be explained by collisions and related processes (Saito et al., 2006; Matsumoto et al., 2016). 25143 Itokawa belongs to the S-class, one of the most abundant *asteroid* spectral types, and space missions like Hayabusa can help provide an answer to how similar their properties are in comparison with *ordinary chondrites* (Burbine et al., 2002). To decipher the physical properties of asteroidal regolith is of great relevance for space exploration.

Different techniques have been developed to infer the properties of the regolith from remote observations (Hiroi, Pieters, and Takeda, 1994), but in situ measurements are still scarce. On the other hand, it is well known that *meteorite* collections are strongly biased toward high tensile strength rocks, so we lack sufficent regolith materials for the direct study in terrestrial laboratories (Chapman et al., 2002). To date, most of our current understanding of regolith comes from the study of the lunar regolith sampled by the Apollo and other Moon missions (Papike, Simon, and Laul, 1982). There are good reasons to study the physical properties of *asteroid* regolith in order to know the possible differences between lunar and asteroidal regolith. Obviously, the first sample returned regolith from an *asteroid* by Hayabusa spacecraft has focused the attention of the scientific community. Remote observations, laboratory studies, and space missions have revealed that regolith covers the surface of many *asteroids*, and might be produced by very different physical processes including the comminution of the surface rock-forming minerals, including impact *gardening* and thermal fatigue (Delbo et al., 2014). For these reasons, sample return missions provide access to unique materials from which valuable data on the physical properties of regolith particles can be extracted. In addition, the properties of the surface materials from well-known *asteroids* are inferred from these studies. This work constitutes the first laboratory study on the mechanical properties of *asteroid* regolith materials that might be of interest to future sample-return missions. In this thesis we gain insight on the mechanical properties of *asteroid* Itokawa's regolith by studying three micron-sized particles collected by the Hayabusa JAXA mission. The data obtained are compared with the materials forming chondritic *meteorites*.

One of the questions to be addressed is whether collisional *gardening* can change the main mechanical properties of the materials forming the surface.

3.2.1 Results

It is of great interest to understand the mechanical properties of the studied regolith grains because 25143 Itokawa can be considered a clear example of a rubble-pile *asteroid* (Saito et al., 2006). Cratering in *asteroids* has been studied in other *asteroids* as well, and the nature and properties of asteroidal regolith seem to be particularly interesting for future exploration missions to minor bodies (Chapman et al., 2002). At the micrometer scale of our samples, Itokawa's regolith can be considered a good example of the materials forming the surface of an *ordinary chondrite* (OC) *asteroid* with recognizable *lithologies* LL4-6. In addition, Itokawa's surface consists of many chondritic fragments that are thermally metamorphosed or fragmented, having experienced the implantation of other nanoscale particles as a consequence of *space weathering* (Nakamura et al., 2011; Noguchi et al., 2011). It is also possible that some regolith grains on the surface of *asteroids* were created by thermal fatigue (Matsumoto et al., 2016). We are going to concentrate on the main mechanical properties inferred for the studied Itokawa regolith grains and the main implications of these results.

TABLE 3.4: Main composition of the studied regolith samples.

Sample	**Size (μm)**	Main mineral phases
#14	131.2 ± 0.1	*Olivine*, low-Ca *pyroxene*, *plagioclase*
#23	149.4 ± 0.1	*Olivine*, troilite
#47	108.0 ± 0.1	*Olivine*, low-Ca and high-Ca *pyroxene*

3.2.1.1 Mechanical properties of Itokawa regolith samples

Representative nanoindentation curves for the three studied particles are shown in Figure 3.9, from which the mean mechanical properties resulting from the analyzed region can be extracted (see Tab. 3.5). As the values of hardness are not remarkably different at 5 and 10 mN, it seems that within this indentation force range, the hardness is not affected by the maximum applied load (Nix and Gao, 1998). This demonstrates that with our chosen loads, hardening phenomena, which could result from the indentation size effect, are avoided (Tanbakouei et al., 2019b).

TABLE 3.5: Average mechanical properties of Itokawa regolith silicates in particles of given S#.

Sample	Applied Force (mN)	E_r (GPa)	H(GPa)	S(mN/μm)	U_{el}/U_{tot}	U_{pl}/U_{tot}
#14	5	83.0± 0.12	8.01±0.01	77.01±0.11	0.64±0.01	0.36±0.01
#14	10	89.00±0.04	9.00±0.014	105.00±0.06	0.66±0.01	0.34±0.01
#23	5	111.01±0.22	10.1±0.02	92.00±0.20	0.73±0.07	0.27±0.07
#23	10	101.00±0.05	10.00±0.01	117.0±0.5	0.66±0.05	0.34±0.05
#47	5	86.01±0.13	13.01±0.03	62.01±0.03	0.87±0.01	0.13±0.01
#47	10	82.00±0.14	11.00±0.02	91.01±0.07	0.86±0.01	0.32±0.01

3.2.2 Discussion

We chose applied forces up to 10 mN in order to keep the maximum penetration depth below one-tenth of the overall thickness of the sample and to minimize the

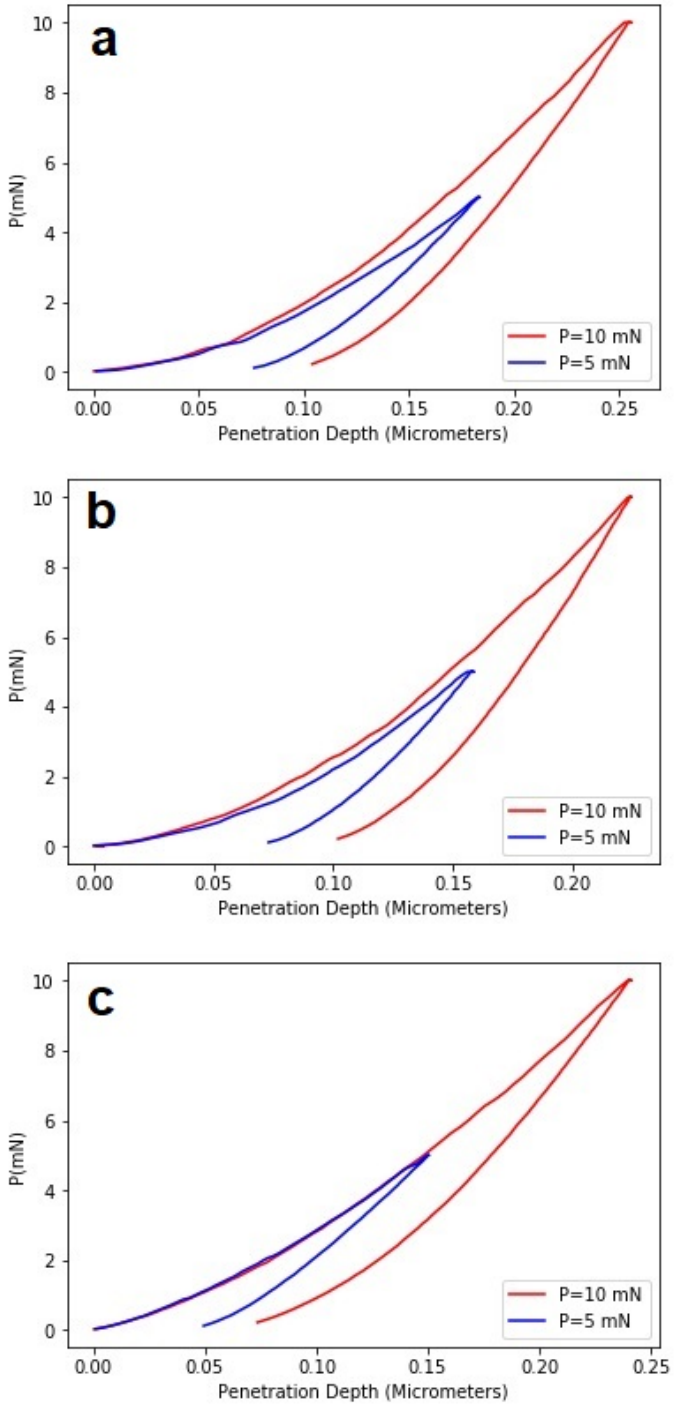

FIGURE 3.9: Indentation curves obtained for Itokawa samples. (a) Indentation curves obtained for S14 sample. (b) Indentation curves obtained for S23 sample. (c) Indentation curves obtained for S47 sample.

eventual influence of the resin on the obtained results (Fischer-Cripps, 2004). We applied some necessary corrections for the contact area and compliance of the instrument. We also kept the thermal drift below 0.05 nm.s^{-1}. The contact stiffness is defined as

$$S = \frac{dP}{dh} \tag{3.1}$$

where P denotes the applied load and h the penetration depth during nanoindentation. The maximum load applied is denoted P_{max}. The hardness is calculated as

$$H = \frac{P_{max}}{A} \tag{3.2}$$

where A is the projected contact area on the horizontal plane. The elastic modulus can be evaluated based on its relationship with the contact area A and the contact stiffness:

$$S = \beta \frac{2}{\sqrt{\pi}} E_r \sqrt{A} \tag{3.3}$$

Here β is a constant that depends on the geometry of the indenter (β= 1.034 for a Berkovich indenter (Fischer-Cripps, 2004) and E_r is the reduced *Young's modulus* defined as follows:

$$\frac{1}{E_r} = \frac{1-\nu^2}{E} + \frac{1-\nu_i^2}{E_i} \tag{3.4}$$

The reduced modulus takes into account the elastic displacements that occur in both the specimen, with *Young's modulus* E and Poisson's ratio ν, and in the diamond indenter, with elastic constants E_i and ν_i. The data for diamond were E_i = 1140 GPa and ν_i= 0.07. We also evaluated the *elastic recovery* as the ratio of the elastic indentation energy U_{el} (calculated as the area enclosed between the unloading indentation curve and the x-axis) to the total indentation energy U_{tot} = U_{el}+U_{pl} (i.e., the area between the loading indentation section and the x-axis). Three Itokawa particles provided by JAXA embedded in epoxy resin and polished to mirror-like appearance, with numbers RA-QD02-0014, RA-QD02-0023, and RA-QD02-0047 (hereafter S14, S23, and S47, respectively) were investigated (see Tab. 3.4). The polished upper sides of the three particles are shown in Figure 3.10. The samples were analyzed via optical microscopy and scanning electron microscopy (Quanta 650 FEG equipped with EDX Inca 250 SSD XMax20 detector). Indentations were applied on the different mineral phases contained in the three particles with applied forces of 5 mN and 10 mN, respectively, in order to extract the nanomechanical properties of the samples. To calculate the gross mechanical properties of the samples the results of the individual indentations applied on the mineral phases were averaged. The results of multiple indentations provided an estimation of the average mechanical properties of different regions, including the uncertainties based on natural deviations in the rock-forming materials.

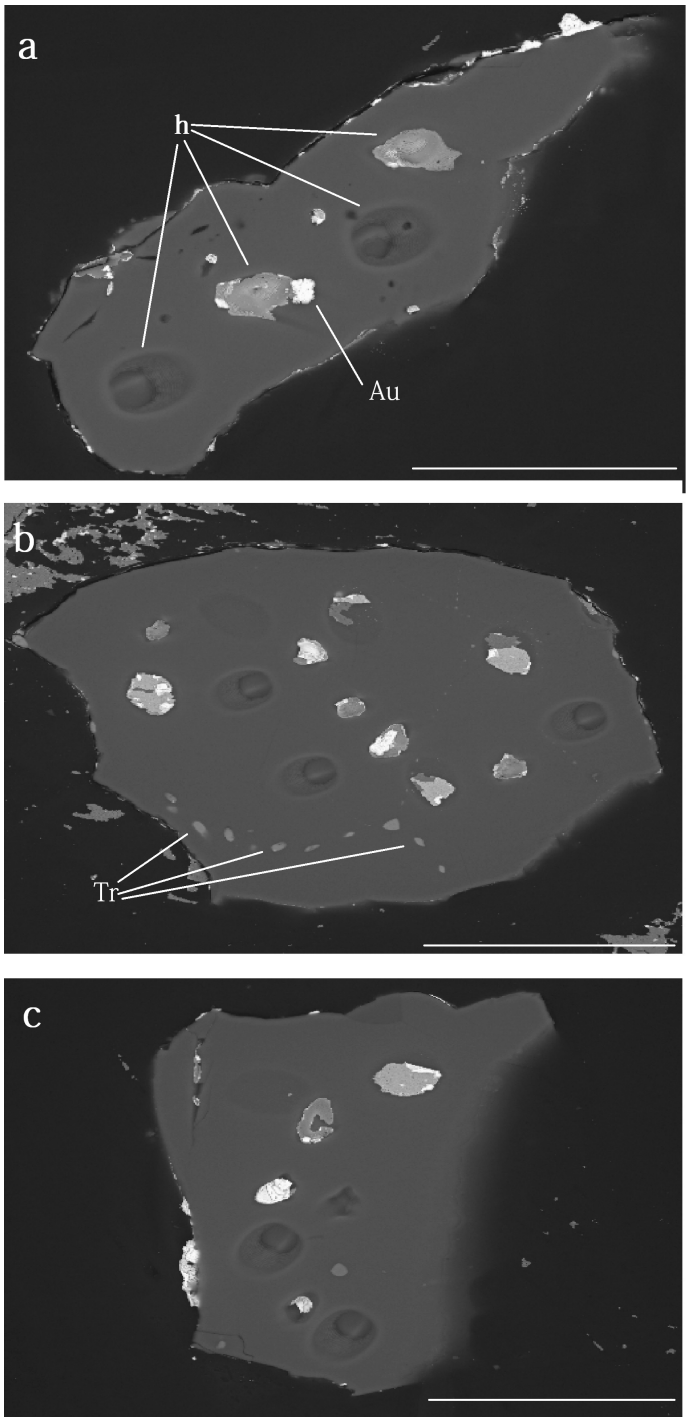

FIGURE 3.10: BSE images of the three Itokawa grains. (a) RA-QD02-0014, (b) RA-QD02-0023, and (c) RA-QD02-0047. The white scale bars are 50, 70, and 60 μm respectively. Labeled in panel a are several holes (h) and Au patches from previous analyses. A chain of troilite (tr) grains is also labeled in panel b.

3.2.3 Comparison with Chelyabinsk meteorite

We compare our results with the mechanical properties of the Chelyabinsk *LL chondrite* specimens obtained with a similar methodology during the nanoindentation experiments (UMIS Nanoindentor from Fischer-Cripps Laboratories) (Moyano-Cambero et al., 2017b). The particles in both cases were embedded in a resin and subsequently

polished to mirror-like appearance using analogous polishing procedures. The size of the particles (hundreds of micrometers) is much larger than the indentation imprint size (on the order of 12 μm, depending on the applied indentation load). Therefore, no effect from the surrounding resin on the evaluated mechanical properties is expected. The mechanical properties were measured by nanoindentation applied on the different mineral parts of this OC with a maximum applied force of 20 mN. For the Chelyabinsk *meteorite* the reduced *Young's modulus* was calculated between 69 and 78 GPa (Moyano-Cambero et al., 2017b), which is lower than the values obtained for Itokawa's samples of 82–111 GPa (Tab. 3.5). Furthermore, the *Young's modulus* measured previously by (Yomogida and Matsui, 1983) for OCs, between 10 and 140 GPa, is quite consistent with the values inferred for Itokawa's regolith grains. Our measurements show lower hardness values than in the *olivine* forming the Chelyabinsk *meteorite*, 10.2 and 13.6 GPa, respectively (Moyano-Cambero et al., 2017b). Assuming that the composition of the two investigated objects is similar (similar minerals and with similar percentages), the lower *Young's modulus* observed in Chelyabinsk suggests that it contains higher *porosity* levels, since *porosity* has a strong detrimental effect on the elastic properties of materials (Pellicer et al., 2012). Different models exist in the literature to correlate the *Young's modulus* with *porosity*, both for metallic and ceramic materials (Tolu et al., 2013). In a first approximation, it has been shown that:

$$\frac{E_{porous}}{E_{bulk}} = (\frac{\rho_{porous}}{\rho_{bulk}})^2 \tag{3.5}$$

where the right-hand term is the relative density and the coefficient n depends on the material (in other words, n = 2 in samples with an open-cell *porosity* (Tolu et al., 2013). This relative density can be related to the material *porosity* volume fraction P_o:

$$\frac{\rho_{porous}}{\rho_{bulk}} = 1 - P_0 \tag{3.6}$$

OCs typically show porosities around 5%–10% (Consolmagno, Britt, and Macke, 2008) and the *porosity* values for Chelyabinsk range between 2% and 11%, with an average value of ∼6%. However, as it is shown in Table 3.6 the posorities of Itokawa are much more less than Chelyabinsk (Moyano Cambero, 2017). It is well known that even a low degree of *porosity* can result in a drastic reduction in the *Young's modulus*. This effect is considered in the approach by Ramakrishnan and Arunachalam, which includes the intensification effects of pressure at the surface of spherical pores due to interactions between the pores and the surrounding bulk solid material (Ramakrishnan and Arunachalam, 1993). For a given *porosity* fraction the elastic modulus of the porous material (E_{porous}) can be then related to the elastic modulus of the fully dense material (E_{bulk}) following:

$$\frac{\rho_{porous}}{\rho_{bulk}} = \frac{(1 - P_0)^2}{1 + 2P_{or} - 3\nu P_{or}} \tag{3.7}$$

where ν is the Poisson ratio of the bulk nonporous material. In the Chelyabinsk compositions, *olivine* (∼Fa_{28}) is two to four times more abundant than *pyroxene* (∼Fs_{23}) (Galimov, 2013). However, the two minerals are homogeneous in composition (Galimov, 2013; Kohout et al., 2014; Righter et al., 2015). In Itokawa particles, *olivine* was found with an average compositional range of $Fa_{28.6}$, low-Ca *pyroxene* of $Fs_{23.1}$, and high- Ca *pyroxene* of $Fs_{8.9}$ (Nakamura et al., 2011). The *porosity* values for Chelyabinsk

range between 2 and 11%, with an average value of 6% (Moyano-Cambero et al., 2017b), which is higher than the Itokawa particles (see Tab. 3.6). The Itokawa and *LL chondrite* samples have *porosities* ranging from approximately 0 to 10% with an average of 1.5 and 1.9%. The values of hardness and *elastic recovery* (U_{el}/U_{tot}) *fall* in the same range as those measured for the Chelyabinsk *meteorite*. This can be understood bearing in mind that these two parameters are less sensitive to *porosity* than the *Young's modulus*. In view of the mechanical properties of Itokawa's regolith particles we expect that these data can be used in future modeling of impact plume formation, and also to interpret the outcome of previous experiments (Michikami et al., 2007; Flynn et al., 2015). If micron-sized particles are strong enough and bear similar mechanical properties to those of *meteorites*, we expect that excavating a *crater* using a kinetic impactor in an area with significant fine-grained regolith will increase the momentum transfer. The reason is that the amount of micron-sized dust released in the creation of the impact plume will naturally increase the total target mass released without the need of grinding up the target during the mechanical excavation phase (Tanbakouei et al., 2019b). Additional experiments to infer the velocity distribution of fine grained regolith particles, from a few to a hundred micron in size should be done with chondritic targets as was done previously (Nakamura, Fujiwara, and Kadono, 1994; Flynn et al., 2015). The Double Asteroid Redirection Test (DART) mission plans to excavate a *crater* in the surface of the (65803) Didymos satellite; our results suggest that this excavation with a kinetic impactor in a significant fine grained regolith area will increase the momentum transfer and release particles in the direction opposite to the movement of the projectile. This would happen without the need of grinding up the target during the mechanical excavation.

TABLE 3.6: Estimated mass of the three Itokawa particles assuming silicate density of 2.2 ×10-12 (g μm^{-3}) taking their porosity into account.

Sample	Volume (μm^{-3})	Estimated mass (g)	Porosity (%)	Estimated mass with porosity (g)
#14	125921	2.76×10^{-7}	0.07	2.75×10^{-7}
#23	781081	1.72×10^{-6}	0.0	1.71×10^{-6}
#47	148570	3.26×10^{-7}	0.0	3.26×10^{-7}

3.2.4 Raman spectroscopy to infer shock in Itokawa and NWA 6013

By studying the regolith particles from Itokawa, we expect to gain precious information about surface processes of *asteroids* which probably cannot be found in *meteorites*. The shape and formation of Itokawa particles is a response to impacts and resulted from mechanical disaggregation (Tsuchiyama et al., 2011; Tsuchiyama et al., 2013). For this reason, the fragments shaped in laboratories by strong collisions are probably similar to the regolith grains forming Itokawa's surface. The selected points to be studied through Raman spectra are identifies in Figure 3.11.

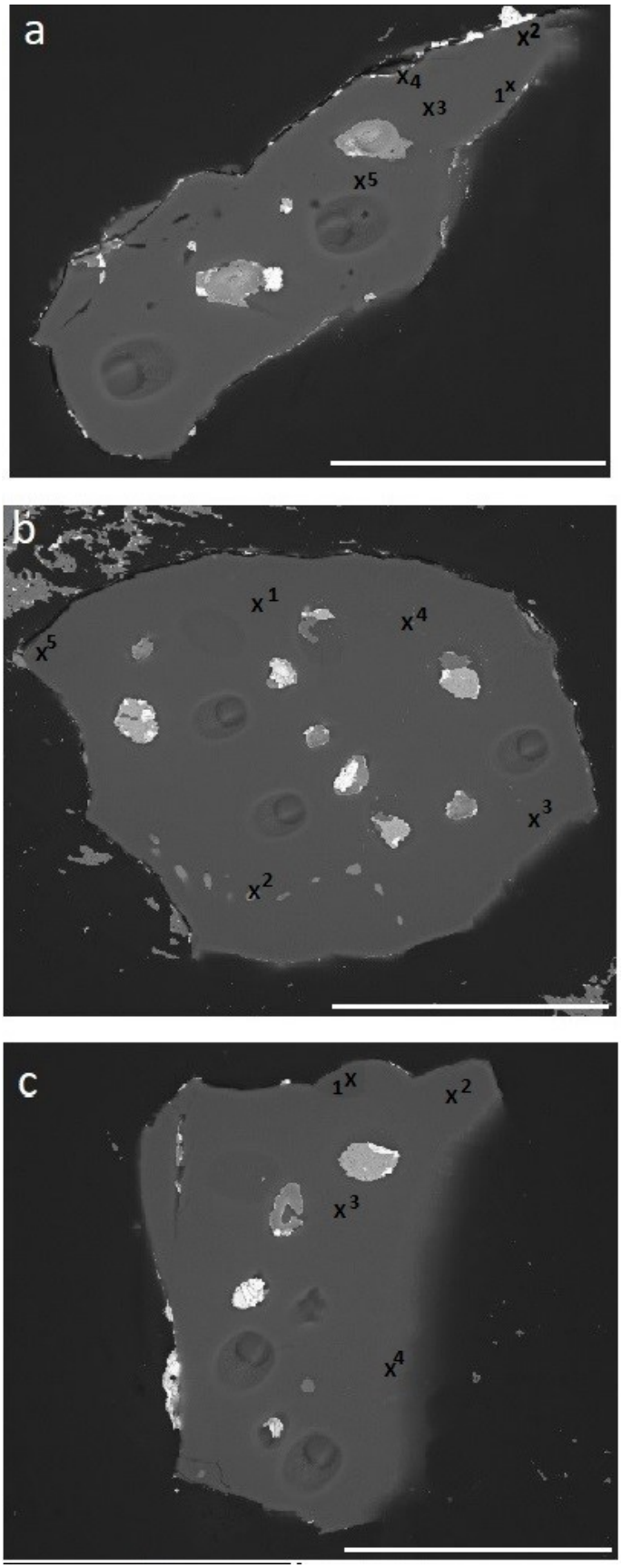

FIGURE 3.11: BSE images of the three Itokawa grains with ROIs (Tab. 3.7 and Tab. 3.8). RA-QD02-0014 (a), RA-QD02-0023 (b) and RA-QD02-0047 (c). The location of the selected Raman points is indicated. The white scale bars are 50, 70 and 60 μm, respectively.

First, we concentrate in the *olivine* phase. Raman spectra of this silicate show two characteristics peaks of P_1 around 820 cm^{-1} and P_2 around 850 cm^{-1} (Mohanan, Sharma, and Bishop, 1993; Kuebler et al., 2006). The shifts in these frequency modes depend on the *forsterite* (Fo) and *fayalite* (Fa) content of the *olivine* (Chopelas, 1991; Kuebler et al., 2006). Several hypervelocity impacts induced strong shocks in the crystal structures of minerals in *asteroids* and caused a permanent shift to lower frequencies in the P_1 and P_2 peak positions of *olivine* (Foster et al., 2013), which thought to be the result of the effects on Si-O bond during the impact.

Raman spectra were obtained from 40 unshocked *olivine* grains by Harriss and Burchell (2016), and the averaged $P_1 = 823.80 \pm 0.12$ and $P_2 = 856.01 \pm 0.16$ were measured. Foster et al. (2013) performed experiments to collide uniform *olivine* grains with an Al foil target with the impact speed of 6.1 $km.s^{-1}$ and then extracted Raman spectroscopy on the remnants in *impact craters*. Their results show a shift to lower wavelengths in the *olivine* P_1 and P_2 Raman peak positions and a change in P_2- P_1, which depended on the Fo composition. They observed that for P_1, a greater shift happened for Fo_{100} (1 cm^{-1}) than that happened for Fo_{40} (0.5 cm^{-1}). The position of P_2 also shifted downward opposite of a greater shift at lower Fo compositions (Fig. 3.12). At high pressures occur the *olivine* into ringwoodite transformation mechanism previously reported in *ordinary chondrites*. (Martinez et al., 2019; Unsalan and Altunayar-Unsalan, 2020). Our Itokawa Raman spectra points toward a high impact shock pressure. Based on the *olivine* doublet (822 and 856 cm^{-1}) and the probable presence of maskelynite (at 509 and 580 cm^{-1}) observed in the Raman spectra.

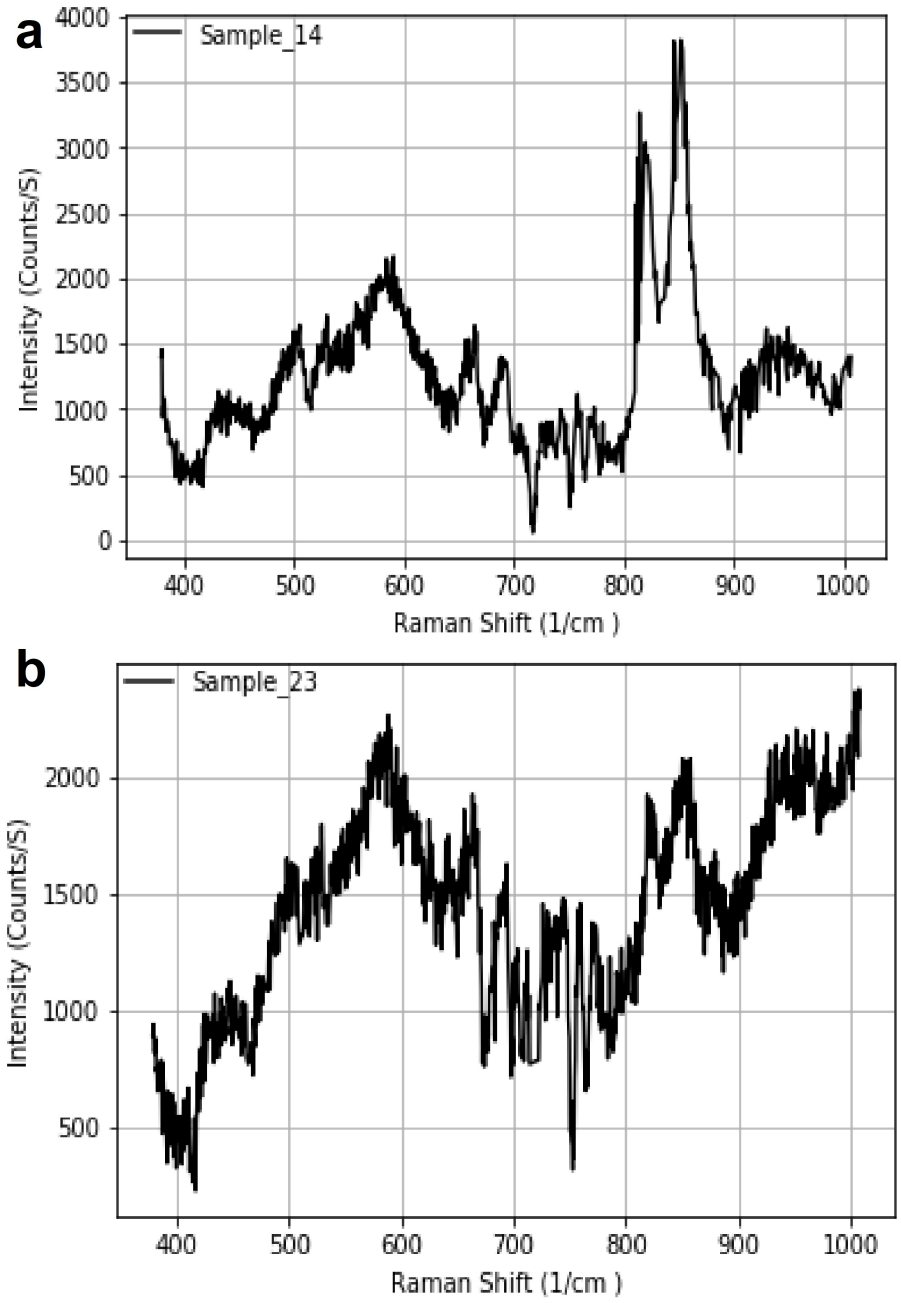

FIGURE 3.12: The Raman spectra of a) S14 and b) S23 of Itokawa particles.

To study the effects of shock in *olivine* we selected a Diogenite olivine-rich *achondrite*, called Northwest Africa 6013 (NWA 6013). Diogenites form one of the *achondrite* groups with suspected origin in *asteroid* 4 Vesta, formely known as the Howardite, Eucrite, and Diogenite (HED) suite. The NWA 6013 sample as also studied using Raman spectroscopy to find the main minerals forming the *meteorite*. NWA 6013 is a coarse-grained rock consisting of cm-sized *chondrules* dominated by *olivine* and *pyroxene*, respectively. The most important characteristic of this *meteorite* is its shock stage S1 and its similar modal composition to Itokawa, so it is perfect to compare with shocked samples.

Although NWA 6013 sample is Diogenite-olivine, in some points, there are evidence of first *olivine* peak around in 822.78 but the second *olivine* peak which is around 854 has not seen in this sample. Table 3.7 shows the minerals found in the selective points from Raman spectroscopy of NWA 6013. 5 points of NWA 6013 have been chosen to study the Raman spectral reflectance properties of the sample (Fig. 3.13).

TABLE 3.7: Main composition of the studied NWA 6013 achondrite sample

Minerals	Raman peaks	Experimental NWA 6013 peaks
Olivine	821 1116	825 1113
Jadeite $NaAlSi_2O_6$	1037.255 990.423	1034.87 1015.03
Orthoensatite $MgSiO_3$	1014.11	1014.90

TABLE 3.8: Olivine mode frequencies in cm^{-1} of Itokawa's regolith particles. Errors are 0.5 cm^{-1}.

Sample#	ROI #	Catalog Raman peaks		Experimental Itokawa peaks	
		P_1	P_2	P_1	P_2
#14	1	822	854	820.4	851.9
#14	2			822.4	854.4
#14	3			822.0	852.0
#14	4			823.7	851.4
#14	5			820.8	852.4
#23	1	822	854	822.0	850.5
#23	2			820.0	851.6
#23	3			826.6	854.0
#23	4			823.2	850.5
#23	5			822.4	854.1

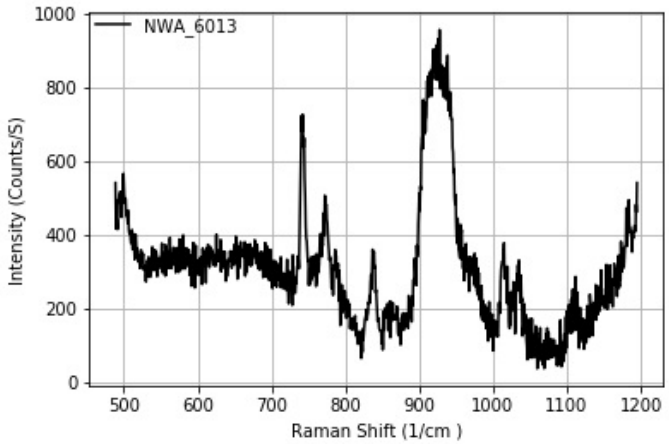

FIGURE 3.13: Raman spectra of olivine in the achondrite NWA 6013

TABLE 3.9: Orthoenstatite mode frequencies in cm^{-1} of Itokawa's regolith particles sample #47. Errors are 0.5 cm^{-1}.

Sample #	ROI #	Catalog Raman peaks					Experimental Itokawa peaks				
		P_1	P_2	P_3	P_4	P_5	P_1	P_2	P_3	P_4	P_5
#47	1	421	665	687	855	938	422.7	665.9	687.9	846.9	938.9
#47	2						423.8	666.5	688.9	853.1	939.4
#47	3						421.3	666.9	688.5	853.8	938.9
#47	4						422.5	665.1	685.5	853.5	937.9

3.2.5 Conclusions

The mechanical properties of μm-sized regolith particles of the *asteroid* Itokawa were studied by using the nanoindentation technique. Given that Hayabusa returned samples come from a rubble-pile *NEA asteroid*, it is worthwhile to remark that the inferred physical properties for these particles are not very different to those exhibited by *meteorites* with similar *ordinary chondrite* composition. Our study provides a method that provides an accurate measurement of the mechanical response of regolith grains on the surface of chondritic *asteroids*. This is relevant, because fine-grained regolith similar to this can be covering the surface of the satellite of *asteroid* 65803 Didymos planned to be impacted by the Double Asteroid Redirection Test (DART) NASA Mission in 2022. The deflection efficiency depends on our ability to release materials in the impact plume in opposite direction to the projectile movement (see Moyano-Cambero et al. (2017b)), so knowing the nature and mechanical properties of the rock-forming materials is of great importance. The conclusions of our current work are summarized as follows:

1. The nano-indentation technique can be successfully applied to study micron-sized particles and larger rocks returned in sample-return missions, providing very valuable information about the physical properties of the materials forming *asteroids*.

2. We found that the mechanical properties of Itokawa regolith particles are comparable with the silicates forming *LL chondrite meteorites*, with relatively minor differences.

   (a) The reduced *Young's modulus* values obtained for Itokawas samples are higher than those measured for Chelyabinsk *chondrite*, so they seem to be more compacted than the minerals forming that particular *LL chondrite*. This might be a natural consequence of being particles surviving long exposure times on the surface of a *NEA*.

   (b) Concerning the *elastic recovery* of Chelyabinsk *chondrite* minerals, it is significantly lower than that measured for the Itokawa samples, whereas hardness values are similar. This indicates that the Itokawa particles have larger ability to absorb elastic energy during an eventual impact as compared to Chelyabinsk *chondrite* minerals.

3. The inferred properties of micron-sized Hayabusa particles offer insights into the cohesion and mechanical response of regolith material on an *asteroid* surface. This is particularly relevant in view of the recent successful touch-down and sampling as well as projectile impact of Hayabusa2 on *asteroid* 162173 Ryugu used to quantify the efficiency of *crater* excavation. It is important to remark that the momentum transfer by a projectile on an *asteroid* will depend

on the mechanical properties of the surface materials as the amount of mass in the impact plume, released in opposite direction to the projectile movement, is directly proportional to the deflection achieved.

4. Our results suggest that excavating a *crater* with a kinetic impactor in an area with significant fine-grained regolith will increase the momentum transfer for a main reason: the amount of micron-sized dust released in the creation of the impact plume will naturally increase the total target mass released without the need of grinding up the target as consequence of the mechanical excavation.

5. The three Itokawa regolith particles studied here formed part of Itokawa's *asteroid* soil. Probably a significant part of the regolith has been processed, ground, powdered by impacts, and affected by shock to a certain extent. At least in two out of three particles we found shocked *olivine*, suggesting that they were broken by collisional gardening.

6. We found that the *olivine* in two regolith grains of Itokawa asteroid is affected by shock, with a distinctive Raman drift usually caused by plastic deformation of the lattice structure.

7. HED *achondrite* NWA 6013 is an olivine-rich diogenite. This *meteorite* does not exhibit shock effect in its silicates. Consequently, It has been found that can be a good calibration standard to compare with Itokawa silicate properties.

A direct application of the parameters measured in this study will be the characterization of the impact outcome of the NASA DART spacecraft with the moon of the *asteroid* binary Didymos in October 2022. DART will perform the first deflection experiment on an *asteroid*. We will then be able to test modeling of *crater* excavation and plume formation with an real deflection experiment. Obviously, the measurements of the dimensions of the *crater* will be required and this can only be achieved by another spacecraft examining the impact outcome after the DART mission. This is the objective of the ESA Hera mission (Michel et al., 2018) that was approved by the ESA Council at Ministerial Level in November 2019.

3.3 2P/Encke comet and comparison of the reflectivity with carbonaceous chondrites

It is known that *carbonaceous chondrites* are unable to survive long time scales in the interplanetary medium as is revealed from the study of Cosmic Ray Exposure Ages in *meteorites* (Eugster, 2003). These are fragile rocks that probably disrupt in space in timescales of few tens of million of years, so they probably reach the near-Earth region being quite small and fractured projectiles (Trigo-Rodriguez and Blum, 2009). These projectiles produce fireballs, but its fragility produce its break-up, ending in quite small *meteorites* on the ground (Trigo-Rodríguez et al., 2010; Jenniskens et al., 2012).

In order to gain insight on the nature of evolved *comets*, we have compared the reflectance spectra of CCs with the reflectance spectrum obtained for *comet* 2P/Encke (Tubiana et al., 2015). In our study we included a significant number of NASA Antarctic CCs. It was not casual, given the small terminal mass expected for meteorite-dropping bolides of the Taurid stream, we think that the Antarctic collection can provide the opportunity to identify the first *meteorites* associated with *comets*.

Gradie and Veverka (1986) studied the visible to NIR spectral dependence in ordinary and *carbonaceous chondrites*. Their models of the surface roughness indicate that the differences found between the visual phase coefficients of S- and C-class *asteroids* are reflecting primarily differences in composition and not necessarily differences in surface roughness. The beam incidence angle of 8° is a particular geometry that cannot be changed in our spectrometer, so we can consider that our data is obtained in almost specular geometry (see e.g. Britt and Pieters (1988)). These authors demonstrate that the amount of metal plays a significant role in the slope of the spectrum as we also previously discussed in (Moyano-Cambero et al., 2016). On the other hand, the incidence angle also might affect the slope of the spectrum, and the overall spectral reflectivity but has not influence in the location of absorption bands (Gradie, Veverka, and Buratti, 1980).

Our reflectance spectra show features that might be different to these obtained using remote sensing. The reason for that is that each feature depth depends on many factors: differences in observation geometry, and also the grain size, shape and roughness. In addition, we recognize that the spectral slope of *carbonaceous chondrites* can change from red to blue depending on whether the sample is prepared as powder or as slab. The slope also changes with grains size, packing density or observation geometry as has been studied for Murchison CC (Cloutis et al., 2018). For these reasons looking at the sample reflectance slope is a multivariate problem, and it provides only a first approach to look for possible proxies of solar system primitive bodies.

Our study on the occurrence of water in CCs (Trigo-Rodriguez and Blum, 2009) pointed out that the hydrated CC groups could be originated in transitional *asteroids* or even evolved *comets*. We used UHR-TEM to better understand the accretion of water into *carbonaceous chondrites*, finding evidence for the accretion of ices and hydrated minerals in materials consolidated in the outer regions of the *protoplanetary disk*. These hydrated minerals have specific absorption bands, but most of the most relevant fall into the mid or far IR. We could not study the presence of such minerals in our samples due to the working range of our UV-NIR spectrometer, and the fact that works under laboratory conditions and not under vacuum. In the literature can be found studies on the importance of hydrated minerals in *meteorites* and remote sensing studies like e.g. (Dotto et al., 2004; Barucci et al., 2008; De Sanctis et al., 2015; Christensen et al., 2018; Hamilton et al., 2019). In order to test our working scenario in which some *carbonaceous chondrites* could be from hydrated *asteroids* or *comets* (Hiroi, Zolensky, and Pieters, 2001) we will compare the spectra of CCs with that of a evolved *comet*. It might be possible that some ungrouped CCs are representative of the surface materials of these bodies, also affected by aqueous alteration and collisional *gardening*.

We have basically compared the reflectance spectrum of the *comet* with those obtained for specimens of *CK, CM* and *CR chondrites* (see e.g. (Trigo-Rodriguez et al., 2014; Tanbakouei et al., 2019b) (Tab. 3.10). No clear similarity with 2P/Encke's spectrum was found as a result of such comparisons for any specimen belonging to these CC groups. Then, we performed a similar one-by-one comparison with the spectra of some ungrouped CCs and we found two quite reasonable matches (Tanbakouei et al., 2020a) (Tab. 3.11).

We did our best to rid off of terrestrial weathering, choosing some areas of the two *meteorites* that were minimally affected by the rusting effect. In any case, both *carbonaceous chondrites* belong to the NASA Antarctic collection and probably spent a significant time in Antarctica. Consequently, while we do not have returned samples

TABLE 3.10: The list of CR, CM and CK carbonaceous chondrites compared here with 2P/Encke spectrum. The total mass of each meteorite are taken from the Meteoritical Bulletin Database.

Meteorites	Group	Weight (g)
QUE 90355	CM2	32.4
Murchison	CM2	10000
EET 92159	CR2	67.6
LAP 02342	CR2	42.4
Renazzo	CR2	1000
PCA 82500	CK4-55	90.9
LAR 12265 thin	CK5	14.3
ALH 85200	CK5	438

from a short period *comet*, we should remark the possible impact of terrestrial weathering in both spectra. There is a possibility that, even with all our efforts made selecting unweathered sections studied by SEM/EDX, the origin of the spectral slope measured for the two anomalous CC could be caused by some oxides formed by terrestrial weathering. In any case, if these *carbonaceous chondrites* were affected by terrestrial weathering the spectral slope could change from red to blue depending on whether the sample is prepared as powder or as slab (Cloutis et al., 2018).

TABLE 3.11: Ungrouped carbonaceous chondrites found to have a reasonable similarity with the spectrum of 2P/Encke. The Masses are taken from the Meteoritical Bulletin and they are the total mass of the meteorite.

Meteorites	Group	Weight (g)
MET 01017	CV3-an	238
GRO 95551	C-ung	213.3

These authors also demonstrated that the slope is very sensitive and could change with the grain size, packing density or the observation geometry. In particular, the particle size can have a strong effect on *albedo*, so a body covered in fine-grained regolith with a particular phase angle has to be taken into account to do a proper comparison with the spectral properties of *meteorites* (Muinonen et al., 2010; Belskaya et al., 2010a).

3.3.1 Comparing the spectral reflectance of Encke comet with carbonaceous chondrites

3.3.1.1 Comparison with ungrouped carbonaceous chondrites

Reflectance spectrum of 2P/Encke covers the full visible spectrum from 400 nm to 900 nm on the detector. Concerning with the comparison with other CC groups, the specimens belonging to most *carbonaceous chondrite* groups exhibited very different reflectance spectra. After many attempts, among the *meteorites* studied, we found likely reflectance similarity in one called Meteorite Hills 01017 (MET 01017). This *meteorite* was initially characterized as a CV3 (possibly reduced) *chondrite* (Busemann, Alexander, and Nittler, 2007) but due to its anomalous properties was reclassified as a CV3-an (MetBull: 88, 2001). In fact, the section used shows evidence of aqueous alteration with half of its exterior having a weathered fusion crust with oxidation haloes. The section also exhibits mm-sized *chondrules* quite well preserved, and has

a fractured and weathered interior. It also contains metal-rich *chondrules* and *CAIs* in a dark *matrix* of FeO-rich phyllosilicates (Brearley, 1997; Krot et al., 2006; Trigo-Rodríguez, 2015). *CV chondrites* usually contain a 45% volume of large *chondrules* with an average size of 1 mm, ∼40% volume of dark *matrix*, and a large abundance of *CAIs* of ∼10% of volume (Brearley and Jones, 1998; Scott and Krot, 2003). The matrices of CV3 *chondrites* are dominated by fine-grained *olivine* plus phyllosilicates and the so-called opaque such as metallic iron, sulphides and *magnetite* (Burbine et al., 2001). Metal grains typically range in size from 50 to 500 nm. Sulphides, up to ∼200 μm in size, are usually associated with metal, and act as opaque as well.

Another sample with a spectral behavior similar to 2P/Encke is Grosvenor Mountains 95551 (GRO 95551). This *meteorite* is an ungrouped CC, an unusual metal-rich breccia formed by two main types of clasts, chondritic and achondritic. The chondritic clasts consist of a variety of *chondrules* and *chondrule* fragments. The silicate composition of GRO 9551; mean *olivine* is $Fa_{1.3}$ (21 analyses) with a range of $Fa_{0.7-3.5}$ and *pyroxene* ranges $Fs_{0.7-39.6}$, $Wo_{0.7-1.6}$ (Weisberg et al., 2015). The *meteorite* is anomalous with a high metal content and some petrographic peculiarities, like e.g. the presence of large silicate nodules, resembling Bencubbin (Kallemeyn et al., 1978; Weisberg et al., 2001). The specimen is of interest because it might be representative of the materials forming from processed objects (Brearley, 1991; Moyano-Cambero and Trigo-Rodríguez, 2015; Trigo-Rodríguez, 2015).

As we can see in Figure 3.14, at first sight the spectral slope of the two studied meteorites is compatible with that of 2P/Encke. The spectrum of the *comet* shows shallower slope above 800 nm. In any case, as we explain in Section 2, our reflectance spectra were taken under a beam angle of 8° so we need to recognize that it implies a significant limitation in the comparison with remote sensing data, particularly in reference with slope. Said that, the spectra of the *comet* is similar to the spectra of primitive *asteroids* and seems to be weird not having some evidence, even when it could be scarce in *meteorite* collections. It is similar to the spectra of primitive *asteroids*, which are believed to be associated with *carbonaceous chondrites* (Tubiana et al., 2015). Figure 3.15 shows that both CC samples and the comet exhibit a common absorption feature at 500 nm (Tab. 3.12). From the spectral similarities, a tentative link between 2P/Encke, MET 01017 and GRO 95551 can be made from their respective reflectance spectra. It is noticeable to know that ungrouped *chondrites* have highly variable spectral properties and Encke *comet* surface was subjected to significant changes due to solar heating (Tubiana et al., 2015).

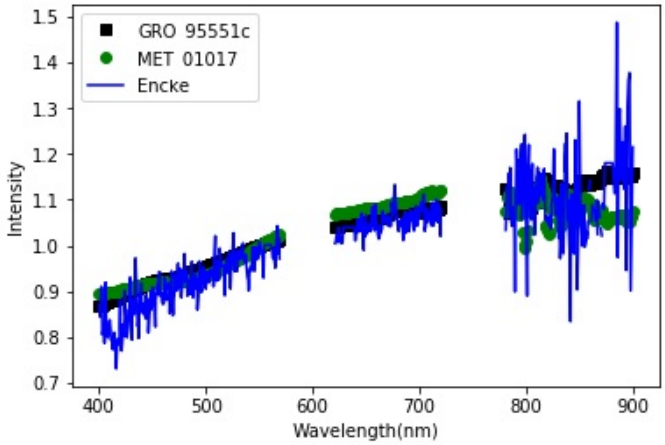

FIGURE 3.14: Reflectance spectra from 400 to 900 nm of the two ungrouped chondrites compared with the 2P/Encke comet spectrum (blue line) (From Tubiana et al. (2015)). MET 01017 is CV3-an chondrite groups and GRO 9551 is an ungrouped carbonaceous chondrites. All spectra were scaled and normalized to 1 at 550 nm.

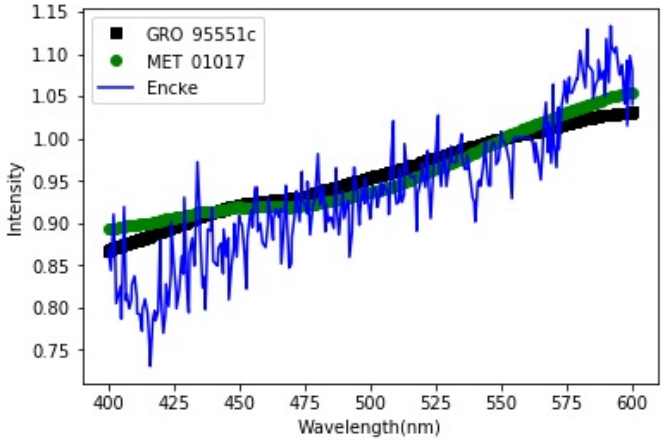

FIGURE 3.15: Reflectance spectra from 400 to 600 nm of the two ungrouped chondrites compared with the 2P/Encke comet spectrum (From Tubiana et al. (2015))

Weisberg et al. (2015) showed the similarities of Bencubbin and GRO 9551, but they are different in *olivine* compositions, oxygen isotope compositions and presence of interstitial sulfides, also the siderophile element compositions of the metal. The siderophile element composition of GRO 95551 is closer to that of ALH 85085 than to that of Bencubbin (Kallemeyn, 2000). There are many of the smaller non-spherical objects in GRO 95551 that show the texture of *chondrule*. The lack of *matrix* in GRO 95551 could be a sign of rapid *accretion*, with significant thermal processing (Metzler, 2012). Obviously some of these features could be also consequence of shock processing and/or heating in close approaches to the Sun (Delbo et al., 2014).

Concerning the reflectance spectra of MET 01017, a weaker absorption feature around 470-520 nm can be also noticed, and appears to be compatible with a weak feature also found in the 2P/Encke reflectance spectrum (Fig. 3.13). It is important to consider that *comet* surfaces are probably extensively processed due to solar heating and collisional *gardening* (Trigo-Rodríguez, 2015). In addition to the reflectance

TABLE 3.12: The location of the main absorption bands in the two ungrouped CC meteorites and their mineral assignments (Cloutis et al., 2010; Cloutis et al., 2012; Trigo-Rodriguez et al., 2014; Weisberg et al., 2015).

MET 01017	495	*Olivine*
	665	*Magnetite*/ maghemite
	700-720	Serpentine (*phyllosilicates*)
	850	*Olivine*
	875	*Orthopyroxene*
GRO 95551	470	*Olivine*
	665	*Magnetite*/ maghemite
	710	Serpentine (*phyllosilicates*)
	850	*Olivine*

data, additional evidence has been recently obtained by fireball networks suggesting that Taurid bolides associated with the largest 2P/Encke meteoroids could produce *meteorites* and even might contribute significantly to impact hazard (Napier, 2010; Madiedo et al., 2014).

For the characteristics of the Encke complex, we expect a quite heterogeneous progenitor, and as consequence of its short period as an evolved comet, we could also propose a brecciated nature consequence of collisional *gardening* (Trigo-Rodríguez, 2015). Therefore, a big diversity of anomalous *meteorites* could be expected from a disrupted and brecciated object. Just as an example of the outcome of a body subjected to strong collisional processing we could cite the heterogeneity found in Almahatta Sitta ureilite body, containing materials from many different rocky projectiles (Bischoff et al., 2010).

3.3.1.2 Comparison with grouped carbonaceous chondrites

Tubiana et al. (2015) found that the 2P/Encke spectrum correspond to one of the primitive *asteroids*, which are supposed to be correlated with CC (Tubiana et al., 2015). We establish a comparison with the rest of the CC spectra belong to *chondrite* groups of *CKs, CRs* and *CMs*. All the spectra we have obtained covered the spectrum in the 400-900 nm range, and are included in Figure 3.16.

CM chondrites are probably originated from a hydrated C-rich *asteroid* that have being fractured or exposed, in order to explain the diverse *petrologic types* (Rubin et al., 2007). It has been recently proposed that members of the 1 Gyr. old 24-Themis *asteroid* family exhibit spectral similarities with*carbonaceous chondrites*, and probably with *CM chondrites* (De Leon et al., 2012). Aqueous alteration of metal and silicate phases in a volatile-rich body, usually produces phyllosilicates and iron oxides (Rivkin et al., 2002; Trigo-Rodriguez, Rubin, and Wasson, 2006). These features had shown as absorption band around 700 nm in Figure 3.16a and are resulted from the hydrated minerals, therefore the feature will be gone after heating the material (Hiroi et al., 1996). As Tubiana et al. (2015) mentioned, by studying *meteorite* samples, we arrive to a similar conclusion: given the *space weathering* exposure the surface spectra of *comets* and primitive *asteroids* are not representative at all of their interior composition. Despite the low overall reflectance, the other absorption features in the 380 to 450 nm region can indicate the presence of insoluble organic matter, or a metal–O charge transfer absorption (Cloutis et al., 2008), while the absorption features in the 450 to 520 nm range exhibit the presence of *magnetite*. The *CM carbonaceous chondrites* we studied here are CM2 *chondrites*: Murchison and QUE 99355.

According to Tholen (1984) taxonomic classification Scheme, there is a relation between CM2 *chondrites* and *asteroids* correspond to an absorption band in the 700-750 nm region and absorption feature near 900 nm (an absorption feature is also in 1100 nm region, although the spectral coverage of this wavelength region is not available). Aqueous alteration of metal and silicate phases in that volatile-rich body have formed phyllosilicates and iron alteration minerals (Zolensky and McSween Jr, 1988; Brearley and Jones, 1998; Krot et al., 2006; Alexander et al., 2012).

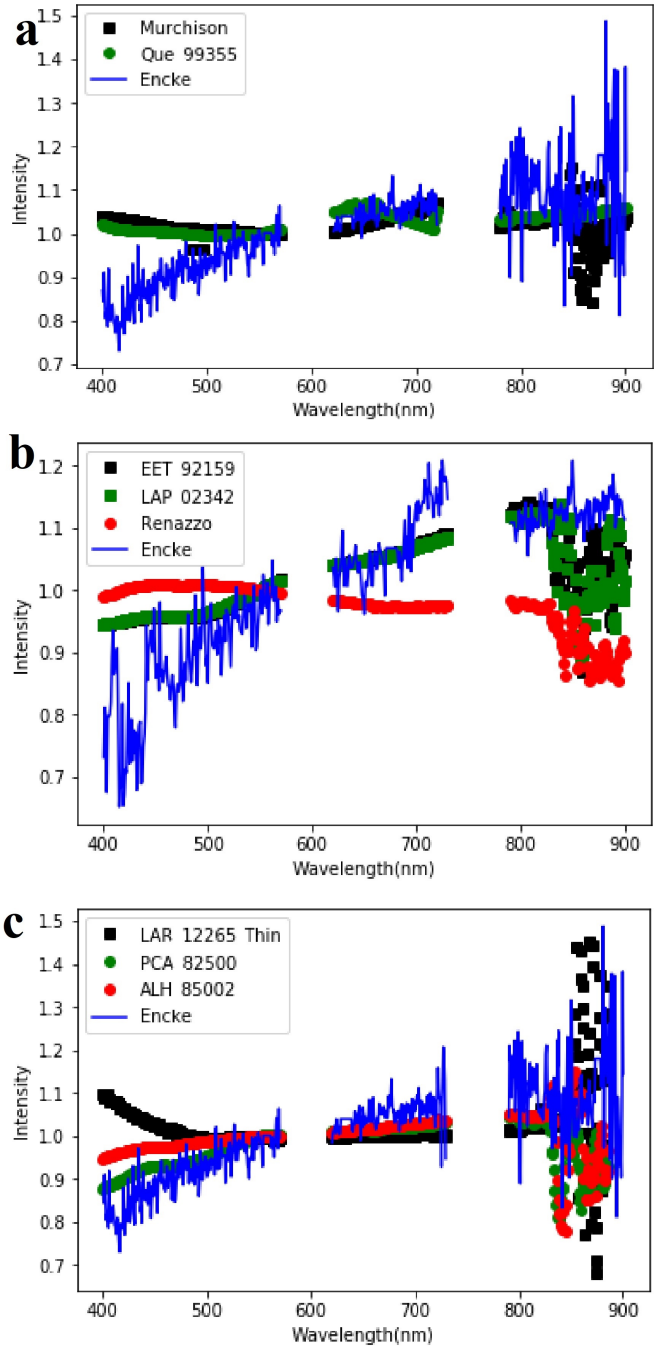

FIGURE 3.16: Comparison of reflectance properties of 2P/Encke comet with selected specimens of CC groups. Two CM2 chondrites are compared in (a), three CR2 chondrites in (b) and three CKs in (c). All data were normalized to 1 at 550 nm.

CR chondrites are one of the major group of CCs with abundant free metal and *magnetite* which show evidence of aqueous alteration (Kallemeyn, Rubin, and Wasson, 1994; Cloutis et al., 2012). *Olivine* is the dominant silicate in CR2 and CR3 *chondrites* (Brearley and Jones, 1998). The spectral reflectance of CR2 (Renazzo) *chondrite* shows that aqueous alteration results in the alteration of *olivine* and *pyroxene* to *phyllosilicates*. Hiroi et al. (1993) and Hiroi, Zolensky, and Pieters (1997) had not found any good *asteroid* match among the C, G, B, and F *asteroids* (see also Cloutis et al. (2012)). The spectral features with CR2 parent bodies are Fe^{2+} phyllosilicate, low-Fe *olivine* absorption features, moderate overall reflectance (∼8–12%), weak silicate absorption bands around 900 and 1100 nm, weak *olivine* absorption bands in 900 nm, and absent or quite weak Fe^{3+}- Fe^{2+} phyllosilicate absorption band in 650-750 nm (Cloutis et al., 2012). The CR2 *carbonaceous chondrites* selected here to compare with Encke spectral properties are EET 92159, LAP 02342 and Renazzo. Figure 3.16b clearly shows a very different spectral behavior for *CR chondrites* compared with 2P/Encke.

Concerning the spectral reflectance data for the CK group, we chose three specimens: LAR 12265 CK5, PCA 82500 CK4/5 and ALH 85002 CK5. This group is of interest here because a previous comparison between CCs and Eos *asteroid* family members provided a good match (Mothé-Diniz et al., 2008). Figure 3.16c exemplifies that there is probably not compositional similitude between Encke comet and the CK group. In all figures, the spectra of *meteorites* do not show a shallow slop beyond 800 nm despite of Encke spectra, which is relatively flat beyond about 800 nm region.

Obviously, in order to compare a *carbonaceous chondrit*e with a *comet* or a transitional *asteroid* belonging to the *Taurid Complex*, is important to consider the vast differences in cohesion that are related with their internal nature, particularly their porosity. While *carbonaceous chondrites* reaching the Earth's surface as *meteorites* exhibit maximum porosities of about 20% (Britt and Consolmagno, 2003; Blum et al., 2006). *comets* are highly porous, with porosities of 60-80% (Blum et al., 2006; Kofman et al., 2015; Pätzold et al., 2016; Fulle et al., 2016; Herique et al., 2019). Most of this porosity could be microporosity, while for rubble piles a significant part could be associated with macroporosity. *Meteorites* possess typical cohesive (tensile) strengths of several MPa (see e.g. Blum et al. (2006) for a compilation), whereas *comets* are extremely weak bodies in comparison. The latest estimate of the tensile strength of comets is only 1 Pa (Skorov and Blum, 2012; Blum et al., 2014; Blum et al., 2017; Attree et al., 2018) for length scales above 1 cm and 1 kPa for length scales below that (Trigo-Rodriguez and Blum, 2009). The latter can be measured in meteoroids penetrating in the Earth's atmosphere (Trigo-Rodríguez and Llorca, 2006; Trigo-Rodríguez and Llorca, 2007), whereas the former is a requirement for the *comet* to become active (Gundlach, Fulle, and Blum, 2020).

It is well known that *meteorites* possess typical cohesive (tensile) strengths of several MPa (see, e.g., Blum et al. (2006) for a compilation), whereas *comets* are extremely weak bodies. The latest estimate of the tensile strength of *comets* is only ∼1 Pa (Skorov and Blum, 2012; Blum et al., 2014; Attree et al., 2018; Blum et al., 2017) for length scales above ∼1 cm and ∼1 kPa for length scales below that (Moyano-Cambero et al., 2016). The latter can be measured in meteor streams (Trigo-Rodríguez and Llorca, 2006; Trigo-Rodríguez and Llorca, 2007)), whereas the former is a requirement for the *comet* to become active (Gundlach, Fulle, and Blum, 2020). Besides this vast difference in cohesion, *meteorites* and *comets* also differ in *porosity*. While *meteorites* exhibit very low *porosities* of $\leq$ 20% (Britt and Consolmagno, 2003), *comets* must be highly porous, with *porosities* of ∼60-80% (Blum et al., 2006; Kofman et al., 2015;

Pätzold et al., 2016; Fulle et al., 2016; Herique et al., 2019).

All primitive bodies in the Solar System date back to the formation era in which protoplanetary dust evolved into *planetesimals*. In the past years, evidence was gathered that *comets* in general (Skorov and Blum, 2012; Blum et al., 2014), *comet* 67P/Churyumov-Gerasimenko (Blum et al., 2017; Fulle et al., 2016) in particular and Kuiper-Belt object (486958) Arrokoth (Pätzold et al., 2016) were formed through the gentle gravitational collapse of a cloud of cm-sized "pebbles" (dust agglomerates). If we also apply such a formation mechanism for the progenitor of the members of the TC, we can state that its maximum size is constrained by several processes: (i) Collisional destruction of the pebbles during the gravitational collapse. Experimental and numerical work has shown that a maximum radius of the final object of ∼50 km is possible, before the pebbles would become collisionally fragmented, which would, thus, lead to a cohesive strength so high that dust activity would be impossible. (ii) Lithostatic destruction or deformation of the pebbles inside the planetesimal. Given the cohesive strength of the pebbles of ∼ 1-10 kPa Blum et al. (2006) and the volume-average lithostatic stress inside a body of radius R of

$$\frac{4}{15}\pi\rho^2 G R^2 \tag{3.8}$$

with $\rho \approx 500$ kg m^{-3} (Pätzold et al., 2016) and G being the mass density of the body and the gravitational constant, we get stresses of

$$4(\frac{R}{1km})^2 Pa \tag{3.9}$$

Thus, the maximum radius before the internal stresses destroy the pebbles is between 16 and 50 km. However, even before the lithostatic stress can destroy the pebbles, the tensile strength may rise to values that would render activity impossible. It was shown experimentally that about 2.5-3% of the compressive stress remains in the body as tensile strength, even after the source for the stress has disappeared (Blum et al., 2014). Setting an upper limit of 1 Pa for the tensile strength of an active *comet*, we get an upper limit for the progenitor body of a radius of 3 km . We conclude here that the progenitor body of the *Taurid complex* and, thus, *comet* 2P/Encke and the source of the *meteorites*, was a rather small body. As it is the fate for small bodies in the *asteroid* belt to eventually get collisionally disrupted and reaggregated (Michel et al., 2001; Beitz et al., 2016; Schwartz et al., 2018), the progenitor planetesimal must have originated in a heavily underpopulated region of the young Solar System.

Although the modelling of the dynamical evolution from planetesimal to *comet* and *meteorites* is beyond the scope of this thesis, we will try to sketch one possible scenario: during the evolutionary process of the Solar System, a high-velocity collision of the *planetesimal* with a much smaller impactor must have locally compacted its near-surface regions (Beitz et al., 2016; Beitz et al., 2013). To achieve *porosities* $\leq$ 20% (measured for *meteorites* (Britt and Consolmagno, 2003), impact speeds of typically 1 kms^{-1} or above are required. If the impactor was sufficiently small, the collision was sub-catastrophic and the comet nucleus remained the largest intact post-collisional residue that suffered neither substantial compaction nor heating (Beitz et al., 2013), whereas sufficient compaction occurred at the impact site to create the low-porosity meteoritic matter (Beitz et al., 2016). Such evolutionary scenario could be consistent with a significant number of ungrouped CCs available in *meteorite* collections (about a 3% of all CCs according to the Meteoritical Bulletin

Database: [1]). These ungrouped CCs are difficult to assign to CC groups because they have experienced significant amorphization (graphitization) of their matrices, as we could expect to result from the heat and compaction produced by impact shock that in addition could explain their peculiar bulk elemental chemistry, with depletion of moderately *volatile elements* (Schwartz et al., 2018). In fact, the *meteorite* matrices exhibit the typical 1300 cm^{-1} disorder band assigned to *graphite* (see e.g. Larsen and Nielsen (2006) Whether such a scenario is plausible, or even likely, remains the task of future studies.

3.3.2 Conclusions

In our search for good *meteorite* proxies of short period *comets*, we compared the reflectance spectrum of *comet* 2P/Encke with the spectral characteristics of several CCs. The absence of a clear spectral match between 2P/Encke and the previously cited CC groups might be not so surprising, given the diversity of rock-forming materials that we expect form C-rich bodies in the Solar System. In that sense, the new results achieved by the OSIRIS-REx mission to *asteroid* (101955) Bennu clearly demonstrate that some *asteroids* are active sources of particles, probably evolving not very differently to the apparently inactive members of the TC (Lauretta et al., 2019). These so-called "transitional asteroids" produce meteoroid ejections and could possess evolved surfaces exhibiting further processing influenced by localized ice sublimation, phyllosilicate dehydration, thermal stress fracturing, and secondary impacts by their own ejected debris (Lauretta et al., 2019). Searching for ungrouped CCs that have experienced thermal processing makes sense as the reflectance spectra of evolved *comet*s, like 2P/Encke, is modelled by the presence of thermally modified minerals, like e.g. amorphous carbon, and mixtures of amorphous and *crystalline* silicates (Kelley et al., 2006). We found that the most common and well established aqueously altered CC groups do not match the spectrum of *comet* 2P/Encke, but two anomalous *meteorites* might be good candidates to be associated with evolved *comets*. Consequently, we have reached the following conclusions:

1. Despite of being almost featureless CC spectra, some spectral similitudes, together with the spectral slope, are reasonably matching the 2P/Encke reflectance spectrum. In any case, we recognize that additional work is needed to establish a more precise link.

2. Such a spectral match is not obvious for other CC groups. Comparison with *CM, CR* and *CK chondrites* exhibits no evidence of compositional similarities with *comet* 2P/Encke.

3. Further search of the reflectance spectra of other CCs could provide additional insight into the real nature, composition and physical properties of periodic *comets*. Given the low *albedo* and overall dark nature of the surfaces of these objects, the characterisation of their rock-forming materials, like is being currently achieved by sample-return missions, is of seminal importance to mitigate future Earth encounters with these dangerous projectiles.

4. Finally, we think that a space mission to study the complex of bodies dynamically associated with *comet* 2P/Encke or other short period *comets* is of key relevance. That mission should include sample return, to recognize and understand the materials forming not only this object, but also those, probably active *asteroids* associated with the TC

[1] https://www.lpi.usra.edu/meteor/metbull.php

3.4 Astrometry and photometry of comets

This final section exemplifies the type of photometric studies performed from remote observations of *comets*. I participated in the follow-up of interstellar *comet* 2I/-Borisov, discovered on August, 2019 by Gennady Borisov using a 0.65 m telescope. The provisional object was named 2019 Q4 until it received the official assignation of 2I/ Borisov (Jewitt and Luu, 2019). From Catalonia we observed *comet* 2I/Borisov using Telescopi Joan Oró (TJO), a m-class telescope working in a completely unattended manner. It operates in the Observatori Astronòmic del Montsec (OAdM: www.oadm.cat), a site devoted to host astronomical research facilities under dark skies. In fact, the TJO is the largest telescope in Catalonia and named after the famous Catalan biochemist and pioneer of astrobiology who promoted the construction of this facility (Tab. 3.13). The photometric follow-up is based in a continuous monitoring like previously made for *comet* 29P/Schwassmann-Wachmann (Trigo-Rodríguez et al., 2008). In this thesis I compile the photometric measurements made from Catalonia and Crimea in order to exemplify the relevance of a systematic photometric study of interstellar visitors using meter-class instruments.

TABLE 3.13: Observatories and instruments used in this study

Observatory	MPC code	Telescope
MARGO Astron. Obs., Ukr.	L51	SC 65 f/10
TJO, Montsec (OAdM), Cat	585	RC 80 f/9.6
Montseny, Cat	B06	SC 25 f/10

The *comet* 2I/ Borisov has shown a uniform photometric behavior, with no clear anomalies. Every night the *comet* seems to suffer small fluctuations of about 0.2-0.3 magnitudes that are attributable to small differences in contrast, change in reference stars and night variations in the sky brightness, but for the rest very minor changes (Fig. 3.17). In reference to its morphology the appearance of Q4 did not change either between the different nights of observation (Sept.-Dec. 2019). No clear jets were found in our imagery, although the resolution of our instruments during the observational period in the inner coma was typically larger than one arcsec. Sky subtraction was used to negate the effects of changing atmospheric extinction. After this correction, no convincing photometric variability was found according to our data.

3.4.1 Conclusions

Interstellar *comet* 2I/ (2019 Q4) Borisov has shown since its discovery an uniform behavior without changes in its morphology. We have noticed little changes in its comma or tail during the few months in which we performed this photometric follow-up. We still need to reduce some of the data collected from TJO, but the general behavior is similar. The *comet* R magnitude increases slightly following a common pattern (see Figure 3.17). The small 0.2-0.3 magnitude changes between successive images that we noticed some nights can be considered the effect of changing atmospheric extinction and stellar fields. In our opinion, there is not convincing photometric variability detected within each night, neither along the observed period. Obviously, given the aperture measurements made for 20 arcsec surrounding the false nucleus, it is likely that any photometric variations are systematically damped. Now the *comet* is moving to the Southern hemisphere, and will be finally lost in

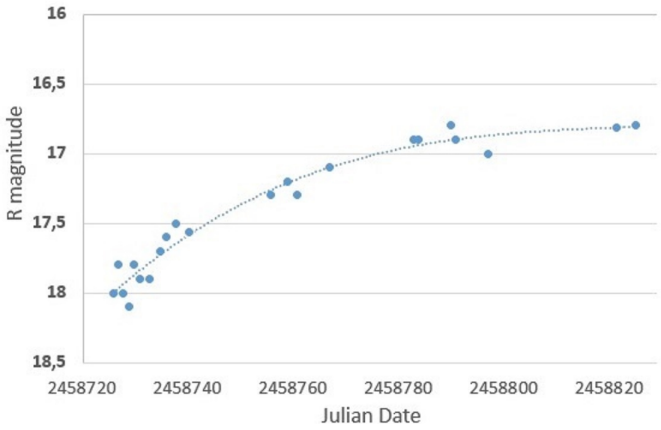

FIGURE 3.17: Unfiltered "R" magnitude for comet 2I/Borisov as a function of the Julian Date. Accuracy is about 0.1 magnitudes.

space for ever so no other observations will be made. In view of the results that we have obtained, we can say that the first interstellar *comet* appearance occurred without sorrow or glory. In any case, it is a clear confirmation that interstellar *comets* also exist.

1. We found small 0.2-0.3 magnitude changes between successive nights that might be considered the effect of changing atmospheric extinction and stellar fields. In our opinion, there is not convincing photometric variability detected within each night, neither along the observed period.

2. The results obtained, given the aperture measurements made for 20 arcsec surrounding the false nucleus, are also limited by low-resolution observing systems. It is likely that any photometric variations are systematically damped

3. The progressive increase in the coma magnitude is similar to other distant comets, but given its large heliocentric distance not significant activations, neither variations were detectable.

The *comet* was moving fast to the Southern hemisphere during the end of 2019, and was finally lost in space for ever so we couldn't do additional observations. In view of the results that we have obtained, we can say that the first interstellar *comet* appearance occurred without sorrow or glory. In any case, it is a nice confirmation that interstellar *comets* also exist. Planning future interception missions to these casual comets could provide very valuable information about the real nature of these objects.

Chapter 4

Summary and Conclusions

In this PhD thesis different techniques have being applied to *meteorites* and sample-return materials to get a deeper understanding of the mineralogy and physical properties of *asteroids* and *comets*. The research focused on the study of the reflectance, and mechanical properties of *meteorites* and regolith particles coming from *asteroids*. I also studied the properties of different rock-forming materials: from ordinary to *carbonaceous chondrites*. In addition I participated in the discovery of a pristine clast that represents a fragment of an ancient comet (Nittler et al., 2019b). A summary and most relevant conclusions of the thesis follows:

- In general the work demonstrates that chondritic *meteorites* are good proxies of the rock-forming materials of undifferentiated *asteroids*. The physical properties of the *meteorites* provide clues to understand the formation and physical evolution of these bodies. Undifferentiated *asteroids* are also a source of cosmogonic information because the materials forming these bodies formed part of the *protoplanetary disk* about 4.6 Ga ago. Since their consolidation the *asteroids* were subjected to different degrees of *metamorphism*, and collisional processing that affected the internal physical and thermal evolution of their forming materials. *Meteorites* and sample-return materials allow us to study these properties. At the same time, a good knowledge about the physico-chemical properties of the *asteroids* is important to successfully achieve sample-return from *near-Earth asteroids*.

- UV-NIR spectroscopy is a valuable remote-sensing technique to infer the main minerals forming the meteorites. Reflectance spectra of 22 *carbonaceous chondrites* from the NASA Antarctic collection and the CSIC-IEEC meteorite collection were obtained, and compared with *asteroid* classes and *comet* 2P/Encke. Reflectance spectroscopy is useful to understand the surface materials on *asteroids*, and to establish proper comparison with *meteorites*. A significant match between two ungrouped CCs and *comet* 2P/Encke has been obtained (Tanbakouei et al., 2020a).

- The surface composition and the effects of shock in *asteroid* Itokawa regolith was studied using samples returned by JAXA Hayabusa mission. The mechanical properties of that regolith were analyzed by nanoindenting the sample. The particles properties exhibit quite minor differences with the materials forming *ordinary chondrite meteorites* (Tanbakouei et al., 2019b).

- Nanoindentation allowed us to quantify hardness, *Young's modulus* and *elastic recovery* of the Itokawa regolith particles. It is a non-destructive technique that can be applied to micron-sized samples. By changing the indentation load, we measured the mechanical properties of each mineral component in each sample, and the properties of larger heterogeneous areas.

- Itokawa's regolith mechanical properties were applied to study how to increase our capacity to release materials from the surface of an *asteroid* during a kinetic impactor experiment like e.g. plans DART NASA mission. Our published study in A&A was highlighted by the European Space Agency (ESA, 2019), and provided a method to infer the mechanical response of regolith grains on the surface of chondritic *asteroids*. The mechanical properties of Itokawa's regolith inferred from nanoindentation are consistent with those found previously for OCs, and differ from those of CCs (Tanbakouei et al., 2018).

- By using SEM and EDS techniques the main minerals forming our samples were characterized. In addition, using a micro-Raman spectrometer at the Institute of Material Sciences of Barcelona (ICMAB-CSIC) had been used to identify mineralogy and allow us to infer the degree of shock experienced by the rock-forming minerals and the structural information of different phases. This technique becomes useful to identify how shock affects minerals by deforming their crystalline structure and producing a subsequent shift in the characteristic Raman peaks. High-pressure phases of *olivine* were found, exhibiting a degree of shock around 40 GPa, corresponding to a common*meteorite* shock stage of 4.

- Through the reflectance spectroscopy study of 2P/Encke *comet*, we have identified two ungrouped *carbonaceous chondrites* that might be good candidates to be associated with evolved *comets* like 2P/Encke. In featureless spectra almost the only available parameter is the spectral slope, which is reasonably matched in our data together with other weak absorption features. The slight difference between the spectrum of 2P/Encke and C-ung or CV3-an *chondrites* are due to the presence of hydrated minerals in these *chondrites* (Tubiana et al., 2015). Due to the low *albedo* and overall dark nature of the surfaces of *comets*, the characterization of their rock-forming materials is non trivial. Future sample-return missions will be addressing such a key goal, being of seminal importance to mitigate future Earth encounters with these dangerous projectiles. A sample return mission would be very useful to materials forming in the active *asteroids* in *Taurid complex* (Tanbakouei et al., 2019a; Tanbakouei et al., 2020a).

- We have also used TEM to better understand the accretion of water into *carbonaceous chondrites*. This research had implications to understand the delivery of water to early Earth. Significant evidence was found for the accretion of ices and hydrated minerals in materials consolidated in the outer regions of the *protoplanetary disk*. The result of this process was the formation of highly porous and fragile C- and water-rich transitional *asteroids* that are currently the *parent bodies* of CCs. We found evidence that some CCs have kept unique features that we interpret as evidence of wet *accretion*. Using these new insights into the water retained in CCs we envision the long and tortuous pathways in which water and other volatile species are delivered to the terrestrial planets (Trigo-Rodríguez et al., 2019)

- Using UV-NIR spectra of CCs we found that they tend to be mostly flat and almost featureless as descending to lower petrographic types, due to the increasing abundance of fine-grained opaque minerals (such as *magnetite* and organics) dispersed in their matrices (Cloutis et al., 2011; Trigo-Rodríguez, 2015; Tanbakouei et al., 2017). In comparing the *CKs* and *CVs* with Cg spectral

class of *asteroids* we infer that such a evidence fits well a evolutionary scenario. Both CC groups could be associated with a common progenitor (the *CV* parent body), but a catastrophic collision produced deep excavation of its surface, and large fragments that evolved separately and were affected by ulterior collisional *gardening*. Such a separated evolution produced increasing aqueous alteration and shock *metamorphism* in the rock forming materials, ending in a slightly different bulk chemistry that was the origin of the *CK* group.

- Finally, as an observational astronomy project I have studied the photometric evolution of 2I/Borisov *comet*, the second interstellar object discovered on 30 August 2019 by Gennady Borisov. A set of observations compiled obtained using medium-sized telescopes to gain insight on its size and nature: given that it is the first time that a clearly cometary interstellar object has been discovered, there is a need to constrain how these type of objects can behave after millions of years in interstellar space. We found that the *comet* experienced a monotonic magnitude increase as consequence of its approach to a relatively distant perihelion. During the five months in which we performed observations we did not detect any evidence for an anomalous magnitude increase, not any outburst (Tanbakouei et al., 2020b).

In summary, in this thesis I have learned how to apply a wide selection of instrumental techniques to explore the physico-chemical properties of *chondrites* and *asteroid* particles into detail. All the data obtained might provide valuable information for the future exploration of *asteroids*, together with practical applications like e.g. the deflection of threatening *asteroids*. Learning about the composition and the physical properties of the small bodies in our Solar System, and about the processes experienced by them along the eons, help us to better understand the evolution of the Solar System. This thesis is an attempt to keep learning about the origin of solid materials in their multiple forms available in a planetary system.

Appendix A

GLOSSARY

Accretion The gradual accumulation of material through the collision of particles or planetesimals within the protoplanetary disk. It produces particles or larger rocks sticking together to form larger bodies that could go up to planetary size.

Achondrite A class of stony meteorites formed by igneous processes. A meteorite whose parent body has gone through melting and differentiation. These meteorites have crystallized from a magma. Achondrites include all stony meteorite types except ordinary, carbonaceous, and enstatite chondrites.

Albedo The percentage of incoming incident light reflecting off the surface of a planetary body.

Asteroid A rocky or metallic orbiting body of subplanetary size showing no cometary activity; usually but not necessarily confined to the main asteroid belt.

CAI Acronym of Ca- and Al-rich Inclusions. These are refractory oxides that appear composing undifferentiated meteorites (chondrites) together with chondrules, metal grains and sulphides (troilite). They were dated as the first surviving minerals in the protoplanetary disk, and result from condensation at high temperatures, or originated as overheating of chondritic materials in the inner region of the protoplanetary disk.

Carbonaceous Chondrites A type of stony chondritic meteorites, mostly characterized by high abundances in carbon and water. They include some of the most primitive known meteorites and subdivided into 8 groups: CB, CH, CI, CK, CM, CO, CR and CV.

CI carbonaceous chondrite A group of carbonaceous chondrites named for the type specimen, Ivuna

CK carbonacous chondrite A group of carbonaceous chondrites named for the type specimen, Karoonda

CM carbonaceous chondrite A group of carbonaceous chondrites named for the type specimen, Mighei

CO carbonaceous chondrite A group of carbonaceous chondrites named for the type specimen, Ornans

CR carbonaceous chondrite A group of carbonaceous chondrites named for the type specimen, Renazzo

CV carbonaceous chondrite A group of carbonaceous chondrites named for the type specimen, Vigarano

CH carbonaceous chondrite A group of carbonaceous chondrites which H stands for "high metal", may contain up to as much as 40% of metal

Chondrite Stony meteorites unmodified by melting or differentiation within their parent body. They are the oldest rocks in our solar system, being the result of the accretion of materials forming the protoplanetary disk about 4.5 Gyrs ago.

Chondrule Millimetre-scale round grains found in chondrites

Chromite A mineral that is an iron chromium oxide. It has a chemical formula of $FeCr_2O_4$. It is an oxide mineral belonging to the spinel group. The element magnesium can substitute for iron in variable amounts as it forms a solid solution with magnesiochromite.

Clinopyroxene A group of important rock-forming inosilicate minerals found in many igneous and metamorphic rocks.

Crystalline A solid material whose constituents are arranged in a highly ordered microscopic structure, with single crystals showing geometrical shapes and flat faces with specific orientations.

Comets An icy, small Solar System body that, when passing close to the Sun, warms and begins to release gases through outgassing. This produces a visible atmosphere or coma, and sometimes also a tail.

Crater A bowl-shaped depression r hole produced by the impact of a meteorite, volcanic activity, or an explosion.

Differentiation A process in which a homogenous planetary body melts and gravitationally separates into layers of different density and composition. The body often separates into a core, mantle and crust.

E chondrites Enstatite chondrites; a highly reduced chondritic meteorite composed of the magnesium-rich orthopyroxene, enstatite, and iron-nickel metal.

Elastic recovery A measure of the ability of a material to return to its orignal shape when a load applied to it is removed.

Enstatite A rock-forming mineral of the orthopyroxene group with general formula $MgSiO_3$.

Fall a meteorite that was seen while it fell to Earth and found

Fayalite The Fe-rich endmember of the olivine solid-solutions series, with ideal composition Fe_2SiO_4.

Find A meteorite that was found without seeing it fall.

Feldspar A general term for aluminum silicate minerals in rocky planets with various amounts of sodium, calcium, and potassium, which also present in metamorphic rocks. Its general formula is $XAl(Al,Si)_3O_8$, where X is commonly K, Na or Ca.

Forsterite The Mg-rich endmember of the olivine solid-solutions series, with ideal composition Mg_2SiO_4.

Gardening Reworking and mixing of a regolith surface by impact from meteorites and asteroids.

Graphite A lustrous soft form of carbon usually forming thin layers; often found as nodular inclusions in iron meteorites.

H chondrite A group of chondritic stony meteorites belonging to the ordinary chondrite clan. They have the highest total iron of the ordinary chondrites.

Impact Craters Craters produced by the collision of a meteorite with the Earth (or another planet or moon) are called impact craters

Kamacite An alloy of iron and nickel (NiFe) found on meteorites, with a proportion of Fe:Ni between 90:10 and 95:5, and small quantities of other elements, such as Co or C.

L chondrite A group within the ordinary chondrite clan containing metal and combined iron in amounts intermediate between the H and LL chondrites.

LL chondrite A group within the ordinary chondrite clan that contains the lowest amounts of metal and combined iron.

Lithology Description of the physical characteristics, such as colour, texture, grain size and composition, of a rock unit. It is commonly used to subdivide a rock into parts with differences in their formation or evolution processes.

Mafic A silicate mineral or igneous rock that is rich in magnesium and iron, and is thus a portmanteau of magnesium and ferric. Most mafic minerals are dark in color, and common rock-forming mafic minerals include olivine, pyroxene, amphibole, and biotite

Magnetite An strongly magnetic iron oxide of the spinel group, with general formula Fe_3O_4, and ocurring naturally in most igneous and metamorphic rocks. It is ferrimagnetic; the most magnetic of all the naturally-occurring minerals on Earth.

Matrix Fine-grained material between inclusions, chondrules and chondrites. This material usually has a similar composition as the chondrules themselves, primarily magnesium-rich olivine and pyroxene.

Metamorphism This word describes rocks thermally modified as a result of physical processes, such as pressure or heat. Self gravity can produce parent body metamorphism, but impacts also might cause shock metamorphism.

Meteorite A solid piece of debris from an object, such as a comet, asteroid, or meteoroid, that originated in outer space and survived its passage through the atmosphere to reach the surface of a planet or moon.

Near Earth Objects, NEO Asteroids or comets of sizes ranging from metres to tens of kilometres that orbit the Sun and whose orbits come close to that of Earth's. Of the more than 600 000 known asteroids in our Solar System, more than 20 000 are NEOs.

Near Earth Asteroids, NEA Refer to those NEOs which are asteroids.

Olivine A magnesium iron silicate mineral with general formula $(Mg,Fe)_2SiO_4$. It forms the solid-solution series of forsterite (Mg-rich endmember) and fayalite (Fe-rich endmember). Its composition is commonly expressed as molar percentatges of forsterite (Fo) and fayalite (Fa).

Ordinary chondrite A chondrite meteorite, where 'ordinary' means that it is the most common found

Orthopyroxene A group of low-Ca, Fe- and Mg-rich pyroxenes crystallizing in the orthorhombic system. Most are in the solid-solution series of enstatite (Mg-rich endmember) and ferrosilite (Fe-rich endmember), and therefore its composition is commonly expressed as molar percentatges of enstatite (En) and ferrosilite (Fs).

Parent body An astronomical body of subplanetary to planetary size that fragments by collision to produce meteorites.

Petrologic type A scale used to denote the texture of chondritic meteorites; denotes increasing metamorphism in chondrites.

Phylosilicate They are an important group of minerals that includes the so-called clay minerals like e.g.: micas, chlorite, serpentine, talc, etc.

Plagioclase A group of silicate feldspars of general formula: $(Na,Ca)Al(Si,Al)Si_2O_8$. They form the solid-solution series of albite (Na-rich endmember) and anorthite (Ca-rich endmember). Their composition is commonly expressed as molar percentatges of albite (Ab) and anorthite (An).

Planetesimals Small bodies up to a few hundred miles in diameter that formed from the first solid grains to condense out of the solar nebula; planetesimals accreted to each other to form the planets of the solar system.

Porosity A percentage of the bulk volume of a rock occupied by pore space.

Protoplanetary disk A circumstellar disk from which all solids in the Solar System formed.

Potentially Hazardous Asteroid, PHA Refer to those PHOs which are asteroids.

Potentially Hazardous Objects, PHO A subgroup of NEOs larger than 150 meters in diameter, and whose orbits exhibit close encounters with the Earth within a Minimum Orbital Distance (MOD) inferior to 7.5 million of km.

Pyroxene A common group of mantle rock-forming silicate minerals, closely related in crystal form and composition and having the general formula $XYSi_2O_6$, where X can be Ca, Na, Mg or Fe^{+2}, and Y is typically Mg, Fe^{+2}, Fe^{+3}, Fe, Cr, Mn or Al, and with Al occasionally substituting Si. They crystallize in the monoclinic (clinopyroxenes) and orthorhombic (orthopyroxenes) systems.

Refractory A material chemically and physically stable at high temperatures, and therefore with a high melting point.

Space weathering Changes in the spectral properties of surface minerals on asteroidal bodies due to impacts by solar wind particles and micrometeorites. Space weathering may disguise the true spectral characteristics of an asteroid.

Taenite An alloy of Fe and Ni, with nickel proportions of 20% up to 65%. Common in meteorites.

Taurid Complex The Taurids are an annual meteor shower, associated with the comet Encke.

Thermal metamorphism Changes in the chemical and physical characteristics due to internal heating of the parent body, probably by the decay of aluminum-26. Melting temperatures are not reached so that all changes are in the solid state. This is responsible for the various petrographic types of ordinary and carbonaceous chondrites.

Thin section A slice of rock or mineral that has been ground to a thickness of 0.03 mm and mounted as a slide in a petrographic microscope.

Troilite An iron sulfide mineral with formula FeS, rarely found on Earth but abundant on meteorites. Is the Fe-rich endmember of the pyrrhotite group.

Volatile elements These are elements that are the last to condense out of a cooling gas. Volatile elements condense from a gas or evaporate from a solid at low temperatures relative to refractory elements. Volatiles are the first materials to be lost when a meteorite is heated.

Young's modulus A measure of the rigidity and flexibility of a solid material, also known as elastic modulus. It defines the relationship between applied force and deformation of a material, in such a way that a high Young's modulus implies

high rigidity.

Bibliography

Abe, M. et al. (2006). "Near-infrared spectral results of asteroid Itokawa from the Hayabusa spacecraft". In: *Science* 312.5778, pp. 1334–1338.

Adams, J.B. and L.H. Goullaud (1978). "Plagioclase feldspars-Visible and near infrared diffuse reflectance spectra as applied to remote sensing". In: *Lunar and Planetary Science Conference Proceedings*. Vol. 9, pp. 2901–2909.

Alexander, C.M.O'D., K.D. McKeegan, and K. Altwegg (2018). "Water reservoirs in small planetary bodies: meteorites, asteroids, and comets". In: *Space science reviews* 214.1, p. 36.

Alexander, C.M.O'D. et al. (2007). "The origin and evolution of chondrites recorded in the elemental and isotopic compositions of their macromolecular organic matter". In: *Geochimica et Cosmochimica Acta* 71.17, pp. 4380–4403.

Alexander, C.M.O'D. et al. (2012). "The provenances of asteroids, and their contributions to the volatile inventories of the terrestrial planets". In: *Science* 337.6095, pp. 721–723.

Armitage, Ph.J. (2011). "Dynamics of protoplanetary disks". In: *Annual Review of Astronomy and Astrophysics* 49.

Attree, N. et al. (2018). "Tensile strength of 67P/Churyumov–Gerasimenko nucleus material from overhangs". In: *Astronomy & Astrophysics* 611, A33.

Barbee, B.W. (2020). In: *Planetary Defence Activities Beyond NASA and ESA*.

Barucci, M.A. et al. (2005). "Asteroid target selection for the new Rosetta mission baseline-21 Lutetia and 2867 Steins". In: *Astronomy & Astrophysics* 430.1, pp. 313–317.

Barucci, M.A. et al. (2008). "Asteroids 2867 Steins and 21 Lutetia: surface composition from far infrared observations with the Spitzer space telescope". In: *Astronomy & Astrophysics* 477.2, pp. 665–670.

Beitz, E. et al. (2013). "Experiments on the consolidation of chondrites and the formation of dense rims around chondrules". In: *Icarus* 225.1, pp. 558–569.

Beitz, E. et al. (2016). "The collisional evolution of undifferentiated asteroids and the formation of chondritic meteoroids". In: *The Astrophysical Journal* 824.1, p. 12.

Belskaya, I.N. et al. (2010a). "Polarimetry of Centaurs (2060) Chiron,(5145) Pholus and (10199) Chariklo". In: *Icarus* 210.1, pp. 472–479.

Belskaya, I.N. et al. (2010b). "Puzzling asteroid 21 Lutetia: our knowledge prior to the Rosetta fly-by". In: *Astronomy & Astrophysics* 515, A29.

Binzel, R.P. et al. (2004). "Observed spectral properties of near-Earth objects: results for population distribution, source regions, and space weathering processes". In: *Icarus* 170.2, pp. 259–294.

Bischoff, A. et al. (2010). "Asteroid 2008 TC3—Almahata Sitta: A spectacular breccia containing many different ureilitic and chondritic lithologies". In: *Meteoritics & Planetary Science* 45.10-11, pp. 1638–1656.

Bland, P.A. et al. (2000). "CV3 chondrites: How oxidized or reduced?" In: *Meteoritics and Planetary Science Supplement* 35, A28.

Blum, J. (2004). "Grain growth and coagulation". In: *Astrophysics of dust*. Vol. 309, p. 369.

Blum, J. and G. Wurm (2000). "Experiments on sticking, restructuring, and fragmentation of preplanetary dust aggregates". In: *Icarus* 143.1, pp. 138–146.

Blum, J. et al. (2006). "The physics of protoplanetesimal dust agglomerates. I. Mechanical properties and relations to primitive bodies in the solar system". In: *The Astrophysical Journal* 652.2, p. 1768.

Blum, J. et al. (2014). "Comets formed in solar-nebula instabilities!–An experimental and modeling attempt to relate the activity of comets to their formation process". In: *Icarus* 235, pp. 156–169.

Blum, J. et al. (2017). "Evidence for the formation of comet 67P/Churyumov-Gerasimenko through gravitational collapse of a bound clump of pebbles". In: *Monthly Notices of the Royal Astronomical Society* 469.Suppl_2, S755–S773.

Bottke, W.F. (2002). *Asteroids III*. University of Arizona Press.

Bouvier, A. and M. Wadhwa (2010). "The age of the Solar System redefined by the oldest Pb–Pb age of a meteoritic inclusion". In: *Nature geoscience* 3.9, pp. 637–641.

Brandt, J.C. and R.D. Chapman (2004). *Introduction to comets*. Cambridge University Press.

Brearley, A.J. (1991). "Subsolidus microstructures and cooling history of pyroxenes in the Zagami shergottite". In: *Lunar and Planetary Science Conference*. Vol. 22.

— (1997). "Disordered biopyriboles, amphibole, and talc in the Allende meteorite: products of nebular or parent body aqueous alteration?" In: *Science* 276.5315, pp. 1103–1105.

Brearley, A.J. and R.H. Jones (1998). "In Planetary materials, edited by Papike JJ Washington". In: *DC: Mineralogical Society of America*, pp. 1–370.

Brearley, A.J. and A. Wagner (2014). "Heterogeneous Matrix Textures in the Highly Oxidized and Sulfidized CV3 Chondrite MET 00430: A Record of Fluid-Rock Interaction and Compaction". In: *LPICo* 77.1800, p. 5335.

Britt, D.T. and G. Consolmagno (2003). "Stony meteorite porosities and densities: A review of the data through 2001". In: *Meteoritics & Planetary Science* 38.8, pp. 1161–1180.

Britt, D.T. and C.M. Pieters (1988). "Bidirectional reflectance properties of iron-nickel meteorites". In: *Lunar and Planetary Science Conference Proceedings*. Vol. 18, pp. 503–512.

Brownlee, D. et al. (2006). "Comet 81P/Wild 2 under a microscope". In: *science* 314.5806, pp. 1711–1716.

Burbine, T.H. et al. (2001). "K asteroids and CO3/CV3 chondrites". In: *Meteoritics & Planetary Science* 36.2, pp. 245–253.

Burbine, Th.H. and R.P. Binzel (2002). "Small main-belt asteroid spectroscopic survey in the near-infrared". In: *Icarus* 159.2, pp. 468–499.

Burbine, Th.H. et al. (2002). "Meteoritic parent bodies: Their number and identification". In: *Asteroids III*.

Bus, S.J. (1999). "Compositional structure in the asteroid belt: Results of a spectroscopic survey". PhD thesis. Massachusetts Institute of Technology.

Bus, S.J. and R.P. Binzel (2002). "Phase II of the small main-belt asteroid spectroscopic survey: The observations". In: *Icarus* 158.1, pp. 106–145.

Busemann, H., M.O'D. Alexander, and L.R. Nittler (2007). "Characterization of insoluble organic matter in primitive meteorites by microRaman spectroscopy". In: *Meteoritics & Planetary Science* 42.7-8, pp. 1387–1416.

Chapman, C.R. (2004). "Space weathering of asteroid surfaces". In: *Annual Review of Earth and Planetary Sciences* 32.

Chapman, C.R., T.V. Johnson, and Th.B. McCord (1971). "A Review of Spectrophotometric Studies of Asteroids". In: *International Astronomical Union Colloquium* 12, 51—65.

Chapman, C.R. and J.W. Salisbury (1973). "Comparisons of meteorite and asteroid spectral reflectivities". In: *Icarus* 19.4, pp. 507–522.

Chapman, C.R. et al. (2002). *Cratering on asteroids from Galileo and NEAR Shoemaker*. this volume. Univ. of Arizona, Tucson.

Chaumard, N. et al. (2014). "Metamorphosed calcium-aluminum-rich inclusions in CK carbonaceous chondrites". In: *Meteoritics & Planetary Science* 49.3, pp. 419–452.

Chopelas, A. (1991). "Single crystal Raman spectra of forsterite, fayalite, and monticellite". In: *American Mineralogist* 76.7-8, pp. 1101–1109.

Christensen, Ph.R. et al. (2018). "The OSIRIS-REx thermal emission spectrometer (OTES) instrument". In: *Space Science Reviews* 214.5, p. 87.

Clark, B.E. et al. (2002). "Asteroid space weathering and regolith evolution". In: *Asteroids III* 585, pp. 90086–2.

Cloutis, E.A. et al. (1986). "Calibrations of phase abundance, composition, and particle size distribution for olivine-orthopyroxene mixtures from reflectance spectra". In: *Journal of Geophysical Research: Solid Earth* 91.B11, pp. 11641–11653.

Cloutis, E.A. et al. (2008). "Ultraviolet spectral reflectance properties of common planetary minerals". In: *Icarus* 197.1, pp. 321–347.

Cloutis, E.A. et al. (2010). "Spectral reflectance properties of ureilites". In: *Meteoritics & Planetary Science* 45.10-11, pp. 1668–1694.

Cloutis, E.A. et al. (2011). "Spectral reflectance properties of carbonaceous chondrites: 2. CM chondrites". In: *Icarus* 216.1, pp. 309–346.

Cloutis, EA et al. (2012). "Spectral reflectance properties of carbonaceous chondrites: 3. CR chondrites". In: *Icarus* 217.1, pp. 389–407.

Cloutis, E.A. et al. (2018). "Spectral reflectance "deconstruction" of the Murchison CM2 carbonaceous chondrite and implications for spectroscopic investigations of dark asteroids". In: *Icarus* 305, pp. 203–224.

Consolmagno, G.J., D.T. Britt, and R.J. Macke (2008). "The significance of meteorite density and porosity". In: *Geochemistry* 68.1, pp. 1–29.

De Leon, J. et al. (2012). "Near-infrared spectroscopic survey of B-type asteroids: Compositional analysis". In: *Icarus* 218.1, pp. 196–206.

De Sanctis, M.CH. et al. (2015). "Ammoniated phyllosilicates with a likely outer Solar System origin on (1) Ceres". In: *Nature* 528.7581, pp. 241–244.

Delbo, M. et al. (2014). "Thermal fatigue as the origin of regolith on small asteroids". In: *Nature* 508.7495, pp. 233–236.

DeMeo, F.E. (2010a). "Impact of parenting styles on academic achievement: Parenting styles, parental involvement, personality factors and peer orientation". PhD thesis. PhD Thesis. Long Island University, The Brooklyn Center.

— (2010b). "La variation compositionnelle des petits corps à travers le système solaire". PhD thesis. Observatoire de Paris.

DeMeo, F.E. et al. (2009). "An extension of the Bus asteroid taxonomy into the near-infrared". In: *Icarus* 202.1, pp. 160–180.

Devouard, B. et al. (2006). "Mineralogy and petrology of TNZ 057 (C4) and comparison to the CV and CK groups". In: *Meteorit. Planet. Sci.* 41, A203.

Dotto, E. et al. (2004). "308 Polyxo: ISO–SWS spectrum up to 26 micron". In: *Astronomy & Astrophysics* 427.3, pp. 1081–1084.

Dunn, T.L. et al. (2013). "Mineralogies and source regions of near-Earth asteroids". In: *Icarus* 222.1, pp. 273–282.

Eugster, O. (2003). "Cosmic-ray exposure ages of meteorites and lunar rocks and their significance". In: *Geochemistry* 63.1, pp. 3–30.

Fischer-Cripps, A.C. (2004). "Contact mechanics". In: *Nanoindentation*. Springer, pp. 1–20.

Flynn, G.J. et al. (2015). "Hypervelocity cratering and disruption of porous pumice targets: Implications for crater production, catastrophic disruption, and momentum transfer on porous asteroids". In: *Planetary and Space Science* 107, pp. 64–76.

Foster, N.F. et al. (2013). "Identification by Raman spectroscopy of Mg–Fe content of olivine samples after impact at 6 km s- 1 onto aluminium foil and aerogel: In the laboratory and in Wild-2 cometary samples". In: *Geochimica et Cosmochimica Acta* 121, pp. 1–14.

Fulle, M. et al. (2016). "Comet 67P/Churyumov–Gerasimenko preserved the pebbles that formed planetesimals". In: *Monthly Notices of the Royal Astronomical Society* 462.Suppl_1, S132–S137.

Gaffey, M.J. (2010). "Space weathering and the interpretation of asteroid reflectance spectra". In: *Icarus* 209.2, pp. 564–574.

Gaffey, M.J., J.F. Bell, and D.P. Cruikshank (1989). "Reflectance spectroscopy and asteroid surface mineralogy." In: *Asteroids II*, pp. 98–127.

Gaffey, M.J., Th.H. Burbine, and R.P. Binzel (1993). "Asteroid spectroscopy: Progress and perspectives". In: *Meteoritics* 28.2, pp. 161–187.

Gaffey, M.J. and Th.B. McCord (1978). "Asteroid surface materials: Mineralogical characterizations from reflectance spectra". In: *Space Science Reviews* 21.5, pp. 555–628.

Gail, H-P. et al. (2013). "Early thermal evolution of planetesimals and its impact on processing and dating of meteoritic material". In: *arXiv preprint arXiv:1312.3509*.

Galimov, E.M. (2013). "Chelyabinsk meteorite–an LL5 chondrite". In: *Solar System Research* 47.4, p. 255.

Garcia-Melendo, E. and C.M. Clement (1997). "NSV 09295: A double-mode RR lyrae variable." In: *The Astronomical Journal* 114, pp. 1190–1194.

Geiger, T. and A. Bischoff (1995). "Formation of opaque minerals in CK chondrites". In: *Planetary and Space Science* 43.3-4, pp. 485–498.

Gillis-Davis, J.J. et al. (2017). "Incremental laser space weathering of Allende reveals non-lunar like space weathering effects". In: *Icarus* 286, pp. 1–14.

Göpel, Ch., G. Manhes, and C.J. Allegre (1994). "U-Pb systematics of phosphates from equilibrated ordinary chondrites". In: *Earth and Planetary Science Letters* 121.1-2, pp. 153–171.

Gradie, J. and J. Veverka (1986). "The wavelength dependence of phase coefficients". In: *Icarus* 66.3, pp. 455–467.

Gradie, J.C., J. Veverka, and B.J. Buratti (1980). "The effects of photometric geometry on spectral reflectance". In: *Lunar and Planetary Science Conference*. Vol. 11, pp. 357–359.

Grady, M.M., R. Hutchison, and A. Graham (2000). *Catalogue of Meteorites Reference Book with CD-ROM*. Cambridge University Press.

Greenwood, R.C. et al. (2004). "The relationship between CK and CV chondrites: A single parent body source (abstract# 1664)". In: *34th Lunar and Planetary Science Conference. CD-ROM*.

— (2010). "The relationship between CK and CV chondrites". In: *Geochimica et Cosmochimica Acta* 74.5, pp. 1684–1705.

Greenwood, R.G., A.T. Kearsley, and I.A. Franchi (2003). "Are CK chondrites really a distinct group or just equilibrated CVs?" In: *66th Annual Meteoritical Society Meeting, Munster, Germany*.

Grimm, R.E. and Jr.H.Y McSween (1989). "Water and the thermal evolution of carbonaceous chondrite parent bodies". In: *Meteoritics* 24, p. 272.

Gundlach, B., M. Fulle, and J. Blum (2020). "On the activity of comets: understanding the gas and dust emission from comet 67/Churyumov–Gerasimenko's south-pole region during perihelion". In: *Monthly Notices of the Royal Astronomical Society* 493.3, pp. 3690–3715.

Hamilton, V.E. et al. (2019). "Evidence for widespread hydrated minerals on asteroid (101955) Bennu". In: *Nature Astronomy* 3.4, pp. 332–340.

Harriss, K.H. and M.J. Burchell (2016). "A study of the observed shift in the peak position of olivine Raman spectra as a result of shock induced by hypervelocity impacts". In: *Meteoritics & Planetary Science* 51.7, pp. 1289–1300.

Hendrix, A.R. and F. Vilas (2006). "The effects of space weathering at UV wavelengths: S-class asteroids". In: *The Astronomical Journal* 132.3, p. 1396.

Henke, S. et al. (2012). "Thermal evolution and sintering of chondritic planetesimals". In: *Astronomy & Astrophysics* 537, A45.

Herique, A. et al. (2019). "Homogeneity of 67P/Churyumov-Gerasimenko as seen by CONSERT: implication on composition and formation". In: *Astronomy & Astrophysics* 630, A6.

Hiroi, T., C.M. Pieters, and H. Takeda (1994). "Grain size of the surface regolith of asteroid 4 Vesta estimated from its reflectance spectrum in comparison with HED meteorites". In: *Meteoritics* 29.3, pp. 394–396.

Hiroi, T., M.E. Zolensky, and C.M. Pieters (2001). "The Tagish Lake meteorite: A possible sample from a D-type asteroid". In: *Science* 293.5538, pp. 2234–2236.

Hiroi, T., M.I. Zolensky, and C.M. Pieters (1997). "Characterization of unusual CI/CM/CR meteorites from reflectance spectroscopy". In: *Lunar and Planetary Science Conference*. Vol. 28, p. 577.

Hiroi, T. et al. (1993). "Evidence of thermal metamorphism on the C, G, B, and F asteroids". In: *Science* 261.5124, pp. 1016–1018.

Hiroi, T. et al. (1996). "Thermal metamorphism of the C, G, B, and F asteroids seen from the 0.7 μm, 3 μm, and UV absorption strengths in comparison with carbonaceous chondrites". In: *Meteoritics & Planetary Science* 31.3, pp. 321–327.

Holsapple, K.A. (2001). "Equilibrium configurations of solid cohesionless bodies". In: *Icarus* 154.2, pp. 432–448.

Howell, S.B. (2006). *Handbook of CCD astronomy*. Vol. 5. Cambridge University Press.

Hsieh, H.H. and D. Jewitt (2006). "A population of comets in the main asteroid belt". In: *Science* 312.5773, pp. 561–563.

Huber, H. et al. (2006). "Siderophile-element anomalies in CK carbonaceous chondrites: Implications for parent-body aqueous alteration and terrestrial weathering of sulfides". In: *Geochimica et Cosmochimica Acta* 70.15, pp. 4019–4037.

Hunt, G.R. and R.P. Ashley (1979). "Spectra of altered rocks in the visible and near infrared". In: *Economic Geology* 74.7, pp. 1613–1629.

Huss, G.R., A.E. Rubin, and J.N. Grossman (2006). "Thermal metamorphism in chondrites". In: *Meteorites and the early solar system II* 943, pp. 567–586.

Hutchison, R. (2006). *Meteorites: A petrologic, chemical and isotopic synthesis*. Vol. 2. Cambridge University Press.

Isa, J., A.E. Rubin, and J.T. Wasson (2012). "Bulk compositions of CV and CK chondrites: support for a close relationship". In: *Lunar and Planetary Science Conference*. Vol. 43.

Jarosewich, E. (2006). "Chemical analyses of meteorites at the Smithsonian Institution: An update". In: *Meteoritics & Planetary Science* 41.9, pp. 1381–1382.

Jenniskens, P. (1998). "On the dynamics of meteoroid streams". In: *Earth, planets and space* 50.6-7, pp. 555–567.

— (2006). "(Mostly) dormant comets in the NEO population and the meteoroid streams that they crumble into". In: *Proceedings of the International Astronomical Union* 2.S236, 87—94.

Jenniskens, P. et al. (2012). "Radar-enabled recovery of the Sutter's Mill meteorite, a carbonaceous chondrite regolith breccia". In: *Science* 338.6114, pp. 1583–1587.

Jewitt, D. and J. Luu (2019). "Initial Characterization of Interstellar Comet 2I/2019 Q4 (Borisov)". In: *The Astrophysical Journal Letters* 886.2, p. L29.

Jogo, K. et al. (2018). "Redistribution of Sr and rare earth elements in the matrices of CV3 carbonaceous chondrites during aqueous alteration in their parent body". In: *Earth, Planets and Space* 70.1, pp. 1–9.

Jones, D. (1967). *The phoneme: Its nature and use*. Heffer.

Jones, R.H. et al. (2000). "Formation of chondrules and CAIs: Theory vs. observation". In: *Protostars and planets IV* 927, p. 962.

Juan-Samsó, J. et al. (2005). "Detection of a classical δ Scuti star in the new eclipsing binary system HIP 7666". In: *Astronomy & Astrophysics* 434.3, pp. 1063–1068.

Kallemeyn, G. W. et al. (1978). "Formation of the Bencubbin polymict meteoritic breccia". In: *Geochimica et Cosmochimica Acta* 42.5, pp. 507–515.

Kallemeyn, G.W. (2000). "The composition of the Grosvenor Mountains 95551 anomalous chondrite and its relationship to other reduced chondrites". In: *Meteoritics and Planetary Science Supplement* 35, A85.

Kallemeyn, G.W., A.E. Rubin, and J. T. Wasson (1991). "The compositional classification of chondrites: V. The Karoonda (CK) group of carbonaceous chondrites". In: *Geochimica et Cosmochimica Acta* 55.3, pp. 881–892.

Kallemeyn, G.W., A.E. Rubin, and J.T. Wasson (1994). "The compositional classification of chondrites: VI. The CR carbonaceous chondrite group". In: *Geochimica et Cosmochimica Acta* 58.13, pp. 2873–2888.

Keil, K. (1968). "Mineralogical and chemical relationships among enstatite chondrites". In: *Journal of Geophysical Research* 73.22, pp. 6945–6976.

Keil, K., Jeffrey F. Bell, and D.T. Britt (1992). "Reflection spectra of shocked ordinary chondrites and their relationship to asteroids". In: *Icarus* 98.1, pp. 43–53.

Kelley, M.S. et al. (2006). "A Spitzer study of comets 2P/Encke, 67P/Churyumov-Gerasimenko, and C/2001 HT50 (LINEAR-NEAT)". In: *The Astrophysical Journal* 651.2, p. 1256.

Kim, J.H. et al. (2014). "Droplet microfluidics for producing functional microparticles". In: *Langmuir* 30.6, pp. 1473–1488.

King, T.V.V. and W.I. Ridley (1987). "Relation of the spectroscopic reflectance of olivine to mineral chemistry and some remote sensing implications". In: *Journal of Geophysical Research: Solid Earth* 92.B11, pp. 11457–11469.

Kofman, W. et al. (2015). "Properties of the 67P/Churyumov-Gerasimenko interior revealed by CONSERT radar". In: *Science* 349.6247, aab0639.

Kohout, T. et al. (2014). "Mineralogy, reflectance spectra, and physical properties of the Chelyabinsk LL5 chondrite–Insight into shock-induced changes in asteroid regoliths". In: *Icarus* 228, pp. 78–85.

Kracher, A. et al. (1985). "The Leoville (CV3) accretionary breccia". In: *Journal of Geophysical Research: Solid Earth* 90.S01, pp. 123–135.

Krause, M. et al. (2011). "Thermal conductivity measurements of porous dust aggregates: I. Technique, model and first results". In: *Icarus* 214.1, pp. 286–296.

Krot, A.N. et al. (2006). "Timescales and settings for alteration of chondritic meteorites". In: *Meteorites and the early solar system II*, pp. 525–553.

Kuebler, K.E. et al. (2006). "Extracting olivine (Fo–Fa) compositions from Raman spectral peak positions". In: *Geochimica et Cosmochimica Acta* 70.24, pp. 6201–6222.

Landolt, A.U. (1992). "UBVRI photometric standard stars in the magnitude range 11.5-16.0 around the celestial equator". In: *The Astronomical Journal* 104, pp. 340–371.

Larsen, K.L. and O.F. Nielsen (2006). "Micro-Raman spectroscopic investigations of graphite in the carbonaceous meteorites Allende, Axtell and Murchison". In: *Journal of Raman Spectroscopy: An International Journal for Original Work in all Aspects of Raman Spectroscopy, Including Higher Order Processes, and also Brillouin and Rayleigh Scattering* 37.1-3, pp. 217–222.

Lauretta, D.S. et al. (2019). "Episodes of particle ejection from the surface of the active asteroid (101955) Bennu". In: *Science* 366.6470.

Lazzarin, M. et al. (2004). "Astronomy and Astrophysics, 425". In: *L25*.

Llorca, J. et al. (2005). "The Villalbeto de la Peña meteorite fall: I. Fireball energy, meteorite recovery, strewn field, and petrography". In: *Meteoritics & Planetary Science* 40.6, pp. 795–804.

Lodders, K. and Jr.B. Fegley (2015). *Chemistry of the solar system*. Royal Society of Chemistry.

Loeffler, M.J., C.A. Dukes, and R.A Baragiola (2009). "Irradiation of olivine by 4 keV He+: Simulation of space weathering by the solar wind". In: *Journal of Geophysical Research: Planets* 114.E3.

Madiedo, J.M. et al. (2014). "Analysis of bright Taurid fireballs and their ability to produce meteorites". In: *Icarus* 231, pp. 356–364.

Martinez, M. et al. (2019). "New observations on high-pressure phases in a shock melt vein in the Villalbeto de la Peña meteorite: Insights into the shock behavior of diopside". In: *Meteoritics & Planetary Science* 54.11, pp. 2845–2863.

Matsumoto, T. et al. (2016). "Nanomorphology of Itokawa regolith particles: application to space-weathering processes affecting the Itokawa asteroid". In: *Geochimica et cosmochimica acta* 187, pp. 195–217.

McLean, I.S. (2008). *Electronic imaging in astronomy: detectors and instrumentation*. Springer Science & Business Media.

McSween, H.Y. and Jr. McSween (1999). *Meteorites and their parent planets*. Cambridge University Press.

Metzler, K. (2004). "Formation of accretionary dust mantles in the solar nebula: Evidence from preirradiated olivines in CM chondrites". In: *Meteoritics & Planetary Science* 39.8, pp. 1307–1319.

— (2012). "Ultrarapid chondrite formation by hot chondrule accretion? Evidence from unequilibrated ordinary chondrites". In: *Meteoritics & Planetary Science* 47.12, pp. 2193–2217.

Michel, P. et al. (2001). "Collisions and gravitational reaccumulation: Forming asteroid families and satellites". In: *Science* 294.5547, pp. 1696–1700.

Michel, P. et al. (2018). "European component of the AIDA mission to a binary asteroid: Characterization and interpretation of the impact of the DART mission". In: *Advances in Space Research* 62.8, pp. 2261–2272.

Michikami, T. et al. (2007). "Ejecta velocity distribution for impact cratering experiments on porous and low strength targets". In: *Planetary and Space Science* 55.1-2, pp. 70–88.

Mohanan, K., Sh.K. Sharma, and F.C. Bishop (1993). "A Raman spectral study of forsterite-monticellite solid solutions". In: *American Mineralogist* 78.1-2, pp. 42–48.

Morris, R.V. et al. (1985). "Spectral and other physicochemical properties of submicron powders of hematite (α-Fe2O3), maghemite (γ-Fe2O3), magnetite (Fe3O4), goethite (α-FeOOH), and lepidocrocite (γ-FeOOH)". In: *Journal of Geophysical Research: Solid Earth* 90.B4, pp. 3126–3144.

Mothé-Diniz, T. et al. (2008). "Mineralogical analysis of the Eos family from near-infrared spectra". In: *Icarus* 195.1, pp. 277–294.

Moyano Cambero, C.E. (2017). *Physico-chemical properties of chondritic meteorites: clues on the origin and evolution of their parent bodies*.

Moyano-Cambero, C.E. and J.M. Trigo-Rodríguez (2015). "Comparative Study of CK Carbonaceous Chondrites and Asteroids Reflectance Spectra Between 0.3 and 2.6 μm". In: *Lunar and Planetary Science Conference*. Vol. 46, p. 1106.

Moyano-Cambero, C.E., J.M. Trigo-Rodríguez, and J. Llorca (2013). "UV-NIR spectra of the most reflective carbonaceous chondrite groups: CH, CR and R". In: *44th Lunar and Planetary Science Conference. Abstract*. Vol. 1533.

Moyano-Cambero, C.E. et al. (2016). "A plausible link between the asteroid 21 Lutetia and CH carbonaceous chondrites". In: *Meteoritics & Planetary Science* 51.10, pp. 1795–1812.

Moyano-Cambero, C.E. et al. (2017a). "Chelyabinsk meteorite as a proxy for studying the properties of potentially hazardous asteroids and impact deflection strategies". In: *Assessment and Mitigation of Asteroid Impact Hazards*. Springer, pp. 219–241.

Moyano-Cambero, C.E. et al. (2017b). "Nanoindenting the Chelyabinsk meteorite to learn about impact deflection effects in asteroids". In: *The Astrophysical Journal* 835.2, p. 157.

Muinonen, K. et al. (2010). "A three-parameter magnitude phase function for asteroids". In: *Icarus* 209.2, pp. 542–555.

Nakamura, A.M., A. Fujiwara, and T. Kadono (1994). "Velocity of finer fragments from impact". In: *Planetary and Space Science* 42.12, pp. 1043–1052.

Nakamura, T. et al. (2011). "Itokawa dust particles: a direct link between S-type asteroids and ordinary chondrites". In: *Science* 333.6046, pp. 1113–1116.

Napier, W.M. (June 2010). "Palaeolithic extinctions and the Taurid Complex". In: *Monthly Notices of the Royal Astronomical Society* 405.3, pp. 1901–1906. ISSN: 0035-8711.

Neumann, W., D. Breuer, and T. Spohn (2012). "Differentiation and core formation in accreting planetesimals". In: *Astronomy & Astrophysics* 543, A141.

Nittler, L.R. et al. (2019a). "A cometary building block in a primitive asteroidal meteorite". In: *Nature Astronomy* 3.7, p. 659.

Nittler, L.R. et al. (2019b). "Reply to: GEMS and the devil in their details". In: *Nature Astronomy* 3.7, pp. 606–606.

Nix, W.D. and H. Gao (1998). "Indentation size effects in crystalline materials: a law for strain gradient plasticity". In: *Journal of the Mechanics and Physics of Solids* 46.3, pp. 411–425.

Noguchi, T. (1993). "Petrology and mineralogy of CK chondrites: Implications for the metamorphism of the CK chondrite parent body". In: *Antarctic Meteorite Research* 6, p. 204.

Noguchi, T. et al. (2011). "Incipient space weathering observed on the surface of Itokawa dust particles". In: *Science* 333.6046, pp. 1121–1125.

Norton, O.R. (2002). "Book Review: The Cambridge encyclopedia of meteorites/-Cambridge University Press, 2002". In: *The Observatory* 122, p. 297.

O'Keefe, J.D. and T.J. Ahrens (1985). "Impact and explosion crater ejecta, fragment size, and velocity". In: *Icarus* 62.2, pp. 328–338.

Oliver, W.C. and G.M. Pharr (1992). "An improved technique for determining hardness and elastic modulus using load and displacement sensing indentation experiments". In: *Journal of Materials Research* 7.6, 1564–1583.

Ormel, C.W. (2008). *The early stages of planet formation: how to grow from small to large*. University Library Groningen][Host].

Papike, J.J., S.B. Simon, and J.C. Laul (1982). "The lunar regolith: Chemistry, mineralogy, and petrology". In: *Reviews of Geophysics* 20.4, pp. 761–826.

Pätzold, M. et al. (2016). "A homogeneous nucleus for comet 67P/Churyumov–Gerasimenko from its gravity field". In: *Nature* 530.7588, pp. 63–65.

Pellicer, E. et al. (2012). "Localized electrochemical deposition of porous Cu-Ni microcolumns: Insights into the growth mechanisms and the mechanical performance". In: *Int. J. Electrochem. Sci* 7.1, pp. 4014–4029.

Petit, J. and A. Morbidelli (2005). "Chronology of solar system formation". In: *Lectures in Astrobiology*. Springer, pp. 61–82.

Popescu, M. (2012). "Techniques for asteroid spectrocopy". PhD thesis.

Popova, O. et al. (2011). "Very low strengths of interplanetary meteoroids and small asteroids". In: *Meteoritics & Planetary Science* 46.10, pp. 1525–1550.

Ramakrishnan, N. and V.S. Arunachalam (1993). "Effective elastic moduli of porous ceramic materials". In: *Journal of the American Ceramic Society* 76.11, pp. 2745–2752.

Rietmeijer, F.J.M. (2002). "The earliest chemical dust evolution in the solar nebula". In: *Geochemistry* 62.1, pp. 1–45.

Righter, K. et al. (2015). "Mineralogy, petrology, chronology, and exposure history of the Chelyabinsk meteorite and parent body". In: *Meteoritics & Planetary Science* 50.10, pp. 1790–1819.

Rivkin, A.S. et al. (2002). "Hydrated minerals on asteroids: The astronomical record". In: *Asteroids III* 1, pp. 235–253.

Rubin, A.E. (2011). "Origin of the differences in refractory-lithophile-element abundances among chondrite groups". In: *Icarus* 213.2, pp. 547–558.

— (2012). "Collisional facilitation of aqueous alteration of CM and CV carbonaceous chondrites". In: *Geochimica et Cosmochimica Acta* 90, pp. 181–194.

Rubin, A.E. and C. Ma (2017). "Meteoritic minerals and their origins". In: *Geochemistry* 77.3, pp. 325–385.

Rubin, A.E. et al. (2007). "Progressive aqueous alteration of CM carbonaceous chondrites". In: *Geochimica et Cosmochimica Acta* 71.9, pp. 2361–2382.

Saito, J. et al. (2006). "Detailed images of asteroid 25143 Itokawa from Hayabusa". In: *Science* 312.5778, pp. 1341–1344.

Salisbury, J.W., G.R. Hunt, and CH.J. Lenhoff (1975). "Visible and near-infrared spectra: X. Stony meteorites." In: *ModGe* 5, pp. 115–126.

Schwartz, S.R. et al. (2018). "Catastrophic disruptions as the origin of bilobate comets". In: *Nature astronomy* 2.5, pp. 379–382.

Scott, E.R.D., K. Keil, and D. Stöffler (1992). "Shock metamorphism of carbonaceous chondrites". In: *Geochimica et Cosmochimica Acta* 56.12, pp. 4281–4293.

Scott, E.R.D and A.N. Krot (2003). "Chondrites and their components". In: *TrGeo* 1, p. 711.

Skorov, Y. and J. Blum (2012). "Dust release and tensile strength of the non-volatile layer of cometary nuclei". In: *Icarus* 221.1, pp. 1–11.

Stetson, P.B. (2000). "Homogeneous photometry for star clusters and resolved galaxies. II. Photometric standard stars". In: *Publications of the Astronomical Society of the Pacific* 112.773, p. 925.

Tanbakouei, S. et al. (2017). "Selective UV-NIR Reflectance Spectra of CM Chondrites to Identify Pristinity, Aqueous Alteration, and Mild Metamorphism in Undifferentiated Asteroids". In: *Lunar and Planetary Science Conference*. Vol. 48.

Tanbakouei, S. et al. (2018). "Mechanical Properties of Silicate-Rich Itokawa Regolith Particles". In: *Lunar and Planetary Science Conference*. Vol. 49.

Tanbakouei, S. et al. (2019a). "Comparing the Reflectivity of Ungrouped Carbonaceous Chondrites with that of 2P/ENCKE Comet: Do We Have Samples from Comets in Meteorite Collection?" In: *Lunar and Planetary Science Conference*. Vol. 50.

Tanbakouei, S. et al. (2019b). "Mechanical properties of particles from the surface of asteroid 25143 Itokawa". In: *Astronomy & Astrophysics* 629, A119.

Tanbakouei, S. et al. (2020a). "Comparing the reflectivity of ungrouped carbonaceous chondrites with that of short period comets like 2P/Encke". In: *arXiv preprint arXiv:2007.06212*.

Tanbakouei, S. et al. (2020b). "Photometric Follow-Up of Interstellar Comet 2I/-BORISOV Since Its Discovery (abstract# 2124)". In: *51st Lunar and Planetary Science Conference, LPI Contribution* 2326.

Tang, J. et al. (2003). "Magnetite Fe3O4 nanocrystals: spectroscopic observation of aqueous oxidation kinetics". In: *The Journal of Physical Chemistry B* 107.30, pp. 7501–7506.

Tholen, D.J. (1984). "Asteroid taxonomy from cluster analysis of Photometry". PhD thesis.

Thomas, C.A. and R.P. Binzel (2010). "Identifying meteorite source regions through near-Earth object spectroscopy". In: *Icarus* 205.2, pp. 419–429.

Tolu, E. et al. (2013). "Highly ordered mesoporous magnesium niobate high-κ dielectric ceramic: synthesis, structural/mechanical characterization and thermal stability". In: *Journal of Materials Chemistry C* 1.32, pp. 4948–4955.

Trigo-Rodríguez, J.M. (2015). "Aqueous alteration in chondritic asteroids and comets from the study of carbonaceous chondrites". In: *Planetary Materials. EMU Notes in Mineralogy* 15, pp. 67–87.

Trigo-Rodriguez, J.M. and J. Blum (2009). "Tensile strength as an indicator of the degree of primitiveness of undifferentiated bodies". In: *Planetary and Space Science* 57.2, pp. 243–249.

Trigo-Rodríguez, J.M. and J. Llorca (2006). "The strength of cometary meteoroids: Clues to the structure and evolution of comets". In: *Monthly Notices of the Royal Astronomical Society* 372.2, pp. 655–660.

— (2007). "Erratum: The strength of cometary meteoroids: clues to the structure and evolution of comets". In: *Monthly Notices of the Royal Astronomical Society* 375.1, pp. 415–415.

Trigo-Rodriguez, J.M., A.E. Rubin, and J.T. Wasson (2006). "Non-nebular origin of dark mantles around chondrules and inclusions in CM chondrites". In: *Geochimica et Cosmochimica Acta* 70.5, pp. 1271–1290.

Trigo-Rodríguez, J.M. et al. (2008). "Outburst activity in comets-I. Continuous monitoring of comet 29P/Schwassmann-Wachmann 1". In: *Astronomy & Astrophysics* 485.2, pp. 599–606.

Trigo-Rodríguez, J.M. et al. (2010). "Outburst activity in comets–II. A multiband photometric monitoring of comet 29P/Schwassmann–Wachmann 1". In: *Monthly Notices of the Royal Astronomical Society* 409.4, pp. 1682–1690.

Trigo-Rodriguez, J.M. et al. (2014). "UV to far-IR reflectance spectra of carbonaceous chondrites–I. Implications for remote characterization of dark primitive asteroids targeted by sample-return missions". In: *Monthly Notices of the Royal Astronomical Society* 437.1, pp. 227–240.

Trigo-Rodríguez, J.M. et al. (2017). "Asteroids, Comets and Meteorite-Dropping Bolides Studied from The Montsec Astronomical Observatory". In: *Assessment and Mitigation of Asteroid Impact Hazards*. Springer, pp. 243–256.

Trigo-Rodríguez, J.M. et al. (2019). "Accretion of water in carbonaceous chondrites: Current evidence and implications for the delivery of water to early Earth". In: *Space Science Reviews* 215.1, p. 18.

Trigo-Rodríguez, J.M. et al. (2010). "Outburst activity in comets – II. A multiband photometric monitoring of comet 29P/Schwassmann–Wachmann 1". In: *Monthly Notices of the Royal Astronomical Society* 409.4, pp. 1682–1690. ISSN: 0035-8711.

Tsuchiyama, A. et al. (2011). "Three-dimensional structure of Hayabusa samples: origin and evolution of Itokawa regolith". In: *Science* 333.6046, pp. 1125–1128.

Tsuchiyama, A. et al. (2013). "Analytical dual-energy microtomography: A new method for obtaining three-dimensional mineral phase images and its application to Hayabusa samples". In: *Geochimica et Cosmochimica Acta* 116, pp. 5–16.

Tubiana, C. et al. (2015). "2P/Encke, the Taurid complex NEOs and the Maribo and Sutter's Mill meteorites". In: *Astronomy & Astrophysics* 584, A97.

Unsalan, O. and C. Altunayar-Unsalan (2020). "Shock–induced olivine–ringwoodite and plagioclase–maskelynite transformations in Bursa L6 chondrite: A Raman and ATR–FTIR spectroscopic study". In: *Spectrochimica Acta Part A: Molecular and Biomolecular Spectroscopy*, p. 118590.

Urzaiz, M., J.M. Trigo-Rodriguez, and N. Mestres (2015). "Identification of a Silico-Phosphate in CK4 Carbonaceous Chondrite Allan Hills 85002". In: *Lunar and Planetary Science Conference*. Vol. 46, p. 1785.

Van Schmus, W.R. and J.A. Wood (1967). "A chemical-petrologic classification for the chondritic meteorites". In: *Geochimica et Cosmochimica Acta* 31.5, pp. 747–765.

Vernazza, P. et al. (2008). "Compositional differences between meteorites and near-Earth asteroids". In: *Nature* 454.7206, pp. 858–860.

Vilas, F. and M.J. Gaffey (1989). "Phyllosilicate absorption features in main-belt and outer-belt asteroid reflectance spectra". In: *Science* 246.4931, pp. 790–792.

Wasson, John T, Junko Isa, and Alan E Rubin (2013). "Compositional and petrographic similarities of CV and CK chondrites: A single group with variations in textures and volatile concentrations attributable to impact heating, crushing and oxidation". In: *Geochimica et Cosmochimica Acta* 108, pp. 45–62.

Wasson, J.T. (1985). "Meteorites: their record of early solar-system history". In: *mtre*.

Watanabe, S. et al. (2019). "Hayabusa2 arrives at the carbonaceous asteroid 162173 Ryugu—A spinning top–shaped rubble pile". In: *Science* 364.6437, pp. 268–272.

Weidenschilling, S.J. and J.N. Cuzzi (1993). "Formation of planetesimals in the solar nebula". In: *Protostars and planets III*, pp. 1031–1060.

Weisberg, M.K., T.J. McCoy, and A.N. Krot (2006). "Systematics and evaluation of meteorite classification". In: *Meteorites and the early solar system II*.

Weisberg, M.K. et al. (2001). "A new metal-rich chondrite grouplet". In: *Meteoritics & Planetary Science* 36.3, pp. 401–418.

Weisberg, M.K. et al. (2015). "Petrology and geochemistry of chondrules and metal in NWA 5492 and GRO 95551: A new type of metal-rich chondrite". In: *Geochimica et Cosmochimica Acta* 167, pp. 269–285.

Wood, X.H. and G.P. Kuiper (1963). "Photometric studies of asteroids." In: *The Astrophysical Journal* 137, p. 1279.

Yano, H. et al. (2006). "Touchdown of the Hayabusa spacecraft at the Muses Sea on Itokawa". In: *Science* 312.5778, pp. 1350–1353.

Yin, Q. et al. (2002). "A short timescale for terrestrial planet formation from Hf–W chronometry of meteorites". In: *Nature* 418.6901, pp. 949–952.

Yomogida, K. and T. Matsui (1983). "Physical properties of ordinary chondrites". In: *Journal of Geophysical Research: Solid Earth* 88.B11, pp. 9513–9533.

— (1984). "Multiple parent bodies of ordinary chondrites". In: *Earth and Planetary Science Letters* 68.1, pp. 34–42.

Zellner, B. (1979). "Asteroid taxonomy and the distribution of the compositional types." In: *aste*, pp. 783–806.

Zellner, B., D.J. Tholen, and E.F. Tedesco (1985). "The eight-color asteroid survey: Results for 589 minor planets". In: *Icarus* 61.3, pp. 355–416.

Zolensky, M. and H.Y McSween Jr (1988). "Aqueous alteration". In: *Meteorites and the early solar system*, pp. 114–143.